Deconstructing squeezed light: Schmidt decomposition versus the Whittaker-Shannon interpolation

C. Drago* and J. E. Sipe†
Department of Physics, University of Toronto, 60 St. George Street, Toronto, Ontario, Canada, M5S 1A7

(Received 4 December 2023; accepted 15 April 2024; published 6 August 2024)

We develop a formalism to describe squeezed light with large spectral-temporal correlations. This description is valid in all regimes, but is especially applicable in the long pulse to continuous-wave limit where the photon density at any particular time is small, although the total number of photons can be quite large. Our method relies on the Whittaker-Shannon interpolation formula applied to the joint temporal amplitude of squeezed light, which allows us to "deconstruct" the squeezed state. This provides a local description of the state and its photon statistics, making the underlying physics more transparent than does the use of the Schmidt decomposition. The formalism can easily be extended to more exotic nonclassical states where a Schmidt decomposition is not possible.

DOI: 10.1103/PhysRevA.110.023710

I. INTRODUCTION

Squeezed light is of interest for applications in quantum sensing and imaging [1,2], and as a resource for quantum computing [3]. For light propagating in one direction in a quasi-one-dimensional (quasi-1D) structure, such as an optical fiber or a channel waveguide in an integrated photonic structure [4], or even light propagating in free space under the approximation that diffraction is negligible, a squeezed state can be written as

$$|\Psi\rangle = e^{\frac{\beta}{2}\int d\omega_1 d\omega_2 \gamma(\omega_1,\omega_2) a^\dagger(\omega_1) a^\dagger(\omega_2) - \text{H.c.}} |\text{vac}\rangle, \tag{1.1}$$

where for simplicity only one polarization and one transverse mode is considered. We label the lowering operator at a frequency shifted by ω from a center reference frequency ω_o by $a(\omega)$ (see Appendix A),

$$[a(\omega_1), a^\dagger(\omega_2)] = \delta(\omega_1 - \omega_2), \tag{1.2}$$

and $|\text{vac}\rangle$ is the vacuum state. Here $\gamma(\omega_1, \omega_2)$ is the joint spectral amplitude,

$$\int |\gamma(\omega_1, \omega_2)|^2 d\omega_1 d\omega_2 = 1, \tag{1.3}$$

and β is the squeezing amplitude. Unless otherwise indicated, we take integrals to range from $-\infty$ to ∞.

Often the properties of interest can be captured by simple functions of frequencies, such as correlation functions of the form

$$G^{(1)}(\omega) = \langle\Psi|a^\dagger(\omega)a(\omega)|\Psi\rangle, \tag{1.4a}$$

$$G^{(2)}(\omega_1, \omega_2) = \langle\Psi|a^\dagger(\omega_1)a^\dagger(\omega_2)a(\omega_2)a(\omega_1)|\Psi\rangle, \tag{1.4b}$$

etc. For a pulse of light where $|\beta| \ll 1$, the state is only slightly different from the vacuum state,

$$|\Psi\rangle \approx |\text{vac}\rangle + \frac{\beta}{2}\int d\omega_1 d\omega_2 \gamma(\omega_1, \omega_2) a^\dagger(\omega_1) a^\dagger(\omega_2)|\text{vac}\rangle, \tag{1.5}$$

where higher-order terms in β have been neglected, and there is only a small probability amplitude for a two-photon state. Then

$$G^{(1)}(\omega) \to |\beta|^2 \int |\gamma(\omega, \omega')|^2 d\omega', \tag{1.6a}$$

$$G^{(2)}(\omega_1, \omega_2) \to |\beta|^2 |\gamma(\omega_1, \omega_2)|^2. \tag{1.6b}$$

In this paper we consider the evaluation of quantities such as these, even when $|\beta|$ is not much less than one. A standard strategy in such a situation is to decompose the joint spectral amplitude in terms of Schmidt modes. If there is only one or a few Schmidt modes, as might occur for squeezed light generated by a short pump pulse in time, the expressions for correlation functions of the squeezed light in terms of Schmidt modes can be easily evaluated even if $|\beta|$ is large, and they immediately identify much of the physics. But large values of $|\beta|$ can also arise for squeezed light generated by pump pulses that are very long, and even if their intensities are very weak. Here, although the rate at which pairs of photons are generated may be quite small, the total number of pairs of photons generated diverges as the pump pulse approaches cw excitation, and thus both $|\beta|$ and the Schmidt number diverge. Our goal is to identify strategies that allow for the calculation of quantities such as correlation functions to be done quickly for such states, and in a way that makes the physics of the squeezed light clear.

We begin by introducing the temporal representation of the joint spectral amplitude $\overline{\gamma}(t_1, t_2)$ and some of its general features in Sec. II. Then in Sec. III we consider a natural first approach, which is to use the Schmidt decomposition of $\overline{\gamma}(t_1, t_2)$ even if the Schmidt number is very large. We find

*Contact author: christian.drago@mail.utoronto.ca
†Contact author: sipe@physics.utoronto.ca

that this approach does not directly make the physics of the state $|\Psi\rangle$ apparent, and this motivates our search for other ways to "deconstruct" the joint amplitude of the squeezed light that better elucidate the physics. In Sec. IV we introduce a new approach suggested by the time-correlation functions of the light; it works well if there is significant degeneracy in the amplitudes of the Schmidt decomposition. In Sec. V we generalize this, based on the Whittaker-Shannon interpolation formula, in a scheme that is applicable even if there is no such degeneracy. We argue that this new way of "deconstructing" the joint amplitude does make the physics of the state more apparent, and in Sec. VI we compare it to the Schmidt decomposition. Then using our formalism we provide a "local decomposition" of the squeezed state, and demonstrate its use in calculations in Sec. VII. We give a discussion of the "strongly squeezed limit" within our framework in Sec. VIII, and end in Sec. IX with a realistic example of a joint spectral amplitude for a squeezed state generated in a ring resonator structure. Our conclusions and suggestions for future work are presented in Sec. X.

II. JOINT TEMPORAL AMPLITUDE

Besides the expression (1.1) for a squeezed state that is based on an integral over frequencies (or wave numbers), it will be useful to have an expression based on integrals over time (or position). For simplicity we assume group-velocity dispersion can be neglected and that light propagates with a velocity v; then putting

$$\overline{a}(t) = \int \frac{d\omega}{\sqrt{2\pi}} a(\omega) e^{-i\omega t}, \tag{2.1}$$

and with

$$\overline{\gamma}(t_1, t_2) \equiv \int \frac{d\omega_1 d\omega_2}{2\pi} \gamma(\omega_1, \omega_2) e^{-i\omega_1 t_1} e^{-i\omega_2 t_2} \tag{2.2}$$

identifying the "joint temporal amplitude," we can write Eq. (1.1) as

$$|\Psi\rangle = e^{\frac{\beta}{2}\int dt_1 dt_2 \overline{\gamma}(t_1,t_2)\overline{a}^\dagger(t_1)\overline{a}^\dagger(t_2) - \text{H.c.}} |\text{vac}\rangle. \tag{2.3}$$

We take $\gamma(\omega_1, \omega_2)$ and $\overline{\gamma}(t_1, t_2)$ to identify the spectral and temporal representations of a "joint amplitude" and refer to their absolute squares $|\gamma(\omega_1, \omega_2)|^2$ and $|\overline{\gamma}(t_1, t_2)|^2$ as the spectral and temporal representations of a "joint intensity." While due to time-ordering corrections we would expect the joint amplitude to change as the pump intensity and thus β is increased [5], here we neglect such effects for simplicity and take the joint amplitude to be fixed when we consider varying β below.

Of course, the ket $|\Psi\rangle$ [Eq. (1.1) or (2.3)] is a Schrödinger ket at a particular time, say $t = 0$. The variables t_1, t_2 can be thought of as surrogates for position, where $\overline{a}(t_1)$ is identified with the electric field at $z = -vt_1$; equivalently, if the ket $|\Psi\rangle$ were allowed to evolve in time, $\overline{a}(t)$ would identify the field operator at $z = 0$ at time t (see Appendix A).

Corresponding to the frequency correlation functions [Eq. (1.4)] we can also introduce time-dependent first- and second-order correlation functions [6]

$$\overline{G}^{(1)}(t_1, t_2) = \langle\Psi|\overline{a}^\dagger(t_1)\overline{a}(t_2)|\Psi\rangle, \tag{2.4a}$$

$$\overline{G}^{(2)}(t_1, t_2) = \langle\Psi|\overline{a}^\dagger(t_1)\overline{a}^\dagger(t_2)\overline{a}(t_2)\overline{a}(t_1)|\Psi\rangle. \tag{2.4b}$$

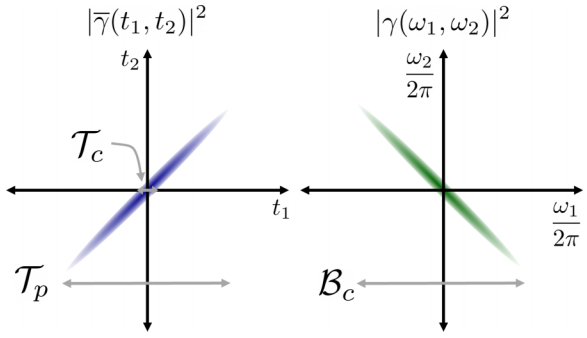

FIG. 1. Schematic of a joint intensity represented in time on the left and frequency on the right. The horizontal width of the joint temporal (spectral) amplitude is denoted by $\mathcal{T}_p$ ($\mathcal{B}_c$), which is the effective pulse duration (bandwidth). The narrow horizontal width at $t_2 = 0$ is denoted by $\mathcal{T}_c = 1/\mathcal{B}_c$ and is the coherence time of photon pairs.

The "equal-time" first-order correlation function, given by $\overline{G}^{(1)}(t) \equiv \overline{G}^{(1)}(t, t)$, is the "photon-density" of the pulse of light, and is used to predict the counting rate of an ideal photodetector; indeed, if we integrate over all time, then

$$N_{\text{pulse}} = \int \overline{G}^{(1)}(t) dt \tag{2.5}$$

is the expected photon number in the pulse. The second-order correlation function $\overline{G}^{(2)}(t_1, t_2)$ has a similar interpretation and is used to predict the probability of detection coincidences at the indicated times.

We will primarily be interested in joint intensities of the form shown schematically in Fig. 1, where there are large spectral-temporal correlations; however, the formalism we introduce is valid for a general joint amplitude. We characterize the joint intensity by two quantities, $\mathcal{T}_p$ and $\mathcal{B}_c$, indicated in Fig. 1. The quantity $\mathcal{T}_p$ is an effective measure of the duration of the generated pulse of squeezed light. The second quantity, $\mathcal{B}_c$, is an effective measure of the bandwidth of generated photons. Associated with this bandwidth we define a time $\mathcal{T}_c = 1/\mathcal{B}_c$, which is on the order of the narrow width of the joint temporal intensity; see Fig. 1. The time $\mathcal{T}_c$ identifies the "coherence time," the typical range of $|t_2 - t_1|$ over which $|\overline{\gamma}(t_1, t_2)|^2$ is non-negligible.

III. SCHMIDT MODES

A natural approach to try to elucidate the physics of a squeezed state and calculate the correlation functions given by Eq. (2.4) is to employ a Schmidt decomposition of the joint amplitude, since the squeezed state can then be written as a direct product of squeezed states associated with the supermodes introduced via the Schmidt decomposition. That is the strategy we explore in this section.

In writing Eq. (1.1) for the squeezed state we took the origin of $\gamma(\omega_1, \omega_2)$ to indicate the same frequency ω_o with respect to which both ω_1 and ω_2 are referenced—this is the case of so-called "degenerate" squeezing—and here without loss of generality the joint amplitude can be taken as symmetric in its variables [$\gamma(\omega_2, \omega_1) = \gamma(\omega_1, \omega_2)$, or equivalently $\overline{\gamma}(t_2, t_1) = \overline{\gamma}(t_1, t_2)$]. From a Takagi factorization [7,8] we can

then construct the Schmidt decomposition,

$$\gamma(\omega_1,\omega_2)=\sum_n \sqrt{p_n} f_n(\omega_1) f_n(\omega_2),$$
$$\overline{\gamma}(t_1,t_2)=\sum_n \sqrt{p_n}\overline{f}_n(t_1)\overline{f}_n(t_2), \tag{3.1}$$

where the Schmidt weights $p_n \geqslant 0$ sum to unity. The elements of the sets $\{f_n(\omega)\}$ and $\{\overline{f}_n(t)\}$ of mutually orthogonal and normalized functions are related by

$$\overline{f}_n(t)=\int \frac{d\omega}{\sqrt{2\pi}} f_n(\omega) e^{-i\omega t}. \tag{3.2}$$

As usual, we take the set $\{f_n(\omega)\}$ of elements with $p_n \neq 0$ to be expanded to be a complete set of functions, assigning $p_n = 0$ to the added elements, and correspondingly for the $\{\overline{f}_n(t)\}$.

The Schmidt number K of the expansion (3.1), which characterizes the effective number of spectral or temporal modes in the sum (3.1), is given by

$$K=\left(\sum_n p_n^2\right)^{-1}. \tag{3.3}$$

It serves as an effective measure of the correlation in the dependence of the joint amplitude on its two variables; in the limit of a Schmidt number of unity the joint amplitude is simply a product of the same function of each variable, and there is no correlation at all in its dependence on those variables.

We can introduce another measure of the correlation of the dependence of the joint amplitude on its two variables by

$$\mathcal{K}=\mathcal{T}_p\mathcal{B}_c=\frac{\mathcal{T}_p}{\mathcal{T}_c}. \tag{3.4}$$

Clearly when $\mathcal{T}_p$ is much greater than $\mathcal{T}_c$ then the dependence of the joint amplitude on its two variables is highly correlated (see Fig. 1), and then $\mathcal{K} \gg 1$. Of course, at the moment we have only defined $\mathcal{T}_p$ and $\mathcal{B}_c$ in a "rough-and-ready" way, and such then is our definition of $\mathcal{K}$; we make the definition more precise below. Often similarly defined quantities are introduced and referred to as the "time-bandwidth product." So to avoid confusion we henceforth refer to $\mathcal{K}$ as an "effective Schmidt number."

Confusions with the phrase "time-bandwidth product" can arise because of different definitions used for "time" and "bandwidth." For example, Fedorov *et al.* calculate a time-bandwidth product by taking the width of the "unconditional" ("single-particle") and "conditional" ("coincidence") widths of the joint intensity; for a general double-Gaussian joint amplitude (considered below), they show that the time-bandwidth product is exactly equal to the Schmidt number [9–11]. Alternatively, Brecht and Silberhorn calculate the time-bandwidth product taking the conditional and unconditional widths of the "chronocyclic Wigner function," which for their double-Gaussian model is equal to the Schmidt number, even when a chirp is included [12]. The agreement—either exact or approximate—between the time-bandwidth product and the Schmidt number suggest a deeper connection between the two quantities.

However, there is an older and more rigorous meaning of the term time-bandwidth product from classical information theory: For a one-dimensional bandlimited signal, it is the number of orthogonal functions optimally concentrated within a given timewidth needed to describe the signal [13], and in this context is referred to as the "Shannon number" [14,15]. Generalizations of the Shannon number exist for higher dimensional signals where one calculates the time-bandwidth product using the bandwidth and timewidth area, volume, etc. [14–17]. Recent work has made the connection between the Shannon number from classical information theory to the Schmidt number in quantum information theory; see, for example, Pires *et al.* [17] or Pors *et al.* [18] for both a theoretical and experimental investigation.

In this spirit we define $\mathcal{K}$ more precisely by defining $\mathcal{T}_p$ and $\mathcal{B}_c$ more precisely. We assume that those quantities are chosen as small as possible but subject to the condition that, to within the level of approximation adopted in calculations, they cover the range of the joint amplitude in time and frequency, respectively. This means that the typical ways used to measure bandwidth or frequency—such as the standard deviation, full-width-at-half-max etc.—are too narrow. In particular, we choose $\mathcal{B}_c$ to be large enough that frequencies larger than $2\pi\mathcal{B}_c/2$ can be completely neglected, and we can treat the joint spectral amplitude as effectively bandwidth limited. For this reason the effective Schmidt number $\mathcal{K}$ will generally be larger than, but typically on the order of, other conventions used for the time-bandwidth product.

In a later section we argue that generally the Schmidt number K and effective Schmidt number $\mathcal{K}$ satisfy the inequality

$$K \leqslant \mathcal{K}. \tag{3.5}$$

One might generally expect this to be true based on a physical argument: Suppose we have squeezed light propagating with an arbitrary joint amplitude with some Schmidt number K and effective Schmidt number $\mathcal{K}$. Now if the squeezed light is sent through a dispersive medium, the joint spectral amplitude is multiplied by a complex but *separable* phase that does *not* change the Schmidt number. However, we know that in a dispersive medium the bandwidth remains constant but the pulse duration broadens, and so $\mathcal{K}$ will generally increase. Thus, in general one might indeed expect that $K \leqslant \mathcal{K}$. Below we discuss when the near exact equality holds.

We find that we can use the effective Schmidt number $\mathcal{K}$ to introduce a "weak squeezing" regime characterized by the condition

$$\frac{|\beta|}{\sqrt{\mathcal{K}}} \ll 1, \tag{3.6}$$

and a "strong squeezing" regime characterized by the condition

$$\frac{|\beta|}{\sqrt{\mathcal{K}}} \gg 1. \tag{3.7}$$

If neither of these conditions are satisfied we refer to the squeezing as "moderate."

Now as a first example of the use of the Schmidt decomposition to evaluate the correlation functions, consider a general

normalized two-photon state,

$$|\mathrm{II}\rangle = \frac{1}{\sqrt{2}} \int dt_1 dt_2 \overline{\gamma}(t_1, t_2) \overline{a}^\dagger(t_1) \overline{a}^\dagger(t_2) |\mathrm{vac}\rangle$$
$$= \frac{1}{\sqrt{2}} \sum_n \sqrt{p_n} A_n^\dagger A_n^\dagger |\mathrm{vac}\rangle, \tag{3.8}$$

where we defined operators associated with the supermodes as

$$A_n^\dagger \equiv \int dt \overline{f}_n(t) \overline{a}^\dagger(t), \tag{3.9}$$

and so

$$\overline{a}(t) = \sum_n \overline{f}_n(t) A_n. \tag{3.10}$$

To write the inverted form [Eq. (3.10)] we have taken the adjoint of Eq. (3.9) and used the completeness relation of the set of functions $\{\overline{f}_n(t)\}$. The set of operators $\{A_n\}$ and their adjoints satisfy the usual harmonic-oscillator commutation relations. Just as the expressions (3.1) can be written in time or frequency form, so the first of (3.8) and (3.9) can also be written involving integrals over frequency of the corresponding quantities. We find

$$\overline{G}^{(1)}(t)|_{|\mathrm{II}\rangle} \equiv \langle \mathrm{II}|\overline{a}^\dagger(t)\overline{a}(t)|\mathrm{II}\rangle = 2\sum_n p_n |\overline{f}_n(t)|^2, \tag{3.11}$$

and

$$\overline{G}^{(2)}(t_1, t_2)|_{|\mathrm{II}\rangle} \equiv \langle \mathrm{II}|\overline{a}^\dagger(t_1)\overline{a}^\dagger(t_2)\overline{a}(t_2)\overline{a}(t_1)|\mathrm{II}\rangle$$
$$= 2\left|\sum_n \sqrt{p_n}\overline{f}_n(t_1)\overline{f}_n(t_2)\right|^2. \tag{3.12}$$

In the first we have a contribution of $|\overline{f}_n(t)|^2$ from each Schmidt mode with a weight p_n, while in the second the amplitudes associated with each of the Schmidt modes add; the factor of two of course arises because we have pairs of photons.

Moving to a squeezed state, in the limit $|\beta| \ll 1$ we can write (2.3) as

$$|\Psi\rangle \to |\mathrm{vac}\rangle + \frac{\beta}{\sqrt{2}}|\mathrm{II}\rangle + \cdots \tag{3.13}$$

[cf. (1.5)], and we find

$$\overline{G}^{(1)}(t) \to \sum_n |\beta_n|^2 |\overline{f}_n(t)|^2 = |\beta|^2 \int |\overline{\gamma}(t, t')|^2 dt',$$
$$\overline{G}^{(2)}(t_1, t_2) \to \left|\sum_n \beta_n \overline{f}_n(t_1)\overline{f}_n(t_2)\right|^2 = |\beta|^2 |\overline{\gamma}(t_1, t_2)|^2, \tag{3.14}$$

where $\beta_n = \beta\sqrt{p_n}$ [cf. (1.6)]. Treating $|\gamma(t_1, t_2)|^2$ as a normalized probability distribution, for $N_{\mathrm{pulse}} = |\beta|^2 \ll 1$ we find $\overline{G}^{(1)}(t)$ is the probability distribution reduced by integrating over the second time variable, and $\overline{G}^{(2)}(t_1, t_2)$ is proportional to $|\overline{\gamma}(t_1, t_2)|^2$ itself, the norm squared of the joint temporal amplitude at the two corresponding times.

More generally, using the Schmidt decomposition (3.1) and the supermode operators (3.9), which are all independent, we can write the squeezed ket (2.3) as

$$|\Psi\rangle = \bigotimes_n S_n |\mathrm{vac}\rangle_n, \tag{3.15}$$

where $|\mathrm{vac}\rangle_n$ is the vacuum state for the corresponding supermode and

$$S_n = e^{\frac{\beta_n}{2} A_n^\dagger A_n^\dagger - \mathrm{H.c.}}. \tag{3.16}$$

With the standard result [19]

$$S_n^\dagger A_n S_n = c_n A_n + e^{i\theta} s_n A_n^\dagger, \tag{3.17}$$

where we have put $\beta = |\beta| e^{i\theta}$ and

$$c_n \equiv \cosh(|\beta_n|), \tag{3.18}$$

$$s_n \equiv \sinh(|\beta_n|). \tag{3.19}$$

Using the expression (3.10) to write $\overline{a}(t)$ in terms of the $\{\overline{f}_n(t)\}$—and using (3.17) to evaluate $\langle\Psi|A_n^\dagger A_m|\Psi\rangle$ and $\langle\Psi|A_n^\dagger A_m^\dagger A_p A_q|\Psi\rangle$—from (2.4), we have

$$\overline{G}^{(1)}(t) = \sum_n |\overline{f}_n(t)|^2 s_n^2,$$
$$\overline{G}^{(2)}(t_1, t_2) = \overline{G}^{(2)}_{\mathrm{coh}}(t_1, t_2) + \overline{G}^{(2)}_{\mathrm{incoh}}(t_1, t_2), \tag{3.20}$$

where

$$\overline{G}^{(2)}_{\mathrm{coh}}(t_1, t_2) = \left|\sum_n s_n c_n \overline{f}_n(t_2)\overline{f}_n(t_1)\right|^2, \tag{3.21a}$$

$$\overline{G}^{(2)}_{\mathrm{incoh}}(t_1, t_2) = \frac{1}{2}\sum_{n,m} |s_n s_m [\overline{f}_n(t_1)\overline{f}_m(t_2) + \overline{f}_n(t_2)\overline{f}_m(t_1)]|^2, \tag{3.21b}$$

and the average photon number is

$$N_{\mathrm{pulse}} = \sum_n s_n^2. \tag{3.22}$$

Of the two contributions to $\overline{G}^{(2)}(t_1, t_2)$, the "coherent" term $\overline{G}^{(2)}_{\mathrm{coh}}(t_1, t_2)$ [20], which involves the square of a sum, is the generalization to a squeezed state of the term $\overline{G}^{(2)}(t_1, t_2)$ for the two-photon state (3.12), and the only term that survives in $\overline{G}^{(2)}(t_1, t_2)$ in the limit $|\beta| \ll 1$, cf. (3.14). The "incoherent" term $\overline{G}^{(2)}_{\mathrm{incoh}}(t_1, t_2)$ [20] involves the sum of squares, and will only be significant at larger values of $|\beta|$. Note that the corresponding expressions for $G^{(1)}(\omega)$ and $G^{(2)}(\omega_1, \omega_2)$ take the same form as Eq. (3.20), with $\overline{f}_n$ replaced by f_n, t_1 by ω_1, etc.

A. Example 1: The double Gaussian

A simple model for the joint amplitude is a double-Gaussian function,

$$\gamma(\omega_1, \omega_2) = \sqrt{\frac{1}{\pi\sigma_p\sigma_c}} e^{-\frac{(\omega_1-\omega_2)^2}{4\sigma_c^2}} e^{-\frac{(\omega_1+\omega_2)^2}{4\sigma_p^2}}, \tag{3.23a}$$

$$\overline{\gamma}(t_1, t_2) = \sqrt{\frac{\sigma_p\sigma_c}{\pi}} e^{-\frac{\sigma_c^2(t_1-t_2)^2}{4}} e^{-\frac{\sigma_p^2(t_1+t_2)^2}{4}}, \tag{3.23b}$$

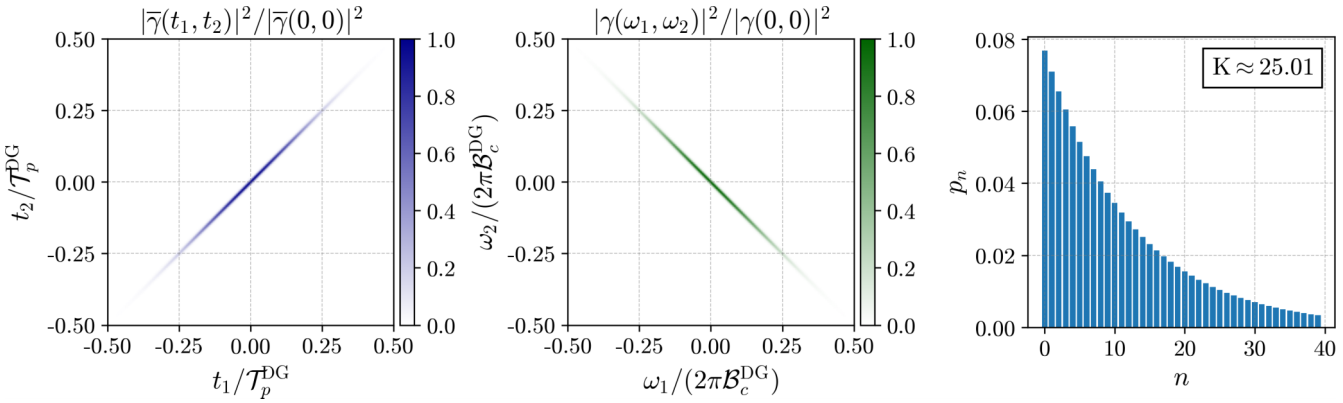

FIG. 2. For the double-Gaussian, from left to right we plot the joint temporal intensity divided by its maximum value with the axes normalized by $\mathcal{T}_p^{\rm DG}$, the joint spectral intensity divided by its maximum value with the axes normalized by $2\pi\mathcal{B}_c^{\rm DG}$, and the Schmidt amplitudes p_n up to $n = 39$.

where σ_p and σ_c are the two parameters. The Schmidt modes are harmonic-oscillator wave functions. This can be seen by noting that the reduced density operator of "particle 1" is equal to the density operator of a harmonic oscillator in thermal equilibrium; its eigenfunctions are the Schmidt modes, and they are obviously the harmonic-oscillator wave functions. The details can be worked out from this, or more mathematically from the Mehler kernel [21,22]. For $\sigma_c \geqslant \sigma_p$, the Schmidt decompositions are given by (3.1), with

$$\gamma(\omega_1,\omega_2) = \sum_{n\geqslant 0} \sqrt{p_n}\mathcal{H}_n(\omega_1)\mathcal{H}_n(\omega_2), \tag{3.24a}$$

$$\overline{\gamma}(t_1,t_2) = \sum_{n\geqslant 0} \sqrt{p_n}\overline{\mathcal{H}}_n(t_1)\overline{\mathcal{H}}_n(t_2), \tag{3.24b}$$

and

$$p_n = \frac{4\sigma_c\sigma_p}{(\sigma_c+\sigma_p)^2}\left(\frac{\sigma_c-\sigma_p}{\sigma_c+\sigma_p}\right)^{2n}, \tag{3.25}$$

with a Schmidt number

$$K = \frac{\sigma_c^2+\sigma_p^2}{2\sigma_c\sigma_p}. \tag{3.26}$$

Here $\overline{f}_n(t) = \overline{\mathcal{H}}_n(t)$, where

$$\overline{\mathcal{H}}_n(t) = \frac{H_n\left(\frac{t}{t_0}\right)e^{-t^2/(2t_0^2)}}{\sqrt{2^n n!\pi^{1/2}t_0}}, \tag{3.27}$$

with $H_n(x)$ the Hermite polynomials, is the standard coordinate-representation harmonic-oscillator energy eigenfunction, but with t playing the role of x and

$$t_0 \equiv \sqrt{\frac{1}{\sigma_p\sigma_c}} \tag{3.28}$$

playing the role of a reference length x_0 that is often introduced [23]. $f_n(\omega) = \mathcal{H}_n(\omega)$, where

$$\mathcal{H}_n(\omega) = (-i)^n\sqrt{\frac{t_0}{2^n n!\pi^{1/2}}}H_n(\omega t_0)e^{-\omega^2 t_0^2/2} \tag{3.29}$$

is the standard momentum-representation harmonic-oscillator energy eigenfunction [23], with ω playing the role of p.

In Fig. 2 we plot the joint intensities $|\overline{\gamma}(t_1,t_2)|^2$ and $|\gamma(\omega_1,\omega_2)|^2$ for $\sigma_c/\sigma_p = 50$, as well as the Schmidt weights p_n as a function of n. For $\sigma_c \gg \sigma_p$, the Schmidt number (3.26) is approximately given by $K \approx \sigma_c/(2\sigma_p) = 25$, indeed we find numerically that $K_{\rm DG} = 25.01$. The joint intensities in Fig. 2 vary over the widths $\mathcal{T}_p^{\rm DG}$ and $\mathcal{B}_c^{\rm DG}$ which we set to be

$$\mathcal{T}_p^{\rm DG} = \frac{a}{\sqrt{2}\sigma_p}, \quad \mathcal{B}_c = \frac{a}{2\pi}\frac{\sigma_c}{\sqrt{2}}, \quad \mathcal{T}_c^{\rm DG} = \frac{2\pi\sqrt{2}}{a\sigma_c}, \tag{3.30}$$

and choose $a = 2\sqrt{2\pi}$ for convenience. This choice of a is large enough that the joint temporal and spectral amplitudes can essentially be taken to be confined within the ranges of $\mathcal{T}_p^{\rm DG}$ and $\mathcal{B}_c^{\rm DG}$, respectively, as can be gleaned from Fig. 2 and will in fact be confirmed by our calculations in later sections. Then the effective Schmidt number is

$$\mathcal{K}_{\rm DG} = \frac{a^2}{2\pi}\frac{\sigma_c}{2\sigma_p} \approx 4K_{\rm DG} = 100. \tag{3.31}$$

To illustrate the behavior of the photon statistics for a large range of photon numbers, we consider the three values of $\beta = 0.1$, 5, and 10, corresponding to $|\beta|/\sqrt{\mathcal{K}_{\rm DG}} = 0.01$, 0.5, 1, and so ranging from weak to moderate squeezing. We dedicate Sec. VIII to the discussion of the strongly squeezed limit.

In Fig. 3 we plot $\overline{G}^{(1)}(t)$ for the three values of β. The expectation value of the number of photons is determined by (3.22), and for $\beta = 0.1$, 5, and 10 we have, respectively, $N_{\rm pulse} \approx 0.01$, 35, and 383; we take an effective photon flux (photons per unit time) to be given by $\Phi = N_{\rm pulse}/\mathcal{T}_p^{\rm DG}$. We also plot the contribution to each $\overline{G}^{(1)}(t)$ from a number of the Schmidt modes [see (3.20)]. For each value of β, the photon density at any particular time t involves contributions from many Schmidt modes, and we cannot associate it with one or even a few Schmidt modes. Clearly as β increases the contribution from the $n = 0$ Schmidt mode increases and the shape of the photon density narrows. This occurs because the scaling of each contribution with $|\beta_n|$ is nonlinear and depends on the quantities c_n and s_n (3.18); since for the double-Gaussian the Schmidt amplitudes p_n decrease as n increases, $|\beta_0|$ has the largest contribution. This behavior suggests that in the strongly squeezed limit the photon statistics

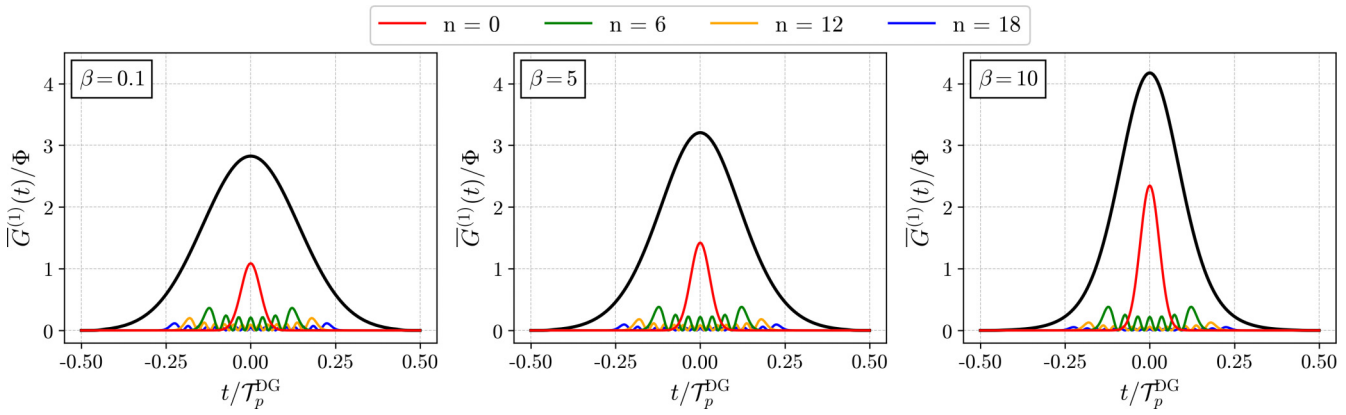

FIG. 3. For the double-Gaussian, from left to right we plot $\overline{G}^{(1)}(t)/\Phi$ and a few contributions from different Schmidt modes in Eq. (3.20) with the horizontal axis normalized by $\mathcal{T}_p^{\mathrm{DG}}$ for $\beta = 0.1$, 5, and 10. In each plot the $n = 0$ term is the largest Schmidt mode contribution and they get smaller as n increases.

can be well approximated by the first few Schmidt modes, a point to which we return in Sec. VIII.

In Fig. 4 we turn to $\overline{G}^{(2)}(t_1, t_2)$ with again the three values of β considered above. In the top row we show this function for the different values of β; at low β the result is proportional to the square of the absolute value of the joint temporal amplitude [see Fig. 2, Eq. (3.14)], while for larger β there are significant corrections to this. In the bottom panel we plot $\overline{G}^{(2)}(t/2, -t/2)$, which corresponds to moving along a diagonal that runs from the upper-left to the lower-right of the plots in the first row; we give the coherent and incoherent contributions separately.

The situation here is of course more complicated than that for $\overline{G}^{(1)}(t)$, because the expression (3.20) for $\overline{G}^{(2)}(t_1, t_2)$ is more complicated than a simple sum over contributions from the individual Schmidt modes. But we see that at least in the weak squeezing regime the coherent contribution to $\overline{G}^{(2)}(t/2, -t/2)$ dominates, and it is nonzero only over a range of t much less than the range of t over which the individual Schmidt modes are nonzero; clearly the interference terms between the different Schmidt modes in (3.20) play a critical role in the result for $\overline{G}^{(2)}(t_1, t_2)$.

Furthermore, the incoherent contribution at $\beta = 5$ has a structure that consists partly of a broad background and partly

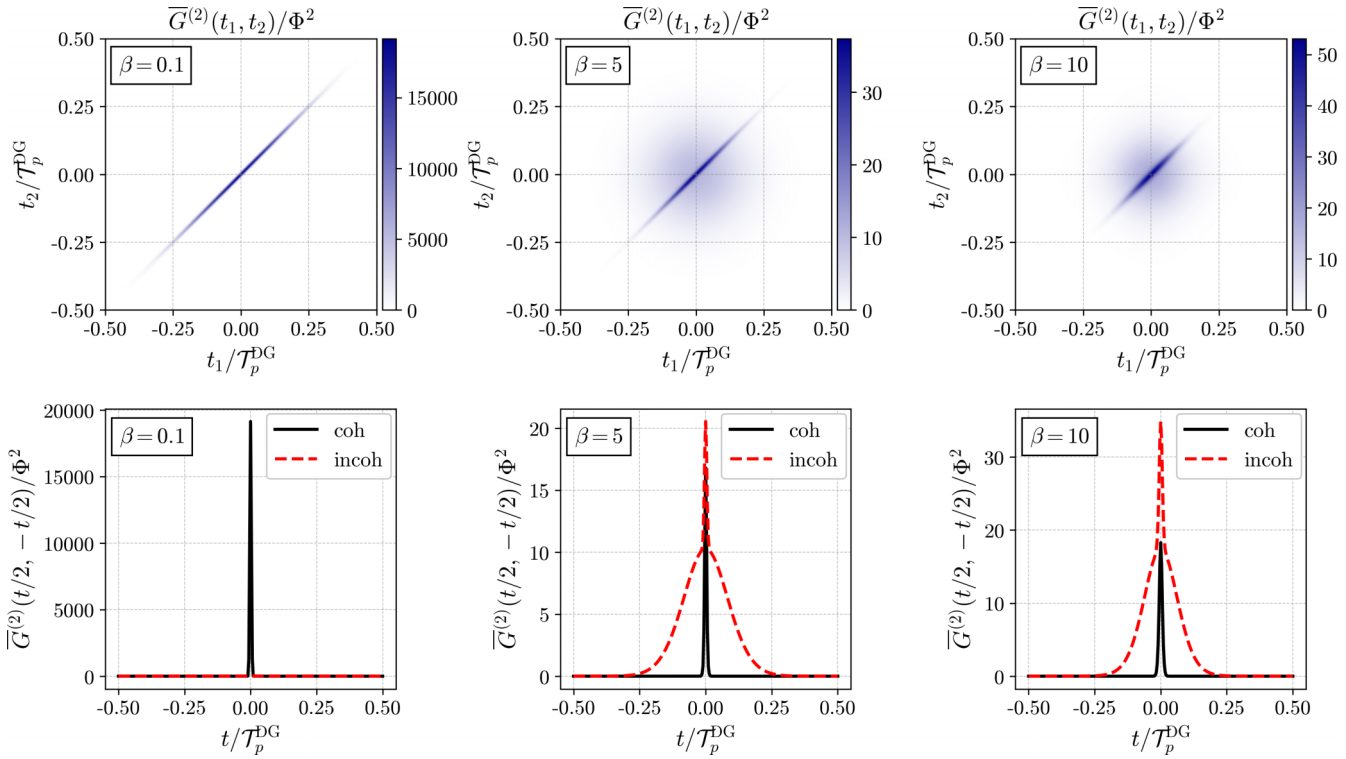

FIG. 4. For the double Gaussian, from left to right we plot $\overline{G}^{(2)}(t_1, t_2)/\Phi^2$ (top) and the coherent and incoherent contribution to $\overline{G}^{(2)}(t/2, -t/2)/\Phi^2$ (bottom) with the axes normalized by $\mathcal{T}_p^{\mathrm{DG}}$ for $\beta = 0.1$, 5, and 10.

of a contribution that mirrors the coherent contribution. Now note that the expression (3.21) for $\overline{G}^{(2)}_{\rm incoh}(t_1,t_2)$ can also be very generally written as

$$\overline{G}^{(2)}_{\rm incoh}(t_1,t_2)=\overline{G}^{(1)}(t_1)\overline{G}^{(1)}(t_2)+|\overline{G}^{(1)}(t_1,t_2)|^2, \tag{3.32}$$

and the broad background in $\overline{G}^{(2)}_{\rm incoh}(t/2,-t/2)$ can be understood as arising from the first term on the right-hand-side. The contribution that mirrors the coherent contribution can be understood as arising from the second term, and in fact it is absent if we consider nondegenerate squeezed light, where signal and idler frequencies are well separated with different center frequencies [24]. The corresponding contribution to $G^{(2)}_{\rm incoh}(\omega_1,\omega_2)$ is often discussed and referred to as the "autocorrelation" [25]. In any case, clearly the different features of $\overline{G}^{(2)}(t/2,-t/2)$ certainly do not follow in any simple way from the features of individual Schmidt modes, but arise from the interference of many of these modes.

As β increases, the range of $\overline{G}^{(2)}(t,t)$ narrows, as does the range of the photon density. However, the coherent and incoherent contribution along $\overline{G}^{(2)}(t/2,-t/2)$ broaden. Thus as the squeezing parameter is increased, the photon statistics begin to look uncorrelated. This behavior matches that of the photon density, in that as β increases fewer Schmidt modes are important in calculating the correlation functions. We also note that the incoherent contribution is approximately twice the coherent contribution, a point to which we return to in Sec. VIII.

While there are many features of interest here, we emphasize that both the value of $\overline{G}^{(1)}(t)$ at a particular t, and that of $\overline{G}^{(2)}(t_1,t_2)$ at a particular t_1 and t_2, receive contributions from *many* of the Schmidt modes. The same holds for the corresponding functions $G^{(1)}(\omega)$ and $G^{(2)}(\omega_1,\omega_2)$. The structure of the Schmidt modes themselves, in and of itself, does not help us understand the structure of the correlation functions.

B. Example 2: The sinc hat

This difference between the features of the Schmidt modes and the features of $\overline{G}^{(1)}(t)$ and $\overline{G}^{(2)}(t_1,t_2)$ is not specific to the double-Gaussian joint amplitude. Consider another form,

$$\gamma(\omega_1,\omega_2)=\alpha(\omega_1+\omega_2)\phi\left(\frac{\omega_1-\omega_2}{2}\right), \tag{3.33}$$

$$\overline{\gamma}(t_1,t_2)=\overline{\alpha}\left(\frac{t_1+t_2}{2}\right)\overline{\phi}(t_1-t_2), \tag{3.34}$$

where

$$\alpha(\omega)=\frac{1}{\sqrt{\Omega_p}}\mathrm{sinc}\left(\frac{\pi\omega}{\Omega_p}\right), \tag{3.35}$$

$$\phi(\omega)=\frac{1}{\sqrt{\Omega_c}}\ \text{for}\ -\frac{\Omega_c}{2}\leqslant\omega\leqslant\frac{\Omega_c}{2}=0\ \text{otherwise} \tag{3.36}$$

$$\bar{\alpha}(t)=\frac{1}{\sqrt{T_p}}\ \text{for}\ -\frac{T_p}{2}\leqslant t\leqslant\frac{T_p}{2}=0\ \text{otherwise}, \tag{3.37}$$

$$\overline{\phi}(t)=\frac{1}{\sqrt{T_c}}\mathrm{sinc}\left(\frac{\pi t}{T_c}\right), \tag{3.38}$$

with $T_p=2\pi/\Omega_p$ and $T_c=2\pi/\Omega_c$, and as usual $\alpha(\omega)$, $\overline{\alpha}(t)$ and $\phi(\omega)$, $\overline{\phi}(t)$, are Fourier transform pairs [cf. (3.2)]. Since both $\gamma(\omega_1,\omega_2)$ and $\overline{\gamma}(t_1,t_2)$ are products of a "sinc" function and "top-hat" function we refer to this example as the "sinc-hat" joint amplitude.

For the sinc-hat joint amplitude, the Schmidt modes must be found numerically. In Fig. 5 we plot the joint intensities $|\overline{\gamma}(t_1,t_2)|^2$ and $|\gamma(\omega_1,\omega_2)|^2$, as well as the Schmidt weights p_n as a function of n, for $T_p/T_c=24$. We see below that for large T_p/T_c we have $K\approx T_p/T_c$, and indeed here we numerically find $K_{\rm SH}=24.78$.

Evaluating $\overline{\gamma}(t_1,t_2)$ along the line $t_1=t_2$ those variables range from $-T_p/2$ to $T_p/2$, and similarly along $\omega_1=-\omega_2$, $\gamma(\omega_1,\omega_2)$ ranges from $-\Omega_c/2$ to $\Omega_c/2$. Naïvely one would guess that we should set $\mathcal{T}_p^{\rm SH}\to T_p$ and $2\pi\mathcal{B}_c^{\rm SH}\to\Omega_c$ or equivalently $\mathcal{T}_c^{\rm SH}\to T_c$, however, this is only the range of t along the *diagonal* (or antidiagonal in frequency) and the joint amplitude exists beyond it. In Appendix B we show that

$$\mathcal{T}_p^{\rm SH}=T_p+\frac{T_c}{2}, \tag{3.39}$$

and

$$\mathcal{B}_c^{\rm SH}=\frac{\Omega_c}{2\pi}+\frac{1}{2}\frac{\Omega_p}{2\pi},\quad \mathcal{T}_c^{\rm SH}=\frac{T_cT_p}{T_p+T_c/2}. \tag{3.40}$$

This leads to an effective Schmidt number

$$\mathcal{K}_{\rm SH}=\frac{\left(T_p+\frac{T_c}{2}\right)^2}{T_pT_c}=1+\frac{T_p}{T_c}+\frac{T_c}{4T_p}, \tag{3.41}$$

and for $T_p/T_c=24$, $\mathcal{K}_{\rm SH}\approx 25$ to very good approximation. In Sec. V we discuss this near equality.

In Fig. 6 we plot $\overline{G}^{(1)}(t)$ for the same three values of β used in the example above, corresponding here to photon numbers $N_{\rm pulse}\approx 0.01$, 35, and 335; we take an effective photon flux to be given by $\Phi=N_{\rm pulse}/\mathcal{T}_p^{\rm SH}$. Then for the three values of β we have $|\beta|/\sqrt{\mathcal{K}_{\rm SH}}\approx 0.02$, 1, 2, which again corresponds to weak to moderate squeezing. In Fig. 6 we also include a few of the contributions from the Schmidt modes; we see that typically those contributions range over the whole duration of the pulse, analogous to what we saw for the double-Gaussian example. In the top row of Fig. 7 we plot $\overline{G}^{(2)}(t_1,t_2)$ for the indicated values of $|\beta|$, and in the bottom row the coherent and incoherent contributions to $\overline{G}^{(2)}(t/2,-t/2)$. Again, the range over which the individual Schmidt modes extend is much larger than these contributions, and so they must be understood as arising from a number of interfering Schmidt modes.

So just as for squeezed states described by the double-Gaussian joint amplitude, the behavior of correlation functions of squeezed states described by the sinc-hat joint amplitude cannot be linked in a simple way to the behavior of the individual Schmidt modes. Quantitatively there are differences between the correlation functions resulting from those two joint amplitudes: The relative amplitudes of the Schmidt modes of a given n in Fig. 6 (sinc-hat joint amplitude) are roughly independent of $|\beta|$, while the relative amplitudes in of those in Fig. 3 (double Gaussian) are not, and the two parts of the structure of $\overline{G}^{(2)}_{\rm incoh}(t/2,-t/2)$ we noticed for the double-Gaussian joint amplitude are even more pronounced and persist to larger β than they did for that amplitude. These differences arise because the Schmidt weights of the sinc-hat joint amplitude are nearly identical in the $T_p/T_c\gg 1$ limit

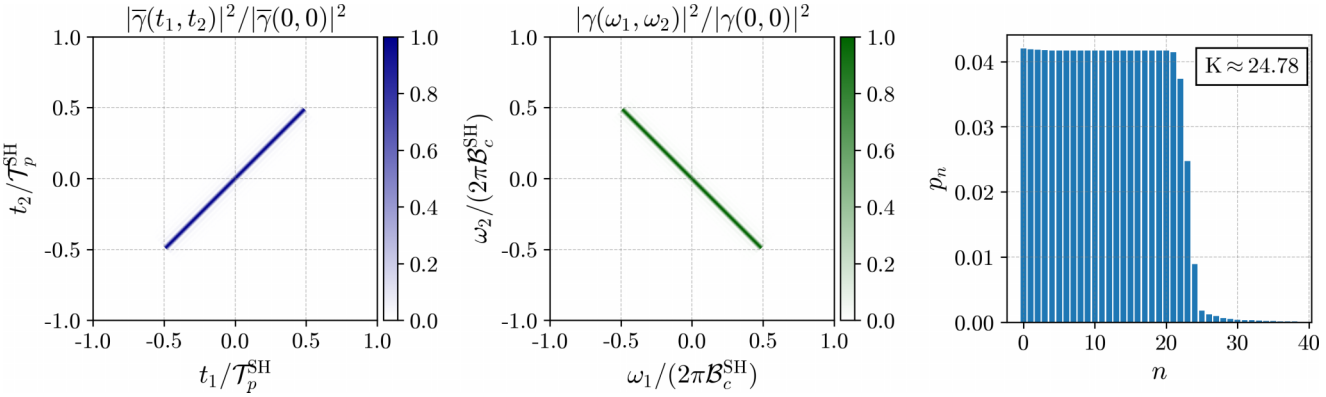

FIG. 5. For the sinc hat, from left to right we plot the joint temporal intensity divided by its maximum value with the axes normalized by $\mathcal{T}_p^{\mathrm{SH}}$, the joint spectral intensity divided by its maximum value with the axes normalized by $2\pi\mathcal{B}_c^{\mathrm{SH}}$, and the Schmidt amplitudes p_n up to $n = 39$.

(see Fig. 5), and thus each Schmidt mode contributes roughly equally to the resulting correlation functions even in the large-β limit.

To see how this near-degeneracy in the Schmidt weights arises, note that in general the Schmidt modes $\overline{f}_n(t)$ of a joint temporal amplitude $\overline{\gamma}(t_1,t_2)$ are eigenfunctions of the operator

$$M(t_1,t_2) \equiv \int \overline{\gamma}(t_1,t)\overline{\gamma}^*(t,t_2)dt, \tag{3.42}$$

with eigenvalue p_n,

$$\int M(t_1,t_2)\overline{f}_n(t_2)dt_2 = p_n\overline{f}_n(t_1), \tag{3.43}$$

which follows immediately from constructing $M(t_1,t_2)$ using (3.1). Now for $T_p/T_c \gg 1$ we can approximate the joint temporal amplitude (3.34) as

$$\overline{\gamma}(t_1,t_2) = \overline{\alpha}\left(\frac{t_1+t_2}{2}\right)\overline{\phi}(t_1-t_2) \tag{3.44}$$

$$\approx \overline{\alpha}(t_1)\overline{\phi}(t_1-t_2), \tag{3.45}$$

and so

$$\begin{aligned} M(t_1,t_2) &\approx \int \overline{\alpha}(t_1)\overline{\alpha}(t_2)\overline{\phi}(t_1-t)\overline{\phi}(t-t_2)dt \\ &= \sqrt{T_c}\overline{\alpha}(t_1)\overline{\alpha}(t_2)\overline{\phi}(t_1-t_2) \\ &= \frac{T_c}{T_p}\frac{\sin\left[\frac{\Omega_c}{2}(t_1-t_2)\right]}{\pi(t_1-t_2)} \quad \text{for} -\frac{T_p}{2} \leqslant t_1,\ t_2 \leqslant \frac{T_p}{2} \\ &= 0 \text{ otherwise.} \end{aligned} \tag{3.46}$$

For specified $\Omega_c T_p/4$, the functions $\overline{\psi}_n(t')$ satisfying the eigenvalue equation

$$\int_{-T_p/2}^{T_p/2} \frac{\sin\left[\frac{\Omega_c}{2}(t-t')\right]}{\pi(t-t')}\overline{\psi}_n(t')dt' = \lambda_n\overline{\psi}_n(t), \tag{3.47}$$

with the label $n = 0, 1, \ldots$, are related to the angular prolate spheroidal functions [13–15,26,27], and are defined with the normalization

$$\int_{-\infty}^{\infty} |\overline{\psi}_n(t)|^2 dt = 1. \tag{3.48}$$

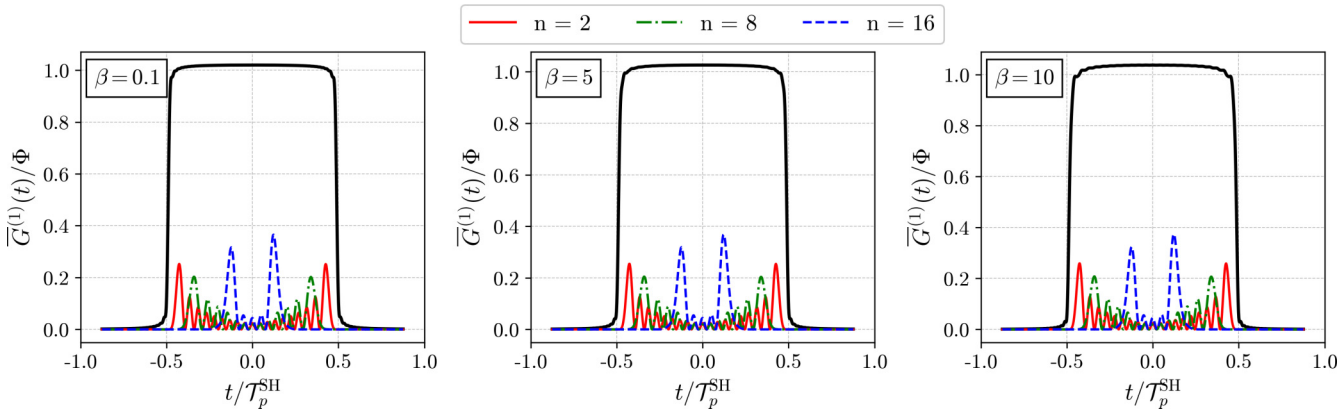

FIG. 6. For the sinc hat, from left to right we plot $\overline{G}^{(1)}(t)/\Phi$ and a few contributions from different Schmidt modes in Eq. (3.20) with the horizontal axis normalized by $\mathcal{T}_p^{\mathrm{SH}}$ for $\beta = 0.1$, 5, and 10.

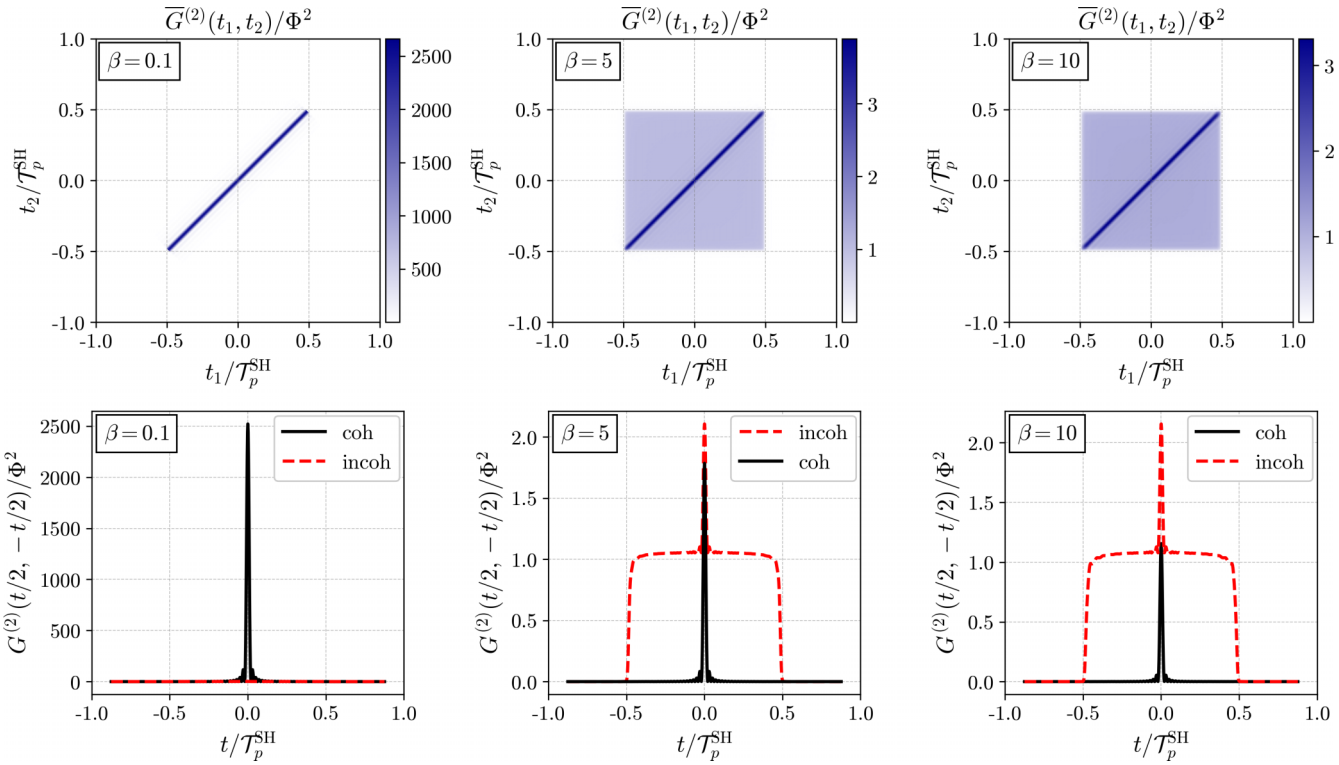

FIG. 7. For the sinc hat, from left to right we plot $\overline{G}^{(2)}(t_1,t_2)/\Phi^2$ (top) and the coherent and incoherent contribution to $\overline{G}^{(2)}(t/2,-t/2)/\Phi^2$ (bottom) with the axes normalized by $\mathcal{T}_p^{\rm SH}$ for $\beta=0.1$, 5, and 10.

The λ_n are close to unity for small n, and fall off quickly to zero for $n > T_p/T_c \equiv K_{\rm app}$; we approximate them as equal to unity for $n < K_{\rm app}$ and zero for $n \geqslant K_{\rm app}$. So within the approximation (3.46) we have

$$\int M(t_1,t_2)\overline{\psi}_n(t_2)dt_2 \to \frac{T_c}{T_p}\lambda_n\overline{\psi}_n(t_1), \tag{3.49}$$

and comparing with (3.43) we can identify

$$\overline{f}_n(t) \to \overline{\psi}_n(t), \quad p_n \to \sqrt{\frac{T_c}{T_p}} = \frac{1}{\sqrt{K_{\rm app}}}, \tag{3.50}$$

for $n < K_{\rm app}$. That is, the Schmidt modes are approximately given by the angular prolate spheroidal functions, and so

$$\overline{\gamma}(t_1,t_2) \to \sum_{n=0}^{K_{\rm app}-1}\sqrt{\frac{T_c}{T_p}}\overline{\psi}_n(t_1)\overline{\psi}_n(t_2), \tag{3.51}$$

exhibiting a huge degeneracy of Schmidt mode amplitudes, with a approximate Schmidt number (3.3) $K_{\rm app} = T_p/T_c \approx K_{\rm SH}$, as expected.

While (3.50) and (3.51) are only approximate (cf. Fig. 5), they do indicate that in the limit $T_p/T_c \gg 1$, which for the sinc-hat function we can characterize as the "long-pulse" limit, a large near-degeneracy of Schmidt mode amplitudes can be expected. Like the exact Schmidt modes, the angular prolate spheroidal functions range over the whole duration T_p associated with the joint temporal amplitude. However, were the degeneracy exact it would imply that the Schmidt modes are not unique and that various superpositions of them could be constructed. While this freedom is only approximate for near degeneracy, we see below that we can use it to deconstruct the joint amplitude in a different way by constructing approximate Schmidt modes that more explicitly reflect the properties of the light.

IV. AN APPROXIMATE SCHMIDT DECOMPOSITION

Focusing on the sinc-hat model (3.33) and (3.35) in the limit where $T_p \gg T_c$ and $\mathcal{T}_p^{\rm SH} \to T_p$ and $\mathcal{T}_p^{\rm SH} \to T_c$, note that while in the second row of Fig. 7 we have plotted $\overline{G}^{(2)}(\bar{t}+t/2,\bar{t}-t/2)$ for $\bar{t}=0$, we would expect such plots to be similar for values of $\bar{t} \equiv (t_1+t_2)/2$ ranging over the pulse duration, especially in the limit of small $|\beta|$. In that limit $\overline{G}^{(2)}(t_1,t_2)$ reflects the behavior of the joint temporal amplitude itself [see (3.14)], and generally $\overline{G}^{(2)}(\bar{t}+t/2,\bar{t}-t/2)$ will be nonzero for t ranging on a timescale of the order of T_c; in our example of Fig. 7 that is $T_p/24$. This suggests that if we want to capture the behavior of the joint temporal amplitude as a function of (t_1-t_2) in each of the terms of an approximate Schmidt decomposition, rather than just when they are all used together, we should look for approximate Schmidt modes that vary over a range of T_c. Since, roughly speaking, frequency components between $-\Omega_c/2$ and $\Omega_c/2$ are then available, one such function can easily be constructed by taking

$$\overline{\eta}(t) \equiv \frac{1}{\sqrt{\Omega_c}}\int_{-\Omega_c/2}^{\Omega_c/2}\frac{d\omega}{\sqrt{2\pi}}e^{-i\omega t} = \frac{1}{\sqrt{T_c}}\mathrm{sinc}\left(\frac{\pi t}{T_c}\right), \tag{4.1}$$

where the prefactor is chosen so the function is normalized [see (4.3) below]. However, we need a set of such functions

that are orthonormal to serve as approximate Schmidt functions; the way to do that is to take the set of functions

$$\overline{\eta}_n(t) = \overline{\eta}(t - nT_c), \tag{4.2}$$

where n is an integer, for then we have

$$\int \overline{\eta}_n^*(t)\overline{\eta}_m(t)dt = \delta_{nm}. \tag{4.3}$$

Note that were time variables replaced by position variables, then the $\{\overline{\eta}_n(t)\}$ would correspond to a set of Wannier functions of the lowest band in a one-dimensional crystal of lattice spacing corresponding to T_c, when the potential of the lattice is neglected ("empty-lattice approximation") [28]. We can then seek an approximate expression $\overline{\gamma}_{\text{app}}(t_1, t_2)$ for the sinc-hat joint temporal amplitude $\overline{\gamma}(t_1, t_2)$ of (3.33) by writing

$$\overline{\gamma}_{\text{app}}(t_1, t_2) = T_c \sum_n u(nT_c)\overline{\eta}_n(t_1)\overline{\eta}_n(t_2), \tag{4.4}$$

which clearly takes the form of a Schmidt decomposition, with $u(nT_c)$ playing the role of an "envelope function"; $\gamma_{\text{app}}(t_1, t_2)$ is normalized as the exact function (3.33) as long as

$$T_c^2 \sum_n |u(nT_c)|^2 = 1. \tag{4.5}$$

The introduction of the functions $\overline{\eta}_n(t)$ allows us to work with "pseudo-Schmidt" modes that are mutually orthogonal (like the real Schmidt modes), but are localized in time and range over different center times. We refer to the approximate Schmidt decomposition (4.4) we construct as the "pseudo-Schmidt decomposition."

Taking the Fourier transform of the approximate joint temporal amplitude (4.4) gives the approximate joint spectral amplitude

$$\begin{aligned}\gamma_{\text{app}}(\omega_1, \omega_2) &\equiv \int \frac{dt_1 dt_2}{2\pi} \overline{\gamma}_{\text{app}}(t_1, t_2) e^{i\omega_1 t_1} e^{i\omega_2 t_2} \\ &= \frac{T_c^2}{2\pi} \widehat{u}(\omega_1 + \omega_2) s(\omega_1) s(\omega_2),\end{aligned} \tag{4.6}$$

where

$$\widehat{u}(\omega) \equiv \sum_n u(nT_c) e^{in\omega T_c}, \tag{4.7}$$

and

$$\begin{aligned}s(\omega) &\equiv \frac{1}{\sqrt{T_c}} \int_{-\infty}^{\infty} \overline{\eta}(t) e^{i\omega t} dt = 1 \quad \text{for} -\frac{\Omega_c}{2} < \omega < \frac{\Omega_c}{2} \\ &= 0 \text{ otherwise.}\end{aligned} \tag{4.8}$$

We need to set $\widehat{u}(\omega)$, which satisfies $\widehat{u}(\omega + mT_c) = \widehat{u}(\omega)$ for any integer m. To ensure that $\overline{\gamma}_{\text{app}}(t_1, t_2)$ is a good approximation to $\overline{\gamma}(t_1, t_2)$ for the sinc-hat model, we want $u(nT_c)$ to be independent of n over an appropriate range. Choosing $\mathcal{N}$ to be a large odd integer, we put

$$\begin{aligned}u(nT_c) &= \frac{1}{T_c\sqrt{\mathcal{N}}} \quad \text{for} -\left(\frac{\mathcal{N}-1}{2}\right) \leqslant n \leqslant \left(\frac{\mathcal{N}-1}{2}\right) \\ &= 0 \text{ otherwise.}\end{aligned} \tag{4.9}$$

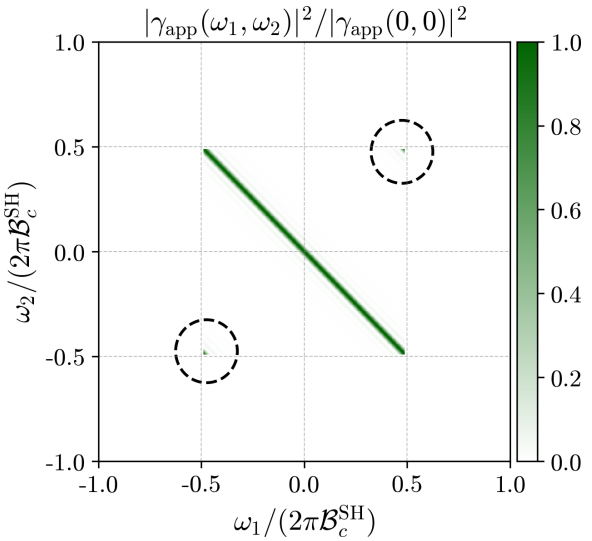

FIG. 8. Plot of the approximate joint spectral intensity divided by its maximum value with the axes normalized by $2\pi\mathcal{B}_c^{\text{SH}}$. The "false" contributions highlighted by the black dashed circles are due to the periodicity of the function $\widehat{u}(\omega)$ with a period T_c; see the discussion in the paragraph above Eq. (4.14).

Then from (4.7) this leads to

$$\widehat{u}(\omega) = \frac{1}{T_c\sqrt{\mathcal{N}}} \frac{\sin\left(\frac{\mathcal{N}\omega T_c}{2}\right)}{\sin\left(\frac{\omega T_c}{2}\right)}. \tag{4.10}$$

Now for the sinc-hat model we want the joint temporal amplitude $\overline{\gamma}(t_1, t_2)$ to be nonvanishing for t_1, t_2 varying from $-T_p/2$ to $T_p/2$. From the approximate form $\overline{\gamma}_{\text{app}}(t_1, t_2)$ that we are trying to construct (4.4), this implies that we should set

$$T_c\left(\frac{\mathcal{N}-1}{2}\right) = \frac{T_p}{2}, \tag{4.11}$$

or

$$\mathcal{N} = 1 + \frac{T_p}{T_c} = \mathcal{K}_{\text{SH}}, \tag{4.12}$$

where the last equality holds to very good approximation when $T_p \gg T_c$. For $T_p \gg T_c$, which is the limit we consider here, we can take $\mathcal{N}$ to be either this or an odd integer close to it. The motivation for calling $\mathcal{K}$ the "effective Schmidt number" is now clear, at least for this joint amplitude; $\mathcal{K}_{\text{SH}}$ is the effective number of pseudo-Schmidt modes required for the decomposition. We can then write (4.10) as

$$\widehat{u}(\omega) = \frac{1}{\sqrt{T_c T_p}} \frac{\sin\left[\frac{\omega}{2}(T_c + T_c)\right]}{\sin\left(\frac{\omega}{2}T_c\right)}. \tag{4.13}$$

Note that with this choice we find $\gamma_{\text{app}}(0,0) = \sqrt{T_c(T_p + T_c)}/(2\pi)$, while for the sinc-hat model we have exactly $\gamma(0,0) = \sqrt{T_c T_p}/(2\pi)$; so for $T_p/T_c \gg 1$, $\gamma_{\text{app}}(0,0)$ is certainly equal to $\gamma(0,0)$ to a good approximation.

In Fig. 8 we plot $|\gamma_{\text{app}}(\omega_1, \omega_2)|^2$ for $T_p/T_c = 24$, taking $\mathcal{N} = \mathcal{K}_{\text{SH}} = 25$. Comparing with the exact plot (middle plot in Fig. 5) we see that there is indeed generally good agreement, with two main differences: First, $\gamma_{\text{app}}(\omega_1, \omega_2)$ is only nonzero for (ω_1, ω_2) satisfying the bandwidth limiting conditions $-\Omega_c/2 \leqslant \omega_1 \leqslant \Omega_c/2$ and $-\Omega_c/2 \leqslant \omega_2 \leqslant \Omega_c/2$, while

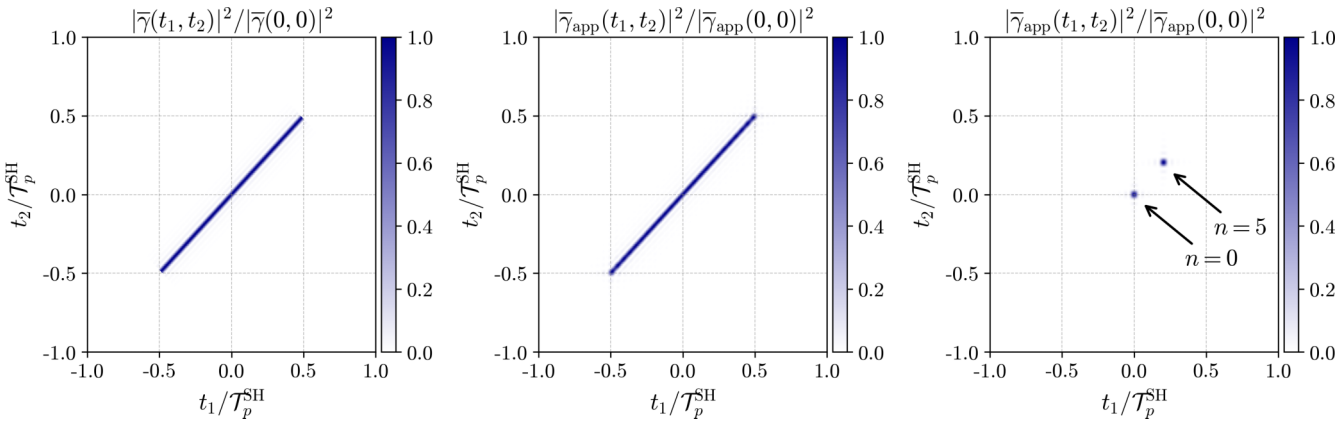

FIG. 9. From left to right we plot the sinc-hat joint temporal intensity divided by its maximum value, the approximate joint temporal intensity divided by its maximum value, and two contributions to the approximate joint temporal intensity divided by its maximum value when $n=0$ and $n=5$ with the axes all normalized by $\mathcal{T}_p^{\rm SH}$.

$\gamma(\omega_1,\omega_2)$ extends beyond that; this is not so apparent in Fig. 5, because outside the bandwidth limiting conditions the true $\gamma(\omega_1,\omega_2)$ is very small. Second, $\gamma_{\rm app}(\omega_1,\omega_2)$ contains "false contributions" near $(\omega_1,\omega_2)=(\Omega_c/2,\Omega_c/2)$ and $(-\Omega_c/2,-\Omega_c/2)$, see the contributions highlighted by the black dashed circles in Fig. 8. This is related to the first difference and arises because the postulated approximate form (4.4) of $\overline{\gamma}_{\rm app}(t_1,t_2)$ involves the function $\widehat{u}(\omega)$ that is periodic in ω with a period $1/T_c$.

We now look at the correlation functions that follow for a squeezed state with the approximate joint temporal amplitude identified here,

$$\overline{\gamma}_{\rm app}(t_1,t_2)=\sum_{n=-\frac{\mathcal{N}-1}{2}}^{\frac{\mathcal{N}-1}{2}}\sqrt{p_n}\overline{\eta}_n(t_1)\overline{\eta}_n(t_2), \tag{4.14}$$

where

$$p_n=\frac{1}{\mathcal{N}}\quad\text{for}\quad -\left(\frac{\mathcal{N}-1}{2}\right)\leqslant n\leqslant\left(\frac{\mathcal{N}-1}{2}\right)$$
$$=0\ \text{otherwise}. \tag{4.15}$$

From this point forward we denote the sums over n leaving the bounds implicit. We plot $|\overline{\gamma}_{\rm app}(t_1,t_2)|^2$ for the sinc-hat model with $T_p/T_c=24$ in the middle diagram of Fig. 9, repeating the exact $|\overline{\gamma}(t_1,t_2)|^2$ for this model in the leftmost diagram; we can see the general level of agreement that might be expected from the results shown in Figs. 5 and 8. In the rightmost plot we show $\overline{\eta}_n(t_1)\overline{\eta}_n(t_2)$ for $n=0$ and $n=5$; all such functions are of course well-localized and from (4.14) we see that the contribution to $\overline{\gamma}_{\rm app}(t_1,t_2)$ from each of these is their product with the (pseudo-) Schmidt weight p_n.

Using the general expressions (3.20) and (3.21) for $\overline{G}^{(1)}(t)$ and $\overline{G}^{(2)}(t_1,t_2)$, we find that for our approximate model (4.14) we have

$$\overline{G}^{(1)}(t)=s^2\sum_n|\overline{\eta}_n(t)|^2,$$
$$\overline{G}^{(2)}(t_1,t_2)=\overline{G}^{(2)}_{\rm coh}(t_1,t_2)+\overline{G}^{(2)}_{\rm incoh}(t_1,t_2), \tag{4.16}$$

where

$$\overline{G}^{(2)}_{\rm coh}(t_1,t_2)=s^2c^2\left|\sum_p\overline{\eta}_p(t_2)\overline{\eta}_p(t_1)\right|^2,$$
$$\overline{G}^{(2)}_{\rm incoh}(t_1,t_2)=\frac{1}{2}s^4\sum_{n,m}|\overline{\eta}_n(t_1)\overline{\eta}_m(t_2)+\overline{\eta}_n(t_2)\overline{\eta}_m(t_1)|^2. \tag{4.17}$$

with

$$s=\sinh\left(\frac{|\beta|}{\sqrt{\mathcal{N}}}\right),\quad c=\cosh\left(\frac{|\beta|}{\sqrt{\mathcal{N}}}\right). \tag{4.18}$$

These are of course the same formulas as for the exact Schmidt modes, except that here s and c are the same for each pseudo-Schmidt mode. But since the pseudo-Schmidt modes are localized over a time of order T_c, we see that this decomposition of $\overline{G}^{(1)}(t)$ identifies contributions from each pseudo-Schmidt mode that are localized in time windows much less than the width of $\overline{G}^{(1)}(t)$, which is on the order of T_p. We show some of these contributions in Fig. 10. Here the range over which n varies indicates the overall range of $\overline{G}^{(1)}(t)$ to very good approximation, and at any given time t the contributions to $\overline{G}^{(1)}(t)$ come from at most a very few of the functions $\overline{\eta}_n(t)$ with nT_c close to t.

At least within the approximate pseudo-Schmidt decomposition we can now justify the use of the condition (3.6) to identify the weak squeezing regime. Since in our example here $\mathcal{N}=\mathcal{K}_{\rm SH}$, the weak squeezing limit can be written as

$$\frac{|\beta|}{\sqrt{\mathcal{N}}}\ll 1, \tag{4.19}$$

the expectation value of the number of photons in any pseudo-Schmidt mode is given by

$$N_{\rm mode}=s^2=\sinh^2\left(\frac{|\beta|}{\sqrt{\mathcal{N}}}\right), \tag{4.20}$$

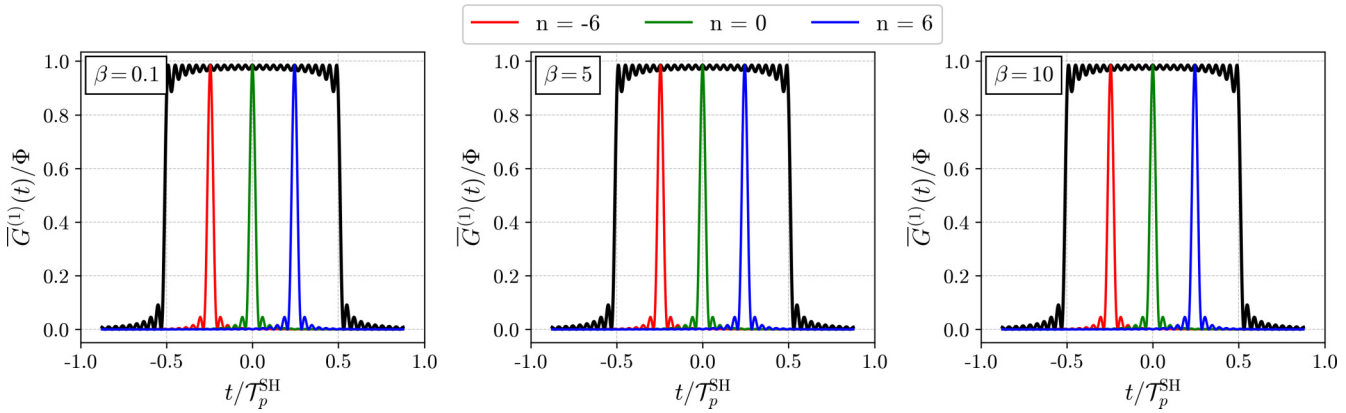

FIG. 10. For the sinc hat calculated from the pseudo-Schmidt decomposition, from left to right we plot $\overline{G}^{(1)}(t)/\Phi$ and a few contributions from different pseudo-Schmidt modes in Eq. (4.16) with the horizontal axis normalized by $\mathcal{T}_p^{\mathrm{SH}}$ for $\beta = 0.1$, 5, and 10. In each plot the $n = -6$ pseudo-Schmidt mode is the leftmost contribution and they move towards to right as n increases.

while the expectation value of the number of photons in the full pulse is

$$N_{\mathrm{pulse}} = \mathcal{N}\sinh^2\left(\frac{|\beta|}{\sqrt{\mathcal{N}}}\right). \tag{4.21}$$

So in the weak squeezing limit (4.19) we have $N_{\mathrm{mode}} \ll 1$; the expected number of photons in any pseudo-Schmidt mode is much less than unity. However, the expected number of photons in the pulse, N_{pulse} can be arbitrarily large; indeed, in the limit of weak squeezing we have $N_{\mathrm{pulse}} \to |\beta|^2$. Very generally, regardless of the level of squeezing, we can understand the cw limit as $|\beta|^2 \to \infty$ and $\mathcal{N} \to \infty$ such that $|\beta|^2/\mathcal{N}$ is a constant.

In Fig. 11 we plot the approximate $\overline{G}^{(2)}(t_1, t_2)$ given by (4.16) and (4.17), and compare with the exact $\overline{G}^{(2)}(t_1, t_2)$ in Fig. 7 for the sinc-hat model; we see very good agreement. Importantly, the decomposition (4.16) and (4.17) of $\overline{G}^{(2)}(t_1, t_2)$ into pseudo-Schmidt modes immediately illustrates the behavior of that function in a way that the decomposition into the exact Schmidt modes does not.

Considering the first plot when $\beta = 0.1$ ($|\beta|/\sqrt{\mathcal{N}} = 0.02$), the dominance of $\overline{G}^{(2)}_{\mathrm{coh}}(t/2, -t/2)$ over $\overline{G}^{(2)}_{\mathrm{incoh}}(t/2, -t/2)$ follows immediately from the prefactors s^2c^2 and s^4 in their expressions (4.17). And in the sum over p in the expression for $\overline{G}^{(2)}_{\mathrm{coh}}(t/2, -t/2)$, of the terms $\overline{\eta}_p(t/2)\overline{\eta}_p(-t/2)$ both $\overline{\eta}_p(t/2)$ and $\overline{\eta}_p(-t/2)$ must be significant for a contribution to be made, which requires p to be close to 0 and $|t| \lesssim T_c$. The same behavior extends for the larger values of β as in the exact sinc-hat Schmidt decomposition. Thus the largest contribution to $\overline{G}^{(2)}(t/2, -t/2)$ when $|t| \lesssim T_c$ comes from only a few terms in the pseudo-Schmidt decomposition, while it involves many terms in the Schmidt decomposition, and their interference.

The expression for $\overline{G}^{(2)}_{\mathrm{incoh}}(t/2, -t/2)$, which in the pseudo-Schmidt decomposition (4.17) involves sums over two indices n and m, contains two types of contributions. In the first, with $m = n$, we get terms that will only be significant if $m = n$ is close to 0 and $|t| \lesssim T_c$, as in the expression for $\overline{G}^{(2)}_{\mathrm{coh}}(t/2, -t/2)$; this gives the contribution to $\overline{G}^{(2)}_{\mathrm{incoh}}(t/2, -t/2)$ that mirrors the form of $\overline{G}^{(2)}_{\mathrm{coh}}(t/2, -t/2)$. This contribution to $\overline{G}^{(2)}_{\mathrm{incoh}}(t/2, -t/2)$, and the term $\overline{G}^{(2)}_{\mathrm{coh}}(t/2, -t/2)$, can thus be seen to arise from pairs of photons, each photon in a pair associated with the same pseudo-Schmidt mode. But the terms with $m \neq n$ can give contributions for t on the order of T_p; they give rise to the broad background, which can be understood as arising from pairs of photons, with the photons in a pair associated with different pseudo-Schmidt modes.

In a similar way one can understand the behavior of $\overline{G}^{(2)}_{\mathrm{coh}}(\bar{t} + t/2, \bar{t} - t/2)$ and $\overline{G}^{(2)}_{\mathrm{incoh}}(\bar{t} + t/2, \bar{t} - t/2)$ for $\bar{t} \neq 0$. Unlike in the decomposition of the joint temporal amplitude in terms of Schmidt modes, the decomposition in terms of pseudo-Schmidt modes immediately reveals the structure of those correlation functions.

And in fact, we can derive an analytic expression for the approximate [(4.16) and (4.17)] $\overline{G}^{(1)}(t)$ and $\overline{G}^{(2)}(t_1, t_2)$ in the cw limit. Noting that

$$\sum_{n=-\infty}^{\infty} \overline{\eta}_n(t_2)\overline{\eta}_n(t_1) = \frac{1}{T_c}\mathrm{sinc}\left(\frac{\pi\ \Delta t}{T_c}\right), \tag{4.22}$$

where $\Delta t \equiv t_2 - t_1$, for t_1 and t_2 in the center of a pulse of duration T_p, when $T_p \to \infty$ we can write

$$\overline{G}^{(2)}_{\mathrm{coh}}(t_1, t_2) \to \frac{s^2c^2}{T_c^2}\mathrm{sinc}^2\left(\frac{\pi\ \Delta t}{T_c}\right), \tag{4.23}$$

while

$$\overline{G}^{(1)}(t) \to \frac{s^2}{T_c}. \tag{4.24}$$

Finally, noting that

$$\overline{G}^{(1)}(t_1, t_2) = s^2\sum_n \overline{\eta}_n(t_2)\overline{\eta}_n(t_1) \to \frac{s^2}{T_c}\mathrm{sinc}\left(\frac{\pi\ \Delta t}{T_c}\right), \tag{4.25}$$

then with the alternate form of $\overline{G}^{(2)}_{\mathrm{incoh}}$ [see Eq. (3.32)] we have

$$\overline{G}^{(2)}_{\mathrm{incoh}}(t_1, t_2) \to \frac{s^4}{T_c^2}\left[1 + \mathrm{sinc}^2\left(\frac{\pi\ \Delta t}{T_c}\right)\right], \tag{4.26}$$

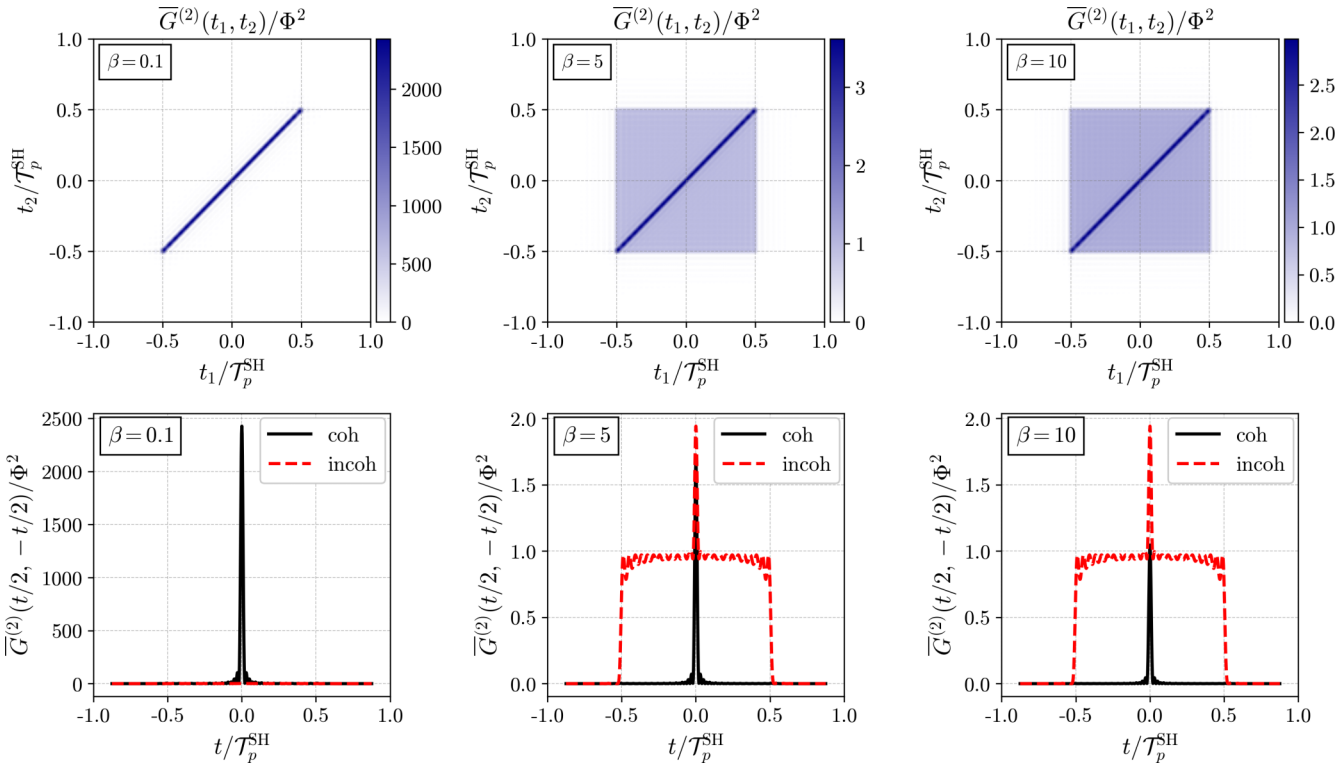

FIG. 11. For the sinc hat calculated from the pseudo-Schmidt decomposition, from left to right we plot $\overline{G}^{(2)}(t_1,t_2)/\Phi^2$ (top) and the coherent and incoherent contribution to $\overline{G}^{(2)}(t/2,-t/2)/\Phi^2$ (bottom) with the axes normalized by $\mathcal{T}_p^{\mathrm{SH}}$ for $\beta=0.1$, 5, and 10.

and so

$$\overline{G}^{(2)}(t_1,t_2)\to\overline{G}^{(2)}(\Delta t) = \frac{s^2c^2}{T_c^2}\mathrm{sinc}^2\left(\frac{\pi\ \Delta t}{T_c}\right)+\frac{s^4}{T_c^2}\left[1+\mathrm{sinc}^2\left(\frac{\pi\ \Delta t}{T_c}\right)\right]. \tag{4.27}$$

We plot this in Fig. 12 (cf. Figs. 7 and 11).

From the above discussion, we are motivated to think of $\overline{G}^{(2)}(\bar{t}+t/2,\bar{t}-t/2)$ for times $|t|\lesssim T_c$ when $n=m$ as arising from one pseudo-Schmidt mode at a time, as it were, on a "mode-by-mode" basis. Since the pseudo-Schmidt decomposition is valid only for joint amplitudes such as the sinc-hat joint amplitude, where there is a high degeneracy in the Schmidt weights, we give this calculation in Appendix F.

V. THE WHITTAKER-SHANNON DECOMPOSITION

The ability to construct approximate pseudo-Schmidt modes for the sinc-hat joint amplitude that are "localized" in time [$\overline{\eta}(t)$, see (4.1)] relied on the near-degeneracy of the Schmidt modes. But this cannot be generally expected; see,

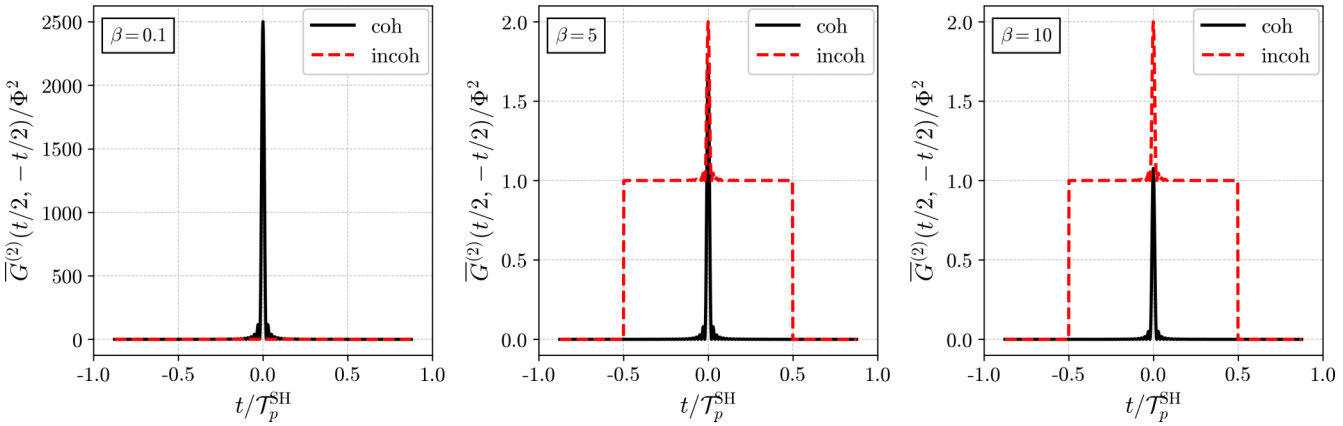

FIG. 12. Using the analytical result (4.27), from left to right we plot $\overline{G}^{(2)}(t_1,t_2)/\Phi^2$ (top) and the coherent and incoherent contribution to $\overline{G}^{(2)}(t/2,-t/2)/\Phi^2$ (bottom) with the axes normalized by $\mathcal{T}_p^{\mathrm{SH}}$ for $\beta=0.1$, 5, and 10.

e.g., Fig. 2 for the Schmidt amplitudes of the double-Gaussian joint amplitude, where there is no such near-degeneracy. Nonetheless, the recognition used above that only a finite frequency range—there from $-\Omega_c/2$ to $\Omega_c/2$—is important can be employed to construct an extension of a Schmidt decomposition more generally; it shares the feature of the pseudo-Schmidt decomposition above that the functions involved are localized in time.

We consider a joint spectral amplitude $\gamma(\omega_1, \omega_2)$ to be bandwidth limited, in that at least approximately it can be taken to be nonzero only for $-\Omega/2 \leqslant \omega_1, \omega_2 \leqslant \Omega/2$, where Ω is a positive frequency. Then we can construct a Whittaker-Shannon decomposition of the joint amplitude based on the Whittaker-Shannon sampling theorem [29–31]. That theorem states that for a function $\overline{g}(t)$ that is bandwidth limited in the sense defined above—i.e., involving only constituent frequencies in the range $-\Omega/2 \leqslant \omega \leqslant \Omega/2$—we can write

$$\overline{g}(t) = \sum_n \overline{g}(n\tau)\mathrm{sinc}\left(\frac{(t-n\tau)\pi}{\tau}\right), \tag{5.1}$$

where n ranges over the integers and

$$\tau = \frac{2\pi}{\Omega}. \tag{5.2}$$

Defining

$$\overline{\chi}(t) = \frac{1}{\sqrt{\tau}}\mathrm{sinc}\left(\frac{\pi t}{\tau}\right) \tag{5.3}$$

and putting

$$\overline{\chi}_n(t) = \overline{\chi}(t - n\tau), \tag{5.4}$$

we have

$$\int \overline{\chi}_n^*(t)\overline{\chi}_m(t)dt = \delta_{nm}, \tag{5.5}$$

and we can write (5.1) as

$$\overline{g}(t) = \sqrt{\tau}\sum_n \overline{g}(n\tau)\overline{\chi}_n(t). \tag{5.6}$$

The Fourier transform of $\overline{g}(t)$ is

$$g(\omega) = \int \frac{dt}{\sqrt{2\pi}}\overline{g}(t)e^{i\omega t} = \sqrt{\tau}\sum_n \overline{g}(n\tau)\chi_n(\omega), \tag{5.7}$$

where

$$\chi_n(\omega) = \frac{e^{i\omega n\tau}}{\sqrt{\Omega}} \quad \text{for} -\frac{\Omega}{2} \leqslant \omega \leqslant \frac{\Omega}{2} \tag{5.8}$$

$$= 0 \text{ otherwise} \tag{5.9}$$

is the Fourier transform of $\overline{\chi}_n(t)$; we have

$$\int \chi_n^*(\omega)\chi_m(\omega)d\omega = \delta_{nm}. \tag{5.10}$$

For frequencies within the band-limited region the set of functions $\{\chi_n(\omega)\}$ and $\{\chi_n(t)\}$ form an approximately complete set of functions and we refer to them as the "Whittaker-Shannon modes."

The "Whittaker-Shannon decomposition" of the joint temporal amplitude $\overline{\gamma}(t_1, t_2)$, and its Fourier transform $\gamma(\omega_1, \omega_2)$, follow immediately from this if $\gamma(\omega_1, \omega_2)$ is bandwidth limited, with frequency bandwidth Ω. Using the sampling theorem for both variables, we have

$$\overline{\gamma}(t_1, t_2) = \tau\sum_{n,m}\overline{\gamma}(n\tau, m\tau)\overline{\chi}_n(t_1)\overline{\chi}_m(t_2),$$

$$\gamma(\omega_1, \omega_2) = \tau\sum_{n,m}\overline{\gamma}(n\tau, m\tau)\chi_n(\omega_1)\chi_m(\omega_2). \tag{5.11}$$

Unlike a Schmidt (or pseudo-Schmidt) decomposition, this involves a double sum. But the Whittaker-Shannon supermodes involved, with raising operators given by

$$B_n^\dagger = \int d\omega\chi_n(\omega)a^\dagger(\omega) = \int dt\overline{\chi}_n(t)\overline{a}^\dagger(t), \tag{5.12}$$

are associated with functions that are localized in time [$\overline{\chi}_n(t)$] and can be inverted so that

$$\overline{a}(t) = \sum_n \overline{\chi}_n(t)B_n. \tag{5.13}$$

It will be useful to define

$$\beta_{nm} = \beta\tau\overline{\gamma}(n\tau, m\tau), \tag{5.14}$$

which is generally complex but symmetric, $\beta_{nm} = \beta_{mn}$. Then we can write the squeezed state $|\Psi\rangle$ [(1.1) and (2.3)] as

$$|\Psi\rangle = e^{\frac{1}{2}\sum_{n,m}\beta_{nm}B_n^\dagger B_m^\dagger - \text{H.c.}}|\text{vac}\rangle. \tag{5.15}$$

Although nondiagonal terms of β_{nm} will be important, since $\overline{\gamma}(t_1, t_2)$ is only significant for $|t_1 - t_2|$ on the order of the coherence time, we can expect β_{nm} to be significant only for m "reasonably close" to n; we examine this in more detail below. Note that our examples of the double-Gaussian and sinc-hat joint spectral amplitudes illustrate that imposing the approximation that those amplitudes are bandwidth limited requires a choice of $\Omega \geqslant 2\pi\mathcal{B}_c$ that corresponds to $\tau \leqslant \mathcal{T}_c$, that is, τ is smaller than, but on the order of, the coherence time.

As a first example, we apply the Whittaker-Shannon decomposition to the sinc-hat joint amplitude (3.33) and (3.35) and show how the approximate pseudo-Schmidt decomposition (4.14) and (4.15) arises as the limiting case when $T_p \gg T_c$. To apply the Whittaker-Shannon decomposition we must choose a bandlimit, and for the sinc-hat example the joint spectral amplitude ranges mostly within the "box" set by the width Ω_c; a natural choice for the bandlimit Ω is then to set $\Omega \to \Omega_c$ and it follows that $\tau \to T_c$. However, the sinc-hat joint spectral amplitude will never fit exactly inside a box of width Ω_c because it is only exactly bandlimited in the diagonal direction set by the range of $\phi((\omega_1 - \omega_2)/2)$, see Eqs. (3.33) and (3.35), so the corners will always exist outside the box, see the discussion surrounding Eq. (3.40) and Appendix B. When we work in the limit that $T_p \gg T_c$, where the contributions that exist outside the boundary of the box are very small, then to good approximation we can treat the sinc-hat joint spectral amplitude as bandlimited with bandwidth $\Omega = \Omega_c$ ($\tau = T_c$).

With this choice of Ω and the sinc-hat joint temporal amplitude [Eq. (3.33)], we evaluate

$$\tau\,\overline{\gamma}(n\tau, m\tau) = \delta_{nm}\sqrt{\frac{T_c}{T_p}} \quad \text{for } -\frac{T_p}{2} \leqslant nT_c \leqslant \frac{T_p}{2}$$
$$= 0 \quad \text{otherwise}, \tag{5.16}$$

where we have used $\mathrm{sinc}((n-m)\pi) = \delta_{nm}$. We find that the range of Whittaker-Shannon modes is then diagonal, and only ranges over the pulse duration set by $\overline{\alpha}(nT_c)$; identifying that $T_p/T_c = \mathcal{N} - 1$ (4.12) and p_n (4.15) as in Sec. IV, it immediately follows that

$$\overline{\gamma}(t_1, t_2) \to \sum_{n=-\left(\frac{\mathcal{N}-1}{2}\right)}^{\left(\frac{\mathcal{N}-1}{2}\right)} \sqrt{p_n}\,\overline{\chi}_n(t_1)\overline{\chi}_n(t_2), \tag{5.17}$$

where $\overline{\chi}_n(t) = \overline{\eta}_n(t)$.

For the sinc-hat model (see Fig. 5), the reduction of the double sum to its diagonal contributions is only possible because the joint spectrum is exactly bandlimited in the $(\omega_1 - \omega_2)$ direction [see (3.33) and (3.35)]; however, the resulting Whittaker-Shannon decomposition will only be accurate as a single sum in the $T_p \gg T_c$ limit for which the contributions that exist outside the box become very small and can safely be neglected.

In general, this reduction will not be possible and we need to include some—but typically only a few—off-diagonal contributions to properly approximate the joint amplitude with the Whittaker-Shannon decomposition. As we see below, the single sum and product state that follows if only diagonal terms are included [see Eq. (3.15)] is much easier and more intuitive to work with, so we always want to be as close to that limit as we can be. This means that for a not-exactly-bandlimited joint spectral amplitude, the choice of a bandwidth $\Omega = 2\pi/\tau$ always involves a trade-off: We want τ as large as possible so that each $\overline{\gamma}(n\tau, n\tau)$ covers most of the $|t_1 - t_2|$ behavior; however, if we choose τ too large then Ω becomes too small to even approximately cover the bandwidth of the joint spectral amplitude.

To see how this plays out in practice, consider the double-Gaussian joint amplitude (3.23). Although it is not strictly bandlimited, if we set $\Omega/2\pi = \mathcal{B}_c^{\mathrm{DG}} = a\sigma_c/(2\pi\sqrt{2})$ [see Eq. (3.30)], to very good approximation we can neglect the high-frequency contributions for a reasonable choice of a. Then $\tau = 2\pi\sqrt{2}/(a\sigma_c)$, and

$$\overline{\gamma}(n\tau, m\tau) \propto e^{-\frac{\sigma_c^2\tau^2(n-m)^2}{4}} \tag{5.18}$$

sets the off-diagonal range; for our choice of τ we have $\sigma_c^2\tau^2 = 8\pi^2/a^2$ and as a increases the bandlimit gets larger, but so does the range over which $|n-m|$ is significant. Setting $a = 2\sqrt{2\pi}$ as in Sec. III, we have $\sigma_c^2\tau^2/4 = \pi$ and the $1/e$ drop-off in Eq. (5.18) occurs when $|n-m| = 1/\sqrt{\pi} \approx 0.5$. In this example, and more generally for only approximately band-limited joint spectral amplitudes, one could investigate optimizing τ constrained by a specified error tolerance on the Whittaker-Shannon interpolation.

Clearly the Whittaker-Shannon decomposition depends on the two index parameter β_{nm}, but to make a comparison to the pseudo-Schmidt decomposition we focus on $\mathring{\beta}$, which we define to be the value of β_{nm} at the n and m for which $|\overline{\gamma}(n\tau, m\tau)|$ takes its maximum value. Denoting the value of $|\overline{\gamma}(n\tau, m\tau)|$ at this n and m by $\overline{\gamma}_{\max}$, we have

$$\mathring{\beta} = \tau\beta\overline{\gamma}_{\max}, \tag{5.19}$$

and

$$\beta_{nm} = \mathring{\beta} r_{nm}, \tag{5.20}$$

with $r_{nm} = \overline{\gamma}(n\tau, m\tau)/\overline{\gamma}_{\max}$. The range of $|n-m|$ over which r_{nm} is significant identifies the range over which β_{nm} varies.

Again using the double-Gaussian joint amplitude as an example, which achieves its maximum at $t_1 = t_2 = 0$, we find

$$|\mathring{\beta}| = \sqrt{2}|\beta|\frac{\tau}{\sqrt{\mathcal{T}_p^{\mathrm{DG}}\mathcal{T}_c^{\mathrm{DG}}}}, \tag{5.21}$$

where we have used $\mathcal{T}_p^{\mathrm{DG}}\mathcal{T}_c^{\mathrm{DG}} = 2\pi/\sigma_c\sigma_p$. From the discussion above, we set $\tau = \mathcal{T}_c^{\mathrm{DG}}$, and obtain

$$|\mathring{\beta}| = \sqrt{2}|\beta|\sqrt{\frac{\mathcal{T}_c^{\mathrm{DG}}}{\mathcal{T}_p^{\mathrm{DG}}}} = \sqrt{2}\frac{|\beta|}{\sqrt{\mathcal{K}_{\mathrm{DG}}}}, \tag{5.22}$$

so the effective Schmidt number naturally arises and—aside from the benign factor of $\sqrt{2}$—identifies the weakly or strongly squeezed limit as $|\mathring{\beta}| \ll 1$ or $|\mathring{\beta}| \gg 1$, respectively, justifying the definition in Sec. III. Since each $\overline{\chi}_n(t)$ has a width $\tau = \mathcal{T}_c^{\mathrm{DG}}$, the effective Schmidt number $\mathcal{K}_{\mathrm{DG}}$ roughly identifies the number of Whittaker-Shannon modes that are relevant along r_{nn}. Furthermore, following the discussion around Eq. (4.19), for a very long pulse such that $\mathcal{K}_{\mathrm{DG}} \gg 1$ the squeezing parameter $|\beta|$ can be quite large but $|\mathring{\beta}|$ remains finite.

In Fig. 13 we plot $|\overline{\gamma}(t_1, t_2)|^2$ and $|\gamma(\omega_1, \omega_2)|^2$, reconstructed from using the Whittaker-Shannon decomposition for the double-Gaussian joint amplitude of Fig. 2, where we have chosen $\Omega = 2\pi\mathcal{B}_c$, and plot r_{nm}. Comparing with Fig. 2, we see very good agreement, and from the zoomed-in plot of r_{nm} in the lower right corner it is clear that only a few neighboring Whittaker-Shannon modes in the $|n-m|$ direction are relevant.

The argument that even though $|\beta|$ can be quite large $|\mathring{\beta}|$ remains finite holds true for *any* joint amplitude, because as long as it is square normalized (1.3) it will carry prefactors on its behavior in the two directions in the plane [of either (t_1, t_2) or (ω_1, ω_2)] over which it is defined. In Appendix C, we show that given a joint temporal amplitude characterized by $\mathcal{T}_p$ and $\mathcal{T}_c$, its maximum value $\overline{\gamma}_{\max}$ is on the order of

$$\overline{\gamma}_{\max} \sim \frac{1}{\sqrt{\mathcal{T}_p\mathcal{T}_c}}. \tag{5.23}$$

To apply the Whittaker-Shannon decomposition we set $\Omega = 2\pi\mathcal{B}_c$ so that $\tau = \mathcal{T}_c$. Then one immediately finds

$$|\mathring{\beta}| = \tau|\beta|\overline{\gamma}_{\max} \sim \frac{|\beta|}{\sqrt{\mathcal{K}}}. \tag{5.24}$$

What remains to be shown is the relation between the Schmidt number K and the effective Schmidt number $\mathcal{K}$. In Appendix D, we show that for a general joint temporal amplitude characterized by widths $\mathcal{T}_p$, $\mathcal{T}_c$ indicated schematically

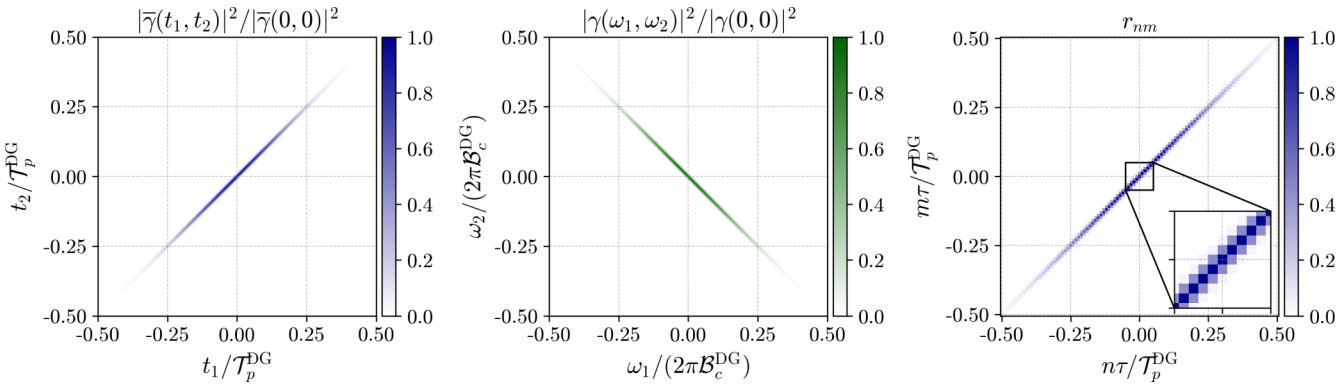

FIG. 13. For the double-Gaussian and using the Whittaker-Shannon decomposition, from left to right we plot the joint temporal intensity divided by its maximum value with the axes normalized by $\mathcal{T}_p^{\mathrm{DG}}$, the joint spectral intensity divided by its maximum value with the axes normalized by $2\pi\mathcal{B}_c^{\mathrm{DG}}$, and the amplitudes r_{nm}.

in Fig. 1, and a given τ which we set to be equal to $\mathcal{T}_c$, the inequality

$$K \leqslant \frac{\mathcal{T}_p}{\tau} = \frac{\mathcal{T}_p}{\mathcal{T}_c} = \mathcal{K}, \tag{5.25}$$

generally holds; of course this is conditioned on τ being sufficiently small that the Whittaker-Shannon decomposition can be accurately used. Thus by applying the Whittaker-Shannon interpolation formula—which previously has not been linked to squeezed light or the Schmidt decomposition—we are able to show that the Schmidt number and effective Schmidt number are intimately related. Furthermore, the Whittaker-Shannon decomposition may be an important stepping stone in formally linking the Schmidt number to other measures of the correlation, like the time-bandwidth product and its generalizations, in the same way that the Whittaker-Shannon interpolation formula is intimately linked to the Shannon number for classical signals and the information content of images [9–18,26,27,29–32].

Finally, we are now in a position to explain why the effective Schmidt number for the sinc-hat example is nearly equal to the exact Schmidt number. First we emphasize that the sinc hat is an idealization with a sharp cutoff in time (frequency) and is constant along $t_1 = t_2$ ($\omega_1 = -\omega_2$). This means that in the limit when $T_p \gg T_c$, to very good approximation it is exactly bandlimited with $\Omega = \Omega_c$ ($\tau = T_c$). Mathematically, the sharp cutoff in frequency results in an exact diagonalization of $\overline{\gamma}(n\tau, m\tau)$, and since $\overline{\gamma}(n\tau, n\tau)$ is identical for all n where it is not zero [see Eq. (4.14)] the sum in Eq. (3.3) can be carried out exactly resulting in $K \approx T_p/T_c$, as we found in Sec. III B. We then expect

$$\frac{\mathcal{K}_{\mathrm{SH}}}{K_{\mathrm{SH}}} = 1 + \frac{T_c}{T_p} \to 1 \tag{5.26}$$

for $T_p/T_c \to \infty$. Physically, the Schmidt amplitudes are near-degenerate, so there is no unique set of Schmidt modes.

VI. EMPLOYING THE WHITTAKER-SHANNON DECOMPOSITION

In using the pseudo-Schmidt decomposition to deconstruct the sinc-hat joint temporal amplitude, we showed that the expressions for the correlation functions $\overline{G}^{(1)}(t)$ and $\overline{G}^{(2)}(t_1, t_2)$ could be easily understood in terms of the properties of the supermodes involved in the decomposition. In this section we look at the corresponding expressions for the correlation functions when we deconstruct the joint amplitudes using the Whittaker-Shannon decomposition instead. The results are more complicated, but again the behavior of the correlation functions can be understood in terms of the properties of the Whittaker-Shannon supermodes in an intuitive way. And since the Whittaker-Shannon decomposition can be much more widely applied than a pseudo-Schmidt decomposition, the results here are much more general.

To simplify the notation we write the squeezed state in Eq. (5.15) as $|\Psi\rangle = \tilde{S}\,|\mathrm{vac}\rangle$, where

$$\tilde{S} = e^{\frac{1}{2}\sum_{n,m}\beta_{nm}B_n^\dagger B_m^\dagger - \mathrm{H.c.}} \tag{6.1}$$

is the squeezing operator. To calculate the correlation functions analogously to what was done with the Schmidt and pseudo-Schmidt decompositions, we use the inverse relation [Eq. (5.13)] and the transformation [33]

$$\tilde{S}^\dagger B_r \tilde{S} = \mu_{rs}B_s + \nu_{rs}B_s^\dagger, \tag{6.2a}$$

$$\tilde{S}^\dagger B_r^\dagger \tilde{S} = \mu_{rs}^* B_s^\dagger + \nu_{rs}^* B_s, \tag{6.2b}$$

where we adopt the convention that repeated indices are to be summed over, and

$$\mu_{rs} = \delta_{rs} + \frac{1}{2!}\beta_{ra}\beta_{as}^* + \frac{1}{4!}\beta_{ra}\beta_{ab}^*\beta_{bc}\beta_{cs}^* + \cdots, \tag{6.3a}$$

$$\nu_{rs} = \beta_{rs} + \frac{1}{3!}\beta_{ra}\beta_{ab}^*\beta_{bs} + \cdots. \tag{6.3b}$$

Note that from the symmetric property of β_{nm} it follows that μ_{rs} is Hermitian and ν_{rs} is symmetric.

For the Schmidt or pseudo-Schmidt decomposition the transformation used always involves a single supermode [see Eq. (3.17)]; for the general Whittaker-Shannon decomposition the squeezing transformation is more complicated. The structure of the squeezing transformation (6.2), and the form of μ_{rs} and ν_{rs}, motivates the use of matrix multiplication; β_{nm} is now treated as a complex square symmetric matrix which we denote by $\boldsymbol{\beta}$ ($\boldsymbol{\beta}^* = \boldsymbol{\beta}^\dagger$). To implement the squeezing transformation it is convenient to use the "left" polar decomposition of $\boldsymbol{\beta}$ (valid for *any* complex square matrix),

given by

$$\boldsymbol{\beta} = \mathbf{UP}, \tag{6.4}$$

where $\mathbf{P} = (\boldsymbol{\beta}^\dagger\boldsymbol{\beta})^{1/2}$ is Hermitian and $\mathbf{U}$ is unitary. Equivalently, if we set $\mathbf{Q} = \mathbf{UPU}^\dagger$ then we have the "right" polar decomposition $\boldsymbol{\beta} = \mathbf{QU}$; since $\boldsymbol{\beta}$ is symmetric, $\mathbf{P}^T = \mathbf{Q}$ and $\mathbf{U}^T = \mathbf{U}$. Using the polar decomposition and its properties, the matrices $\boldsymbol{\mu}$ and $\boldsymbol{\nu}$ are given by [34]

$$\boldsymbol{\mu} = \cosh(\mathbf{UPU}^\dagger) = \cosh\mathbf{Q}, \tag{6.5a}$$

$$\boldsymbol{\nu} = \mathbf{U}\sinh\mathbf{P} = (\sinh\mathbf{Q})\mathbf{U}. \tag{6.5b}$$

The form of $\boldsymbol{\mu}$ and $\boldsymbol{\nu}$ guarantees that the transformation in Eq. (6.2) preserves the commutation relations of the B_n operators, as expected since the transformation is unitary.

In Appendix E we calculate the correlation functions [Eq. (2.4)]; we find

$$\overline{G}^{(1)}(t_1, t_2) = \overline{\boldsymbol{\chi}}^\dagger(t_1)(\sinh^2\mathbf{P})\overline{\boldsymbol{\chi}}(t_2), \tag{6.6}$$

and

$$\overline{G}^{(2)}(t_1, t_2) = |\overline{\boldsymbol{\chi}}^T(t_1)\mathbf{U}(\sinh\mathbf{P})(\cosh\mathbf{P})\overline{\boldsymbol{\chi}}(t_2)|^2 + \overline{G}^{(1)}(t_1)\overline{G}^{(1)}(t_2) + |\overline{G}^{(1)}(t_1, t_2)|^2, \tag{6.7}$$

where $\overline{\boldsymbol{\chi}}(t) = (\ldots, \overline{\chi}_{-1}(t), \overline{\chi}_0(t), \overline{\chi}_1(t), \ldots)^T$ is the column vector formed from the set $\{\overline{\chi}_n(t)\}$ for a given t.

Since the functions $\overline{\chi}_n(t)$ are similar to the pseudo-Schmidt modes $\overline{\eta}_n(t)$, Eqs. (6.6) and (6.7) for the correlation functions calculated using the Whittaker-Shannon decomposition are the generalization of the pseudo-Schmidt results (4.16) and (4.17), valid for an approximately bandlimited but otherwise general joint amplitude. Both the pseudo-Schmidt and Whittaker-Shannon mode functions are localized, so for short time differences the structure of Eq. (6.7) reduces to that of the pseudo-Schmidt decomposition, and we can again think of the correlation function on a "mode-by-mode" basis; however, since this correspondence is only approximate, we discuss it in Appendix F.

A. Packet expansion

From Eq. (6.6), we can immediately write the photon density as

$$\overline{G}^{(1)}(t) = \sum_n \Gamma_n^2 |\overline{\rho}_n(t)|^2, \tag{6.8}$$

where $\overline{\rho}_n(t)$ is a normalized function set by

$$\overline{\rho}_n(t) = \frac{1}{\Gamma_n}\sum_m (\sinh\mathbf{P})_{nm}\overline{\chi}_m(t), \tag{6.9}$$

and

$$\Gamma_n = \sqrt{(\sinh^2\mathbf{P})_{nn}}, \tag{6.10}$$

which is real. The expression (6.8) for $\overline{G}^{(1)}(t)$ is the generalization of Eq. (4.16) in the pseudo-Schmidt decomposition and clearly has the same form; indeed, if we were to set β_{nm} to be diagonal and independent of n for the n for which it does not vanish, we would have $\overline{\rho}_n(t) \to \overline{\chi}_n(t)$. Even more generally, the expression (6.8) mirrors the form of the expansion (3.20) of $\overline{G}^{(1)}(t)$ in terms of Schmidt modes, with Γ_n here taking the role of s_n there. But the $\overline{\rho}_n(t)$ cannot be identified as a supermode; while the functions in the set $\{\overline{\chi}_n(t)\}$ are mutually orthogonal, the functions in the set $\{\overline{\rho}_n(t)\}$ are not, because in general $\sinh\mathbf{P}$ is not unitary. Nonetheless, the functions in the latter set are generally localized compared with the duration of the pulse, especially for weak squeezing. We refer to the $\overline{\rho}_n(t)$ simply as "packets," and to the expansion (6.8) for $\overline{G}^{(1)}(t)$ as its "packet expansion." We will see packet expansions of other correlation functions below.

The expected number of photons in the pulse is given by integrating $\overline{G}^{(1)}(t)$ over all time; we find

$$N_{\text{pulse}} = \text{Tr}(\sinh^2\mathbf{P}) = \sum_n \Gamma_n^2, \tag{6.11}$$

where $\text{Tr}(\cdot)$ denotes the trace. This is reminiscent of the corresponding expressions (3.22) and (4.21) for the Schmidt and pseudo-Schmidt expansions, respectively. From Eq. (6.11) it is clear that Γ_n^2 is the number of photons in each packet, and summing over all packets gives the total number of photons.

For the double-Gaussian and three values of β chosen in Sec. III A, we have $|\mathring{\beta}| \approx 0.014$, 0.7, and 1.4 which is on the order of the three values $|\beta|/\sqrt{K}$, in agreement with the discussion surrounding Eq. (5.24). In Fig. 14 we plot $G^{(1)}(t)$ calculated using Eq. (6.6), as well as the contributions given by Eq. (6.8) for a few values of n, together with the exact $\overline{G}^{(1)}(t)$ for the three chosen values of β, which correspond to $N_{\text{pulse}} \approx 0.01, 35, 383$. We find excellent agreement between the exact and Whittaker-Shannon decomposition. From Fig. 14 we see that each $\overline{\rho}_n(t)$ is clearly localized compared with the duration of the pulse, and so using the packets we can deconstruct the squeezed light and provide a simple description of the photon density [Eq. (6.8)]. This extends our understanding from the pseudo-Schmidt decomposition valid for the sinc-hat joint amplitude to more general joint amplitudes, such as the double-Gaussian, where a Whittaker-Shannon decomposition is necessary.

Notice that as $|\beta|$ ($|\mathring{\beta}|$) increases so does the width of each $\overline{\rho}_n(t)$. Referring back to Eq. (6.9), this occurs because elements of $\sinh\mathbf{P}$ that are further off-diagonal become more important as $|\beta|$ increases. And this is a consequence of the fact that more powers of $\mathbf{P}$ become important in the expansion of $\sinh\mathbf{P}$ as $|\beta|$ increases, since $\mathbf{P}$ depends on $\boldsymbol{\beta}$ [see Eq. (6.4)]. Thus the off-diagonality of $\sinh\mathbf{P}$ is extended beyond that of $\boldsymbol{\beta}$, and elements of $\sinh\mathbf{P}$ further from the diagonal become larger as $|\beta|$ increases; see Fig. 15 for plots of $\sinh\mathbf{P}$ with increasing $|\beta|$, which demonstrates this effect.

We can now construct the expansions for $\overline{G}^{(2)}_{\text{coh}}(t_1, t_2)$ and $\overline{G}^{(2)}_{\text{incoh}}(t_1, t_2)$. For the first of these, comparing the expression (6.7) for the full $\overline{G}^{(2)}(t_1, t_2)$ with our earlier general expression (3.32) for $\overline{G}^{(2)}_{\text{incoh}}(t_1, t_2)$, we can identify

$$\overline{G}^{(2)}_{\text{coh}}(t_1, t_2) = |\overline{\boldsymbol{\chi}}^T(t_1)\mathbf{U}(\sinh\mathbf{P})(\cosh\mathbf{P})\overline{\boldsymbol{\chi}}(t_2)|^2 = \left|\sum_{n,m}(\mathbf{U}(\sinh\mathbf{P})(\cosh\mathbf{P}))_{nm}\overline{\chi}_n(t_1)\overline{\chi}_m(t_2)\right|^2. \tag{6.12}$$

This can be compared with the corresponding expressions (3.21) and (4.17) for the Schmidt and pseudo-Schmidt

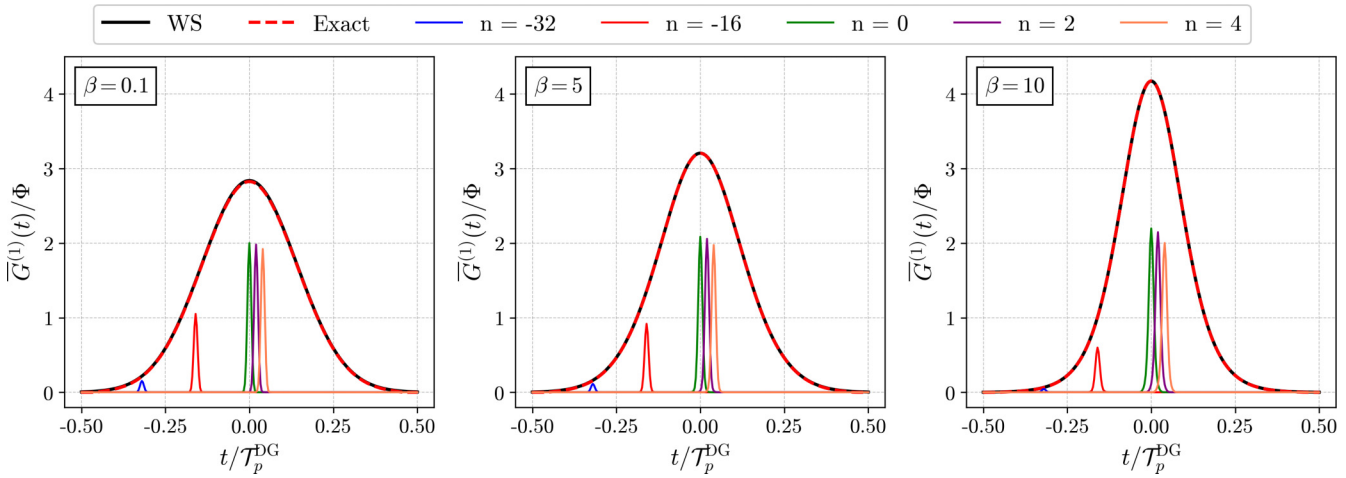

FIG. 14. For the double-Gaussian, from left to right we plot $\overline{G}^{(1)}(t)/\Phi$ calculated using the Whittaker-Shannon decomposition and a few contributions from different packets in Eq. (6.8) compared with the exact calculation (3.20), with the horizontal axis normalized by $\mathcal{T}_p^{\mathrm{DG}}$ for $\beta = 0.1, 5$, and 10. In each plot the $n = -32$ packet is the leftmost contribution and they move towards to right as n increases.

decompositions, respectively. The appearance of terms with $m \neq n$ here, as opposed to the single summation that appears in the Schmidt and pseudo-Schmidt expansion, is expected given that the squeezed state written using the Whittaker-Shannon decomposition involves a double sum (6.1).

We show in Appendix G that the expression (6.12) for $\overline{G}^{(2)}_{\mathrm{coh}}(t_1, t_2)$ can also be written using the set of packet functions $\{\overline{\rho}_n(t)\}$,

$$\overline{G}^{(2)}_{\mathrm{coh}}(t_1, t_2) = \left| \sum_{n,m} \Gamma_n \Gamma_m (\mathbf{U} \coth \mathbf{P})_{mn} \overline{\rho}_m(t_1) \overline{\rho}_n(t_2) \right|^2, \quad (6.13)$$

but this is not a convenient expression to use in practice, for if $\boldsymbol{\beta}$ is close to diagonal some functions of $\boldsymbol{\beta}$, such as $\tanh\mathbf{P}$, will be as well, but not $\coth\mathbf{P}$. Furthermore, the weakly squeezed limit is not directly apparent from the form of Eq. (6.13), so it seems preferable to write $\overline{G}^{(2)}_{\mathrm{coh}}(t_1, t_2)$ using $\{\overline{\chi}_n(t)\}$ instead of $\{\overline{\rho}_n(t)\}$. Perhaps this is not surprising, for earlier we found that when $|\beta| \ll 1$, $\overline{G}^{(2)}(t_1, t_2) \to |\beta|^2 |\overline{\gamma}(t_1, t_2)|^2$ (3.14), which directly depends on the correlations contained in the joint temporal amplitude; in same limit, using the Whittaker-Shannon decomposition, we expect it to depend on the analogous quantity β_{nm}. So unlike $G^{(1)}(t)$, where the photon density at a particular time involves contributions from all possible pairs and is written in terms of $\{\overline{\rho}_n(t)\}$, $\overline{G}^{(2)}_{\mathrm{coh}}(t_1, t_2)$—at least in the weakly squeezed limit—should directly depend on the temporal correlations, and so it is more suitable to write $\overline{G}^{(2)}_{\mathrm{coh}}(t_1, t_2)$ in terms of $\{\overline{\chi}_n(t)\}$, as is done in Eq. (6.12).

Turning finally to the general expression (3.32) for $\overline{G}^{(2)}_{\mathrm{incoh}}(t_1, t_2)$, using the definition of $\overline{\rho}_n(t)$ and Γ_n [(6.9) and (6.10)] we can write a packet expansion for the incoherent contribution as

$$\overline{G}^{(2)}_{\mathrm{incoh}}(t_1, t_2) = \frac{1}{2} \sum_{n,m} |\Gamma_n \Gamma_m (\overline{\rho}_n(t_1) \overline{\rho}_m(t_2) + \overline{\rho}_n(t_2) \overline{\rho}_m(t_1))|^2, \quad (6.14)$$

which has the same form as the Schmidt (3.21) and pseudo-Schmidt (4.17) decompositions but is in terms of the set of packets $\{\overline{\rho}_n(t)\}$.

In Fig. 16 we plot $G^{(2)}(t_1, t_2)$ calculated using Eq. (6.7) for the double-Gaussian joint amplitude, as well as the coherent and incoherent contributions; comparing with Fig. 4 for the

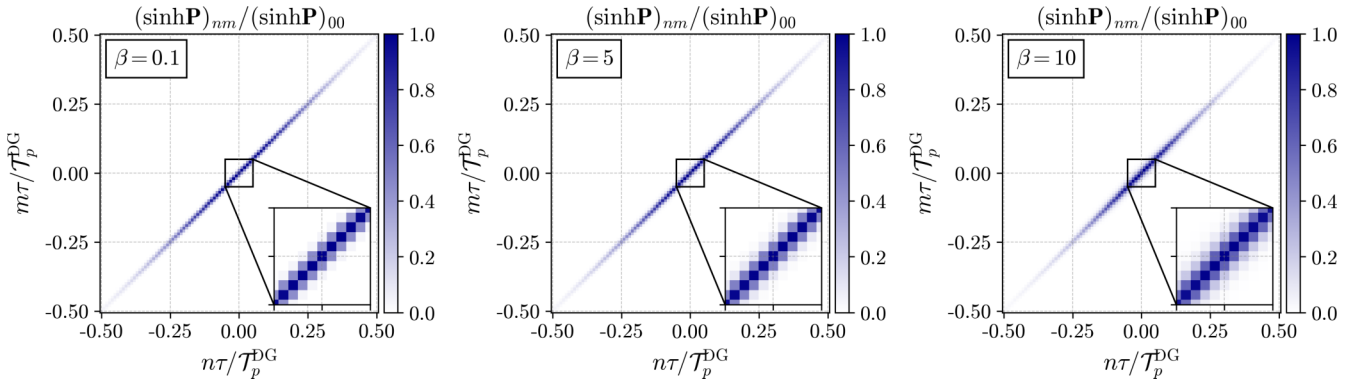

FIG. 15. For the double-Gaussian, from left to right we plot $(\sinh\mathbf{P})_{nm}$ normalized by the respective maximum values for $\beta = 0.1, 5$, and 10 with the horizontal axis normalized by $\mathcal{T}_p^{\mathrm{DG}}$.

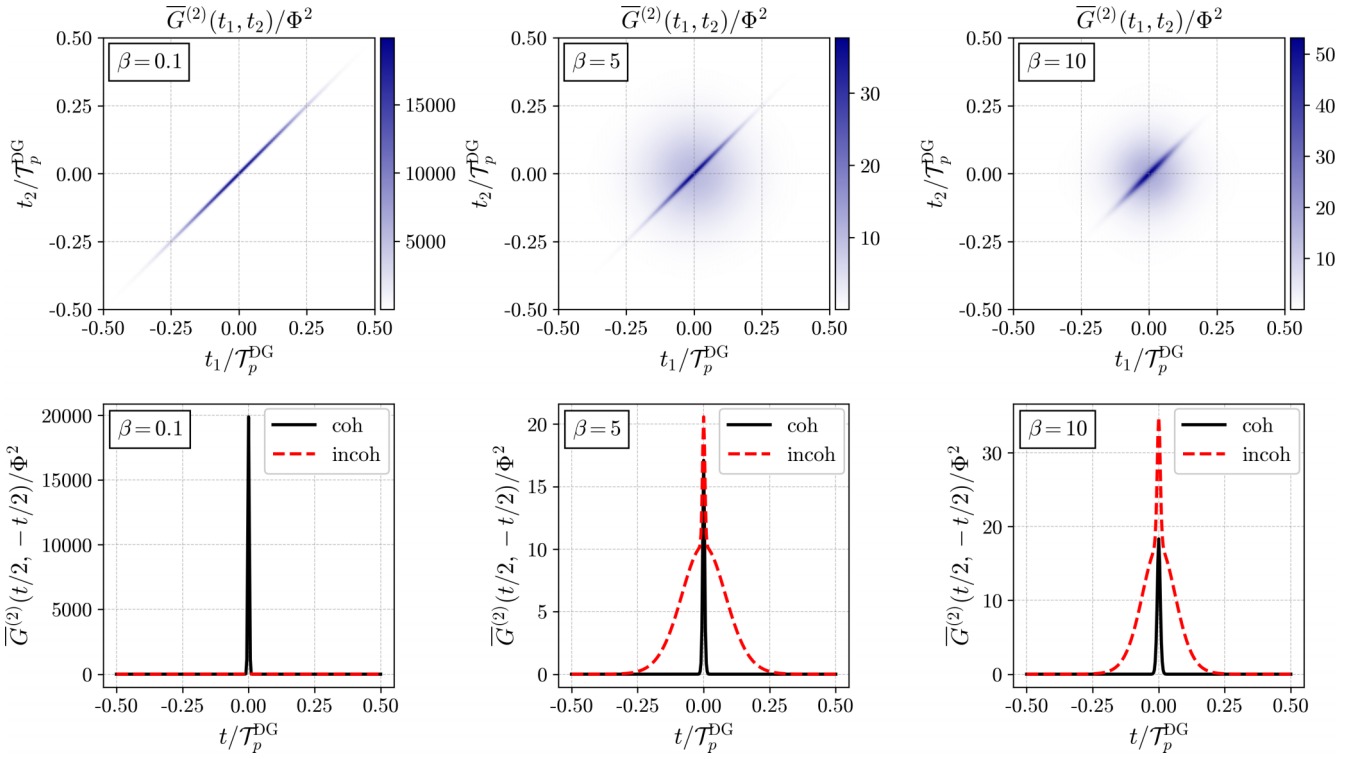

FIG. 16. For the double-Gaussian and using Whittaker-Shannon decompositions, from left to right we plot $\overline{G}^{(2)}(t_1,t_2)/\Phi^2$ (top) and the coherent and incoherent contribution to $\overline{G}^{(2)}(t/2,-t/2)/\Phi^2$ (bottom) with the axes normalized by $\mathcal{T}_p^{\rm DG}$ for $\beta=0.1$, 5, and 10.

exact calculation we find excellent agreement between the two. Although the Whittaker-Shannon decomposition does not allow the simple factorization of the ket into product kets associated with each Schmidt or pseudo-Schmidt mode, correlation functions can still be evaluated. And, since the off-diagonal elements of the squeezing matrix $\boldsymbol{\beta}$ typically drop off quickly away from the diagonal, the correlation functions can be written in a form involving either the set of functions $\{\overline{\chi}_n(t)\}$ or the set of functions $\{\overline{\rho}_n(t)\}$; all these functions are localized compared with the Schmidt modes.

B. Correlation functions in the weakly squeezed limit

In this section we identify approximate expressions for the correlation functions valid in the weakly squeezed limit when $|\mathring{\beta}|\ll 1$. The correlation functions for the Whittaker-Shannon decomposition involve the matrix $\mathbf{P}$, which using the form of Eq. (5.20) is given by $\mathbf{P}=|\mathring{\beta}|\sqrt{\mathbf{r}^{\dagger}\mathbf{r}}$. Taking the weakly squeezed limit we approximate

$$\sinh\mathbf{P}\to\mathbf{P},\quad \cosh\mathbf{P}\to\mathbf{1}, \tag{6.15}$$

where $\mathbf{1}$ is the identity matrix. Then $\Gamma_n\to[(\mathbf{P}^2)_{nn}]^{1/2}$,

$$\overline{\rho}_n(t)\to\frac{1}{\Gamma_n}\sum_m P_{nm}\overline{\chi}_m(t), \tag{6.16}$$

and for r_{nm} nonzero only for $|n-m|$ less than a small integer, the set $\{\overline{\rho}_n(t)\}$ will be localized. The expression (6.8) then gives

$$\overline{G}^{(1)}(t)\to\sum_{n,m}|P_{nm}\overline{\chi}_m(t)|^2. \tag{6.17}$$

Turning to $\overline{G}^{(2)}(t_1,t_2)$, for the coherent contribution $\overline{G}^{(2)}_{\rm coh}(t_1,t_2)$, the general expression (6.12), using the result

$$\mathbf{U}(\sinh\mathbf{P})(\cosh\mathbf{P})\to\mathbf{UP}=\boldsymbol{\beta}, \tag{6.18}$$

to find

$$\overline{G}^{(2)}_{\rm coh}(t_1,t_2)\to|\overline{\boldsymbol{\chi}}^T(t_1)\boldsymbol{\beta}\overline{\boldsymbol{\chi}}(t_2)|^2=\left|\sum_{n,m}\overline{\chi}_n(t_1)\beta_{nm}\overline{\chi}_m(t_2)\right|^2, \tag{6.19}$$

which clearly shows that the resulting photon statistics depends on β_{nm}. Finally, in this limit the expression (6.14) for $\overline{G}^{(2)}_{\rm incoh}(t_1,t_2)$ gives

$$\overline{G}^{(2)}_{\rm incoh}(t_1,t_2)\to\frac{1}{2}\sum_{n,m}\left|\sum_{u,v}P_{nu}P_{mv}(\overline{\chi}_u(t_1)\overline{\chi}_v(t_2)+\overline{\chi}_u(t_2)\overline{\chi}_v(t_1))\right|^2. \tag{6.20}$$

VII. LOCAL STATES AND CORRELATION FUNCTIONS

The general equations we derived for $\overline{G}^{(1)}(t)$ (6.8) and $\overline{G}^{(2)}(t_1,t_2)$ (6.7), and their weakly squeezed approximations, are valid for any times t,t_1,t_2. In the discussion surrounding Fig. 14 for the photon density, it was noted that since each packet is localized we only need a few to properly represent the photon density at any particular time. This suggests that for some calculations, including some more general than the

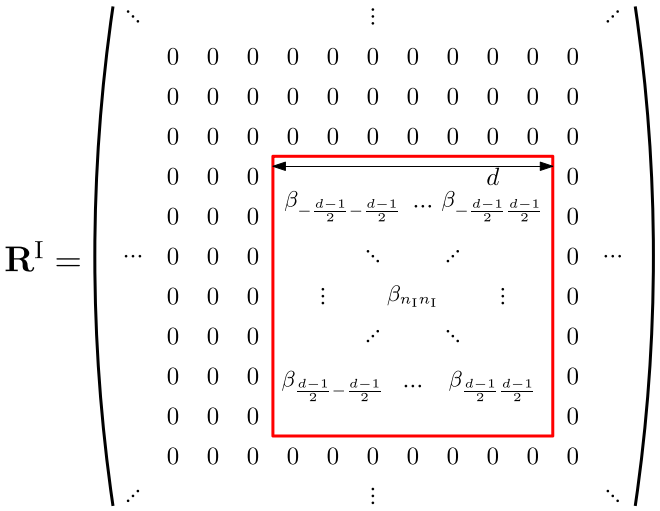

FIG. 17. Schematic of the matrix $\mathbf{R}^{\mathrm{I}}$ which has nonzero entries centered at $\beta_{n_{\mathrm{I}}n_{\mathrm{I}}}$ with a width d and zeros everywhere else. The matrix $\mathbf{K} = \boldsymbol{\beta} - \mathbf{R}^{\mathrm{I}}$ and consists of every nonzero element that we set to zero in $\mathbf{R}^{\mathrm{I}}$.

correlation functions considered above, we can rely on an approximate form of the ket itself.

Suppose we are interested in features of the state around a small neighborhood centered at the time t_{I}. Now for a correlated joint temporal amplitude β_{nm} will typically only be nonzero for $|n-m|$ ranging up to a small integer, so for times around a small neighborhood of t_{I} only a few Whittaker-Shannon modes centered around $n_{\mathrm{I}} = [t_{\mathrm{I}}/\tau]$ will be relevant; here we use $[\cdot]$ to denote the closest integer. We identify the range of m around n_{I} for which $\beta_{n_{\mathrm{I}}m}$ will be non-negligible by the odd integer d, assuming that $\beta_{n_{\mathrm{I}}m}$ is sufficiently small for $|n_{\mathrm{I}} - m| > (d-1)/2$ that for those values of m it can be neglected.

We then split the matrix $\boldsymbol{\beta}$ into two contributions

$$\boldsymbol{\beta} = \mathbf{R}^{\mathrm{I}} + \mathbf{K}, \tag{7.1}$$

where $\mathbf{R}^{\mathrm{I}}$ is a symmetric matrix with nonzero entries centered at $\mathrm{R}^{\mathrm{I}}_{n_{\mathrm{I}}n_{\mathrm{I}}}$. It contains the elements of $\boldsymbol{\beta}$ as the row and column indices range over $(d-1)/2$ in all directions from the center at $(n_{\mathrm{I}}, n_{\mathrm{I}})$, and all its other elements are set to zero. The matrix $\mathbf{R}^{\mathrm{I}}$ is shown schematically in Fig. 17 with the nonzero contributions existing inside the red "box" containing d^2 elements; all the other elements of $\boldsymbol{\beta}$ are contained in $\mathbf{K}$. For times of interest we assume that d is chosen large enough so that significant contributions to the quantities of interest, such as correlation functions involving times near t_{I}, only involve the elements of $\boldsymbol{\beta}$ contained in $\mathbf{R}^{\mathrm{I}}$.

The squeezing operator (6.1) is then approximated by

$$\tilde{S} = e^{\frac{1}{2}\sum_{n,m}(R^{\mathrm{I}}_{nm}+K_{nm})B^{\dagger}_n B^{\dagger}_m - \mathrm{H.c.}} \approx e^{\frac{1}{2}\sum_{n,m}R^{\mathrm{I}}_{nm}B^{\dagger}_n B^{\dagger}_m - \mathrm{H.c.}}, \tag{7.2}$$

where in the second line we dropped all the terms from $\mathbf{K}$. The dimension of $\mathbf{R}^{\mathrm{I}}$ can be quite large if the pulse is long, but since most of its entries are zero and the only nonzero entries have a width given by d, we use a "prime" symbol below to indicate that we can restrict the sum to be only over the nonzero elements of $\mathbf{R}^{\mathrm{I}}$. In practice, this can drastically increase the efficiency of numerical computations involving only a limited region of time. The state is then taken to be $|\Psi_{\mathrm{I}}\rangle = \tilde{S}_{\mathrm{I}}|\mathrm{vac}\rangle_{\mathrm{I}}$, where $|\mathrm{vac}\rangle_{\mathrm{I}}$ is the vacuum state corresponding to the modes associated with the nonzero elements in $\mathbf{R}^{\mathrm{I}}$, and we set

$$\tilde{S}_{\mathrm{I}} = e^{\frac{1}{2}\sum'_{n,m}R^{\mathrm{I}}_{nm}B^{\dagger}_n B^{\dagger}_m - \mathrm{H.c.}}. \tag{7.3}$$

From the approximate state $|\Psi_{\mathrm{I}}\rangle$ we can apply the same steps as above to calculate the correlation function, but instead of using the full matrix $\boldsymbol{\beta}$ for the transformation and polar decomposition we use the reduced matrix $\mathbf{R}^{\mathrm{I}}$. Then for times of interest we have [see Eq. (5.13)]

$$\overline{a}(t) = \sum_n \overline{\chi}_n(t)B_n \approx \sum_n{}' \overline{\chi}_n(t)B_n, \tag{7.4}$$

where again we restrict the sum to be over the modes associated with the nonzero elements of $\mathbf{R}^{\mathrm{I}}$, as in the approximate state $|\Psi_{\mathrm{I}}\rangle$. The equations for the correlation functions, (6.6) and (6.7), can be applied with $\boldsymbol{\beta}$ replaced by $\mathbf{R}^{\mathrm{I}}$ for times near t_{I}, with the appropriate restriction of the sums.

In Fig. 18 we plot a zoomed-in version of $\overline{G}^{(1)}(t)$ calculated from the full state $|\Psi\rangle$ and the approximate state $|\Psi_{\mathrm{I}}\rangle$ around the time $t_{\mathrm{I}} = 0$ for the double-Gaussian, the three values of β ($\mathring{\beta}$), and $d = 7$, 9 and 11. We see that the choice of d generally determines over how wide a neighborhood around t_{I} the contributions from the full state are well approximated by the contributions from $|\Psi_{\mathrm{I}}\rangle$. For $\beta = 0.1$ ($\mathring{\beta} = 0.014$), which is well within the weakly squeezed limit, only three Whittaker-Shannon modes on each side of the center mode are relevant to accurately determine the photon density at $t = 0$; this is much less then the total number of modes along r_{nn} which is set by $\mathcal{K}$, and for this example is $\mathcal{K}_{\mathrm{DG}} = 100$. Thus, the state $|\Psi_{\mathrm{I}}\rangle$ provides a "local" description of the photon density around $t = t_{\mathrm{I}}$. With the state $|\Psi_{\mathrm{I}}\rangle$ one can also calculate $G^{(2)}(t_1, t_2)$ as long as both times are near the time t_{I}. We find similar agreement and trends with β and d as for the photon density.

As $|\beta|$ ($|\mathring{\beta}|$) increases more neighboring Whittaker-Shannon modes are required to accurately reproduce the photon statistics at a given time and we need to increase the size of the nonzero box of elements in $\mathbf{R}^{\mathrm{I}}$. For as $|\beta|$ increases there is a larger amplitude for photons to be described by different modes spread further apart from each other; see the discussion in the paragraph after Eq. (6.11). In the same way that $(\sinh\mathbf{P})_{nm}$ spreads in the $|n-m|$ direction as $|\beta|$ increases (see Fig. 15) we need to choose a larger box to capture all the possible contributions near a given t_{I}. We return to this point below.

Suppose now we are interested in the properties of the state associated with two or more times $t_{\mathrm{I}}, t_{\mathrm{II}}, t_{\mathrm{III}}, \ldots$, "sufficiently far apart" from one another. Then we can split $\boldsymbol{\beta}$ into a *set* of contributions given by

$$\boldsymbol{\beta} = \mathbf{R}^{\mathrm{I}} + \mathbf{R}^{\mathrm{II}} + \mathbf{R}^{\mathrm{III}} + \cdots + \mathbf{K}, \tag{7.5}$$

with $\mathbf{R}^{\mathrm{I}}$ associated with t_{I}, $\mathbf{R}^{\mathrm{II}}$ associated with t_{II}, etc., and where by "sufficiently far apart" we mean that the corresponding boxes of sizes $d_{\mathrm{I}}, d_{\mathrm{II}}$, etc. associated with the regions of $\mathbf{R}^{\mathrm{I}}, \mathbf{R}^{\mathrm{II}}$, etc. that contain nonzero elements do not overlap; this is shown schematically in Fig. 19, where we indicate the regions of $\mathbf{R}^{\mathrm{I}}$, $\mathbf{R}^{\mathrm{II}}$, etc. that contain nonzero elements by I, II,

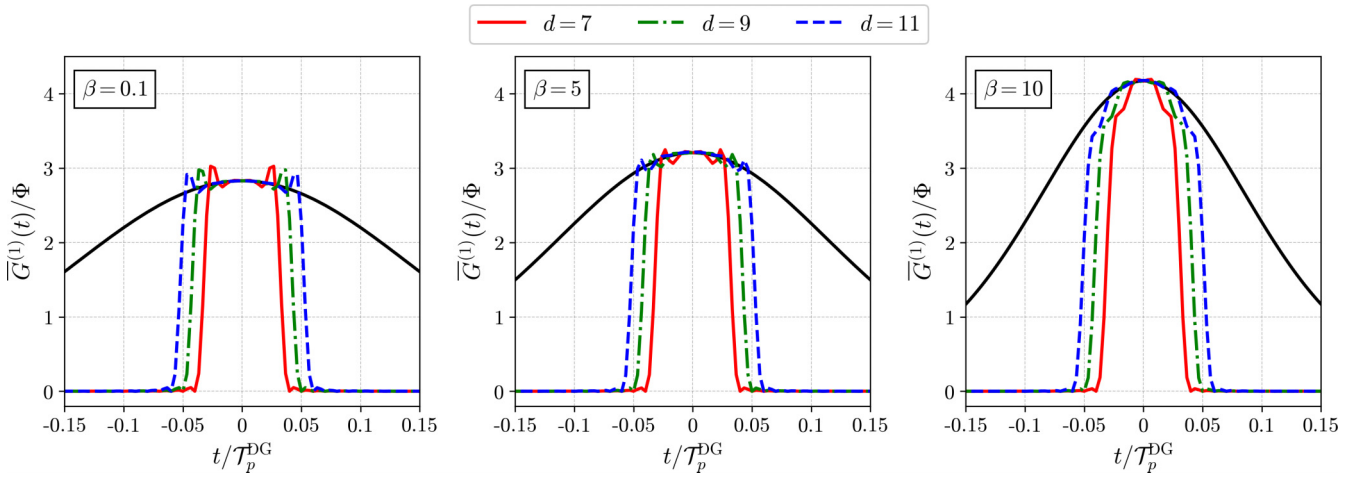

FIG. 18. For the double-Gaussian, from left to right we plot $\overline{G}^{(1)}(t)/\Phi$ calculated using the Whittaker-Shannon decomposition with the full β_{nm} compared with the approximate calculation using R^{I} near $t_{\mathrm{I}} = 0$ for $d = 7, 9$ and 11, with the horizontal axis normalized by $\mathcal{T}_p^{\mathrm{DG}}$ for $\beta = 0.1$, 5, and 10.

etc. Again, the matrix $\mathbf{K}$ contains the remaining contributions to $\boldsymbol{\beta}$ not in any of the nonzero regions of the $\mathbf{R}^J$ matrices, $J = \mathrm{I}, \mathrm{II}$, etc. Then since each $\mathbf{R}^J$ has nonzero elements only in the region where the others do not, each matrix in $\{\mathbf{R}^J\}$ commutes with the rest and each contribution to the squeezing operator can be split apart. So for the times of interest the state is given by

$$|\Psi\rangle \approx \bigotimes_J |\Psi_J\rangle = \bigotimes_J \tilde{S}_J\,|\mathrm{vac}\rangle_J\,, \tag{7.6}$$

where $|\Psi_J\rangle$, $\tilde{S}_J$, and $|\mathrm{vac}\rangle_J$ are the obvious generalization of $|\Psi_I\rangle$, $\tilde{S}_I$, and $|\mathrm{vac}\rangle_I$. Using equation (6.11) for the average photon number we similarly calculate that each time region t_J has

$$N_J = \mathrm{Tr}(\sinh^2\mathbf{P}^J) \tag{7.7}$$

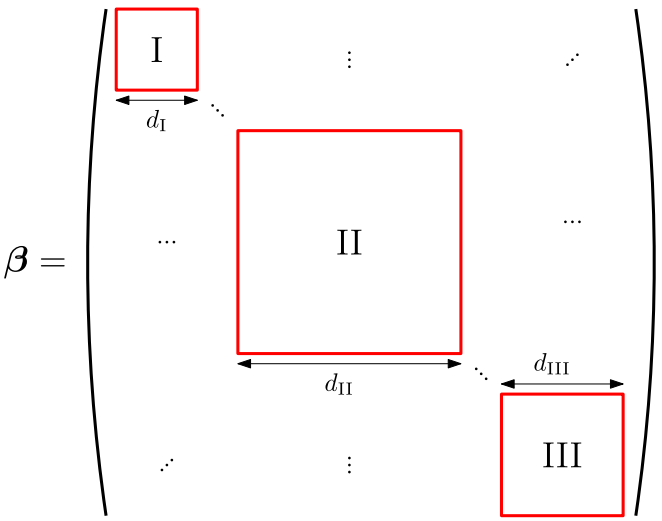

FIG. 19. Schematic of the matrix $\boldsymbol{\beta}$ partitioned into a set of nonoverlapping matrices $\mathbf{R}^J$, each with nonzero values centered at $\beta_{n_J n_J}$ of size d_J denoted by the red squares. The matrix $\mathbf{K} = \boldsymbol{\beta} - \mathbf{R}^{\mathrm{I}} - \mathbf{R}^{\mathrm{II}} - \cdots$ and consists of every other nonzero element contained in $\boldsymbol{\beta}$.

photons, where $\mathbf{P}^J$ is the matrix calculated from doing a polar decomposition of the corresponding $\mathbf{R}^J$.

To calculate the correlation functions in the neighborhood of a time t_J we again use Eqs. (6.6) and (6.7) with the replacement of β_{nm} with the appropriate $\mathbf{R}^J$ as discussed above. If instead we want to calculate $\overline{G}^{(2)}(t_J, t_{J'})$ for $J \neq J'$ then the corresponding operators $a(t_J)$ and $a^\dagger(t_{J'})$ in Eq. (2.4) commute and the resulting second-order correlation function is

$$\overline{G}^{(2)}(t_J, t_{J'}) = \overline{G}^{(1)}(t_J)\overline{G}^{(1)}(t_{J'}), \tag{7.8}$$

where the photon densities evaluated at the times $t_J, t_{J'}$ are evaluated using the respective contributions from $|\Psi_J\rangle$ and $|\Psi_{J'}\rangle$.

A. Disentangling the squeezing operator

While the approximation of the state $|\Psi\rangle$ into the set of states $\{|\Psi_J\rangle\}$, deconstructs the squeezed state and provides a local calculation of the correlation functions, it does not really give us intuition of the state itself. To gain insight into that, we make use of the general "disentangling formula" [34] applied to each squeezing operator $\tilde{S}_J$,

$$\tilde{S}_J = |\mathbf{W}^J|^{\frac{1}{2}} e^{\frac{1}{2}\sum'_{n,m} T^J_{nm} B^\dagger_n B^\dagger_m} e^{\sum'_{n,m} L^J_{nm} B^\dagger_n B_m} e^{-\frac{1}{2}\sum'_{n,m} T^{J,*}_{nm} B_n B_m}, \tag{7.9}$$

where

$$|\mathbf{W}^J|^{\frac{1}{2}} = \sqrt{\det[\mathrm{sech}(\mathbf{Q}^J)]}, \tag{7.10a}$$

$$\mathbf{T}^J = (\mathbf{T}^J)^T = \tanh(\mathbf{Q}^J)\mathbf{U}^J = \mathbf{U}^J\tanh(\mathbf{P}^J), \tag{7.10b}$$

$$\mathbf{L}^J = \ln(\mathrm{sech}(\mathbf{Q}^J)), \tag{7.10c}$$

and with $\mathbf{Q}^J$, $\mathbf{U}^J$, and $\mathbf{P}^J$ the same as before (6.4) but calculated from the reduced matrix $\mathbf{R}^J$. Then acting the disentangled squeezing operator on the vacuum state we have for each $|\Psi_J\rangle$,

$$|\Psi_J\rangle = |\mathbf{W}^J|^{\frac{1}{2}} e^{\frac{1}{2}\sum'_{n,m} T^J_{nm} B^\dagger_n B^\dagger_m}\,|\mathrm{vac}\rangle_J \equiv \overline{S}_J\,|\mathrm{vac}\rangle_J\,, \tag{7.11}$$

where $\overline{S}_J$ is the disentangled squeezing operator after acting on the vacuum state. We point out that one could also apply the disentangling formula to the whole state valid at all times, but

this is not very illuminating because one can already calculate the full correlation functions; further, had we first applied the disentangling formula and then reduced the state by getting rid of the terms that are negligible, the resulting state would not be normalized, whereas $|\Psi_J\rangle$ as given in Eq. (7.11) always is.

Unlike the squeezing operator in its "entangled form" (6.1), all the operators in the exponent of Eq. (7.11) are creation operators which always commute so we can equivalently write the state for each J as

$$|\Psi_J\rangle = |\mathbf{W}^J|^{\frac{1}{2}} \bigotimes_{n,m} e^{\frac{1}{2}T^J_{nm}B^\dagger_n B^\dagger_m} |\text{vac}\rangle_J \,. \tag{7.12}$$

Unfortunately this form of the state is not as intuitive as the *single* product state in the pseudo-Schmidt decomposition because for a given n we must include contributions from every other m in the range of T^J_{nm}.

B. The ket in the weakly squeezed limit

Instead, in situations where $|\beta|$ can be quite large but $|\mathring{\beta}|$ is sufficiently small, as in a long pulse, we can take advantage of the fact that it is $|\mathring{\beta}|$ that sets the magnitude of the matrix T^J_{nm}. Given that the sum in Eq. (7.11) is only over the modes of interest, and not the whole joint amplitude, in the weakly squeezed limit when $|\mathring{\beta}| \ll 1$ we can Taylor expand the exponential so that

$$|\Psi_J\rangle \approx |\mathbf{W}^J|^{\frac{1}{2}} \left(|\text{vac}\rangle_J + \sqrt{\frac{N_J}{2}} \, |\text{II}\rangle_J + \cdots \right), \tag{7.13}$$

where we have used $(\mathbf{T}^J)^\dagger \mathbf{T}^J \to (\mathbf{R}^J)^\dagger \mathbf{R}$, Eq. (7.7) reduces to

$$N_J \to \text{Tr}((\mathbf{R}^J)^\dagger \mathbf{R}^J), \tag{7.14}$$

and we have introduced the normalized two-photon state for each J by

$$|\text{II}\rangle_J = \frac{1}{\sqrt{2}} \sum_{nm} \frac{T^J_{nm}}{\sqrt{N_J}} B^\dagger_n B^\dagger_m |\text{vac}\rangle_J \,. \tag{7.15}$$

The state $|\Psi_J\rangle$ has $N_J \ll 1$ photons and the prefactor $|\mathbf{W}^J|$ in the weakly squeezed limit is

$$|\mathbf{W}^J| \approx 1 - \frac{N_J}{2}, \tag{7.16}$$

so to good approximation, the state remains normalized, as expected. The two-photon state $|\text{II}\rangle_J$ is a superposition of all the ways in which pairs of photons can be associated with the same Whittaker-Shannon supermode, or different supermodes, within a neighborhood of the time t_J; one can easily extend the state in Eq. (7.13) to higher order in which two pairs, three pairs, etc. are considered. For a set of times, $\{t_J\}$, in the weakly squeezed limit the full state in equation (5.15) can be expanded as

$$|\Psi\rangle \approx \bigotimes_J |\mathbf{W}^J|^{\frac{1}{2}} \left(|\text{vac}\rangle_J + \sqrt{\frac{N_J}{2}} \, |\text{II}\rangle_J + \cdots \right), \tag{7.17}$$

providing a localized description of squeezing light for correlated but otherwise arbitrary joint amplitudes. In the long-pulse limit, despite the fact that $|\beta| \to \infty$, $|\mathring{\beta}|$ remains finite and we can describe the light in the weakly squeezed limit as being composed of approximately two-photons within a neighborhood around each time t_J.

VIII. THE STRONGLY SQUEEZED LIMIT

In this section we consider the strongly squeezed limit, where $|\beta|/\sqrt{\mathcal{K}} \gg 1$, or equivalently $|\mathring{\beta}| \gg 1$. The results we derived in Secs. V and VI are valid for any approximately bandlimited joint amplitude and for any squeezing parameter β. However, following the discussion around Fig. 3, for the double-Gaussian with $\mathcal{K}_{\text{DG}} = 100$ we found that as $|\beta|$ increased fewer Schmidt modes were required to calculate the correlation functions, although many were required to calculate the joint amplitude.

To explore this further, consider the double-Gaussian joint amplitude (Fig. 2, with $\mathcal{K}_{\text{DG}} = 100$) but for $\beta = 150$, corresponding to $|\beta|/\sqrt{\mathcal{K}_{\text{DG}}} \approx 15$ or $|\mathring{\beta}| \approx 21$, well in the strongly squeezed regime. In Fig. 20 we plot $\overline{G}^{(1)}(t)$ calculated using the Schmidt and Whittaker-Shannon decompositions. Clearly the first Schmidt mode is sufficient to produce an accurate $\overline{G}^{(1)}(t)$, despite the fact that all Schmidt modes are required to correctly calculate the joint amplitude. This is because the correlation functions depend on s_n and c_n [recall Eqs. (3.20) and (3.21)], but when $|\beta|$ is large these scale exponentially; since the Schmidt modes drop off as n increases, $s_0 \gg s_1$ and the sums in Eq. (3.20) for the correlation functions are well approximated by the $n = 0$ term. For the Whittaker-Shannon decomposition we still find very good agreement with the Schmidt calculation. However, as in Fig. 14, we find each packet is significantly broadened. In the strongly squeezed limit, the amplitude that many photon pairs will contribute is large, and so the contribution of photons corresponding to two Whittaker-Shannon modes for which $|n - m| \gg 1$ is significant; since the $\overline{\rho}_n(t)$ include contributions from all other m for a given n, they are necessarily broader. More mathematically, in the strongly squeezed limit many matrix multiplications are involved in calculating $\sinh\mathbf{P}$, and so (following the discussion in Sec. VI A and surrounding Figs. 15 and 18) the width of each packet is significantly broadened.

Since packets can then significantly overlap with a number of their neighbors, the local description of the photon statistics and resulting state breaks down. This is not surprising, given that the second-order correlation function, calculated using the Schmidt decomposition and plotted in Fig. 21, is completely uncorrelated, a local description to identify the photon correlations is not necessary. Note that here we do not include the plot of $\overline{G}^{(2)}(t_1, t_2)$ calculated using the Whittaker-Shannon decomposition, because it is essentially identical to Fig. 21.

Finally, we point out that in Fig. 21 the incoherent contribution is approximately twice the coherent contribution. If we restrict the sum in Eqs. (3.20) and (3.21) to the first term we have

$$\overline{G}^{(1)}(t) \to s_0^2 |\overline{f}_0(t)|^2, \tag{8.1a}$$

$$N_{\text{pulse}} \to s_0^2, \tag{8.1b}$$

$$\overline{G}^{(2)}_{\text{coh}}(t_1, t_2) \to N^2_{\text{pulse}} |\overline{f}_0(t_1)|^2 |\overline{f}_0(t_2)|^2, \tag{8.1c}$$

$$\overline{G}^{(2)}_{\text{incoh}}(t_1, t_2) \to 2N^2_{\text{pulse}} |\overline{f}_0(t_1)|^2 |\overline{f}_0(t_2)|^2, \tag{8.1d}$$

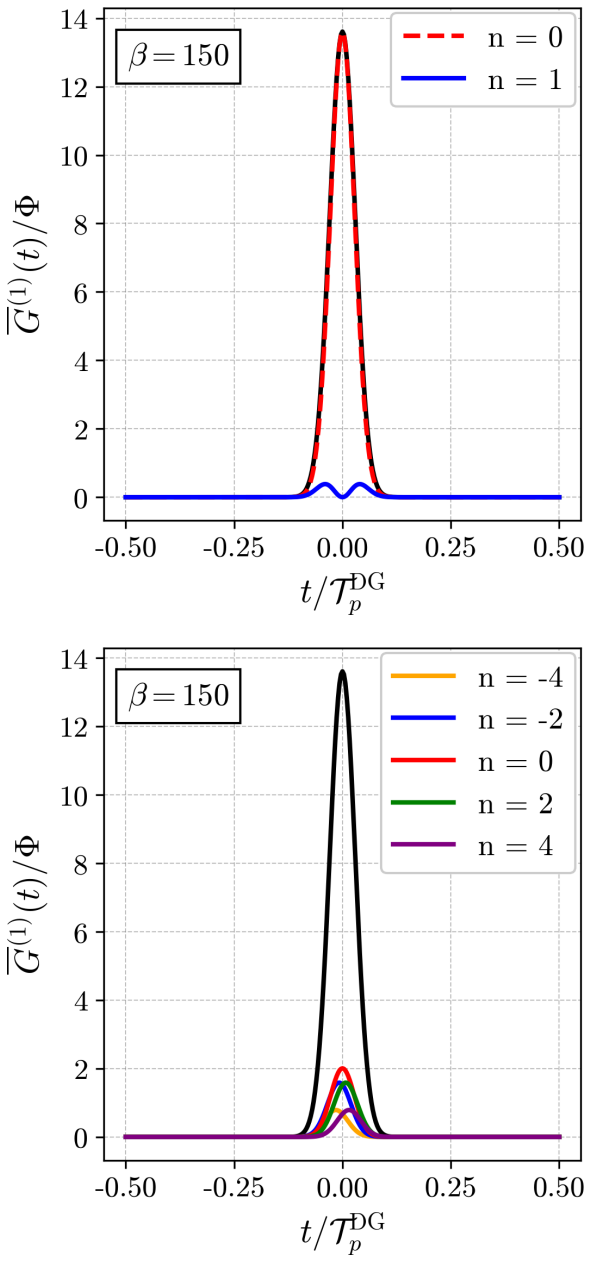

FIG. 20. For the double-Gaussian joint amplitude, we plot $\overline{G}^{(1)}(t)/\Phi$ calculated using the Schmidt decomposition (top) and Whittaker-Shannon decomposition (bottom) as well as a few contributions from each calculation, for $\beta = 150$ with the horizontal axis normalized by $\mathcal{T}_p^{\mathrm{DG}}$. In the bottom plot, the smallest and leftmost contribution is from the $n = -4$ packet and the largest is the $n = 0$ packet.

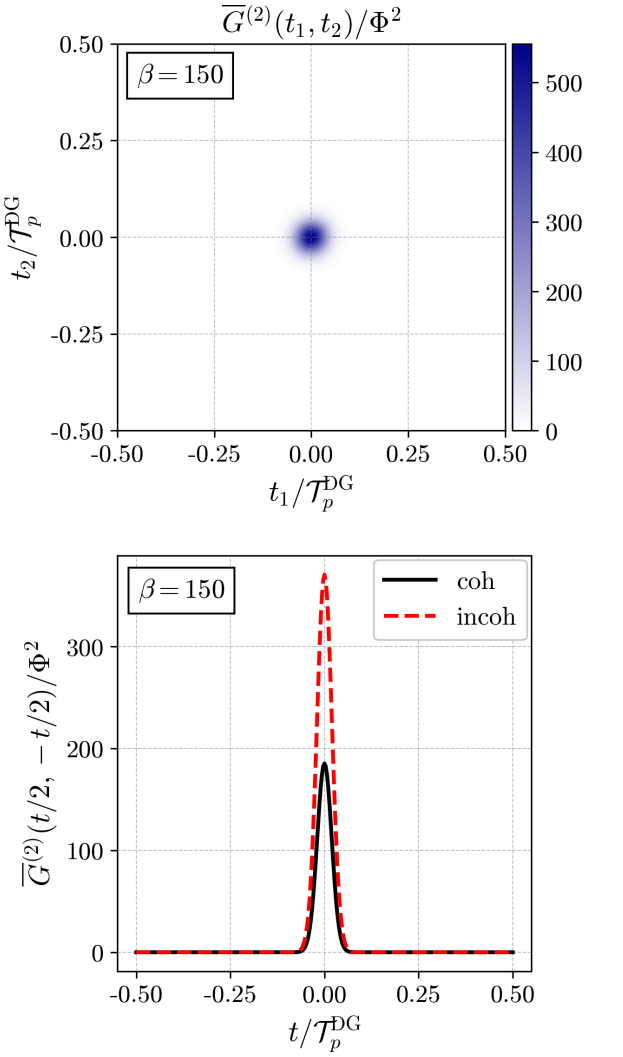

FIG. 21. For the double-Gaussian joint amplitude, we plot $\overline{G}^{(2)}(t_1, t_2)/\Phi^2$ (top), and the coherent and incoherent contribution to $\overline{G}^{(2)}(t/2, -t/2)/\Phi^2$ (bottom) calculated using the Schmidt decomposition, for $\beta = 150$ with the horizontal and vertical axis normalized by $\mathcal{T}_p^{\mathrm{DG}}$.

where we have used the fact that, for large $|\beta|$, $c_n \approx s_n$; it is clear from these expressions that $\overline{G}^{(2)}_{\mathrm{incoh}}(t_1, t_2) \approx 2\overline{G}^{(2)}_{\mathrm{coh}}(t_1, t_2)$. Then putting them together we have

$$\overline{G}^{(2)}(t_1, t_2) = 3N_{\mathrm{pulse}}^2 |\overline{f}_0(t_1)|^2 |\overline{f}_0(t_2)|^2. \tag{8.2}$$

Since the calculation in Appendix F was done for a pseudo-Schmidt mode, it can be applied to this instance of a single Schmidt mode, so we identify $3N_{\mathrm{pulse}}^2$ as the expectation value of the number of ways of "picking" two photons in the large $|\beta|$ limit from the first Schmidt mode.

IX. A FINAL EXAMPLE

In this section we consider a realistic joint amplitude generated from a dual-pump spontaneous four-wave mixing process, in a ring resonator system, when time-ordering effects and self- and cross-phase modulation are included [4]. In Fig. 22 we plot the joint intensity and the Schmidt amplitudes. The joint intensity has widths $\mathcal{T}_p^{\mathrm{R}} = 200$ ns and $\mathcal{B}_c^{\mathrm{R}} \approx 1.03$ GHz ($\mathcal{T}_c^{\mathrm{R}} \approx 0.97$ ns) corresponding to an effective Schmidt number $\mathcal{K}_{\mathrm{R}} \approx 206$, and the joint amplitude has a Schmidt number $K_{\mathrm{R}} \approx 108$, where we use "R" to identify this "ring" calculation. The squeezing parameter for the generation is $\beta = 3.72$, corresponding to $N_{\mathrm{pulse}} \approx 11$ photons. Other system parameters, such as the center wavelengths and pump duration, are given in the caption of Fig. 22. Comparing

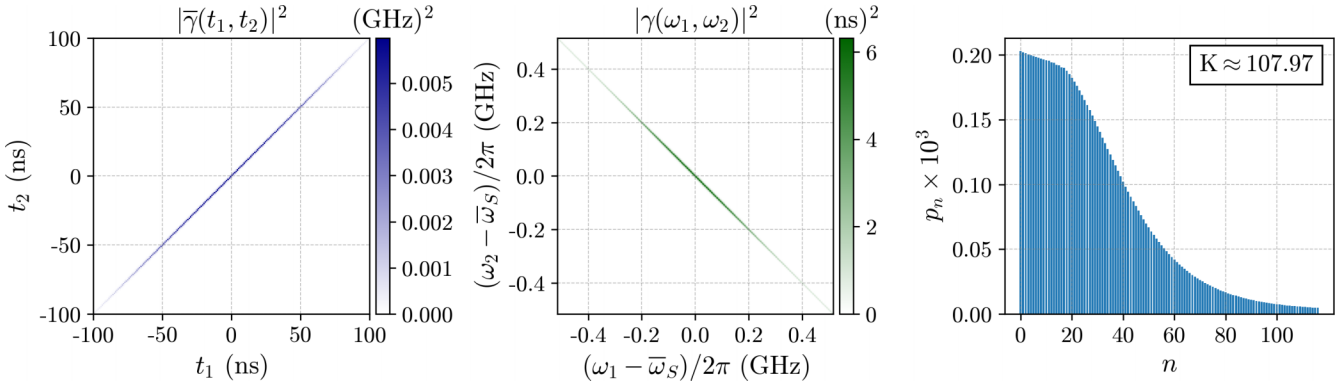

FIG. 22. From left to right we plot the joint temporal intensity, the joint spectral intensity, and the Schmidt amplitudes generated from a dual-pump spontaneous four-wave mixing process. The two pump functions are centered at the wavelengths $\overline{\lambda}_{\mathrm{P1}} = 1.556$ μm and $\overline{\lambda}_{\mathrm{P2}} = 1.547$ μm and each have temporal FWHM of 100 ns and an energy of 10^3 pJ. The generated photons are centered at $\overline{\lambda}_{\mathrm{S}} = 1.552$ μm ($\overline{\omega}_{\mathrm{S}}/2\pi = 193.164$ THz) and have a bandwidth on the order of a GHz. The ring resonator has quality factors $Q_{\mathrm{P1}} = 1\,529\,378$, $Q_{\mathrm{P2}} = 3\,844\,257$, and $Q_{\mathrm{S}} = 2\,704\,405$ for the three modes and a nonlinear coupling $\Lambda = 5$ THz [4].

Fig. 22 with Fig. 23 for the joint temporal intensity calculated using the Whittaker-Shannon decomposition, with $\Omega/2\pi = \mathcal{B}_c^{\mathrm{R}}$ ($\tau = \mathcal{T}_c^{\mathrm{R}}$), we see excellent agreement.

In Fig. 24 we plot $\overline{G}^{(1)}(t)$ for the Schmidt (top) and Whittaker-Shannon (bottom) decompositions, as well as a few contributions to each. We see a dramatic difference: at any particular time a huge number of Schmidt modes are required to capture the overall photon density, while in our packet decomposition only a small range of packets are required to describe the behavior at any time.

In Fig. 25 we plot $\overline{G}^{(2)}(t_1,t_2)$ (top) and the coherent and incoherent contributions to $\overline{G}^{(2)}(t/2,-t/2)$ (bottom) calculated using the Whittaker-Shannon decomposition. Here we only plot the Whittaker-Shannon results because the Schmidt results look the same. The contributions to $\overline{G}^{(2)}(t_1,t_2)$—strong peak near $t_1 = t_2$ and smaller broad background—match that of the double-Gaussian example for the three values of β. This

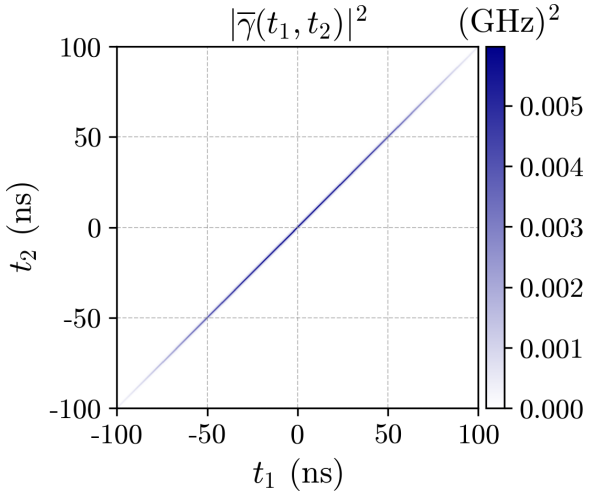

FIG. 23. Joint temporal intensity calculated using the Whittaker-Shannon decomposition.

is unsurprising because, although $\beta = 3.72$ in this example, $\mathring{\beta} = 0.28$, and so the state is weakly squeezed.

Since the state is weakly squeezed, the formalism provided in Sec. VII can be directly applied, providing a localized description of the pulse of light into a set of states with different time labels, each containing approximately two photons.

X. CONCLUSION

In this article we have developed a formalism to describe squeezed light with a large spectral-temporal correlation. As opposed to the usual strategy of employing the Schmidt decomposition, we feel it makes the physics more apparent. We began by characterizing general joint amplitudes by their timewidth $\mathcal{T}_p$ and bandwidth $\mathcal{B}_c$ (or equivalently the coherence time $\mathcal{T}_c = 1/\mathcal{B}_c$). Using the double-Gaussian joint amplitude as an example, we calculated the correlation functions using the Schmidt decomposition and found that for weak squeezing the form of $\overline{G}^{(2)}(t_1,t_2)$ matches that of the joint temporal amplitude and reaches its maximum value when $|t_1 - t_2| < \mathcal{T}_c$. However, the Schmidt modes themselves extend on a much broader timescale given by $\mathcal{T}_p$. When calculating the correlation functions using the Schmidt decomposition, we found that a large amount of interference is present. We cannot associate a single Schmidt mode, or even a few, with a particular time.

Next we considered another example, the sinc-hat joint amplitude, which demonstrated that this behavior of the double-Gaussian is not unique. And although it is somewhat artificial, the sinc-hat joint amplitude is interesting in that its Schmidt amplitudes are nearly degenerate, allowing us to construct an approximate pseudo-Schmidt decomposition where the pseudo-Schmidt modes are displaced, localized "sinc" functions. Using this decomposition we could immediately identify contributions contained in $\overline{G}^{(1)}(t)$ or $\overline{G}^{(2)}(t_1,t_2)$ at a particular time as arising from a single pseudo-Schmidt mode, allowing us to deconstruct the photon statistics, elucidating the physics. We also demonstrated that the weakly squeezed limit corresponds to $|\beta|/\sqrt{\mathcal{N}} \ll 1$, where $\mathcal{N}$ is the effective

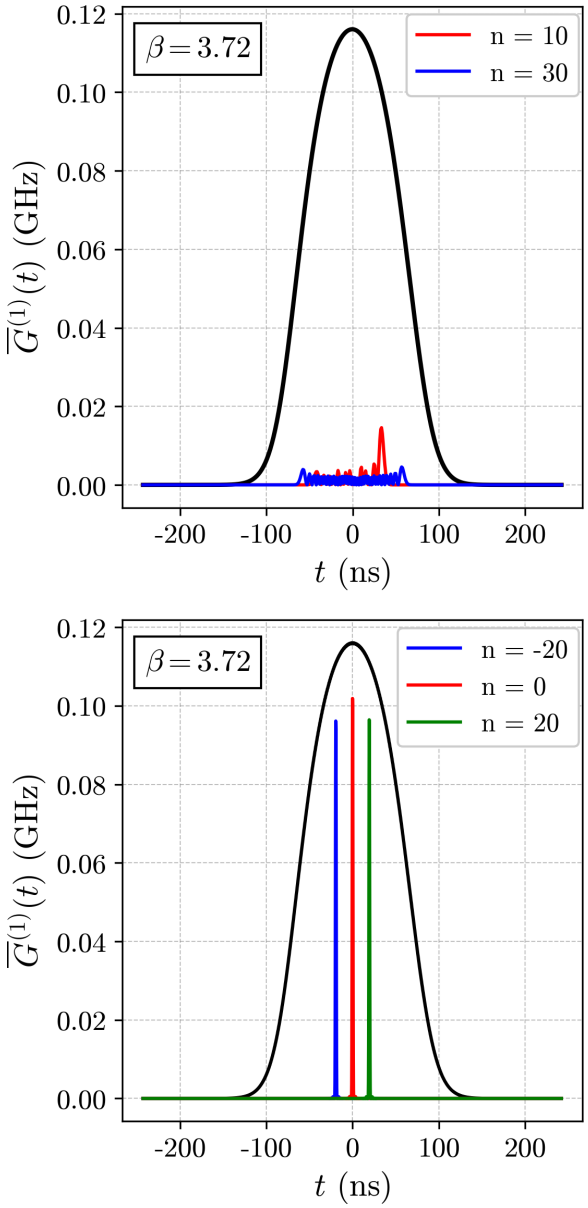

FIG. 24. Plot of $\overline{G}^{(1)}(t)$ calculated using the Schmidt decomposition (top) and Whittaker-Shannon decomposition (bottom). In the top plot the $n = 10$ Schmidt corresponds to the larger contribution. In the bottom plot the $n = -20$ is the leftmost packet.

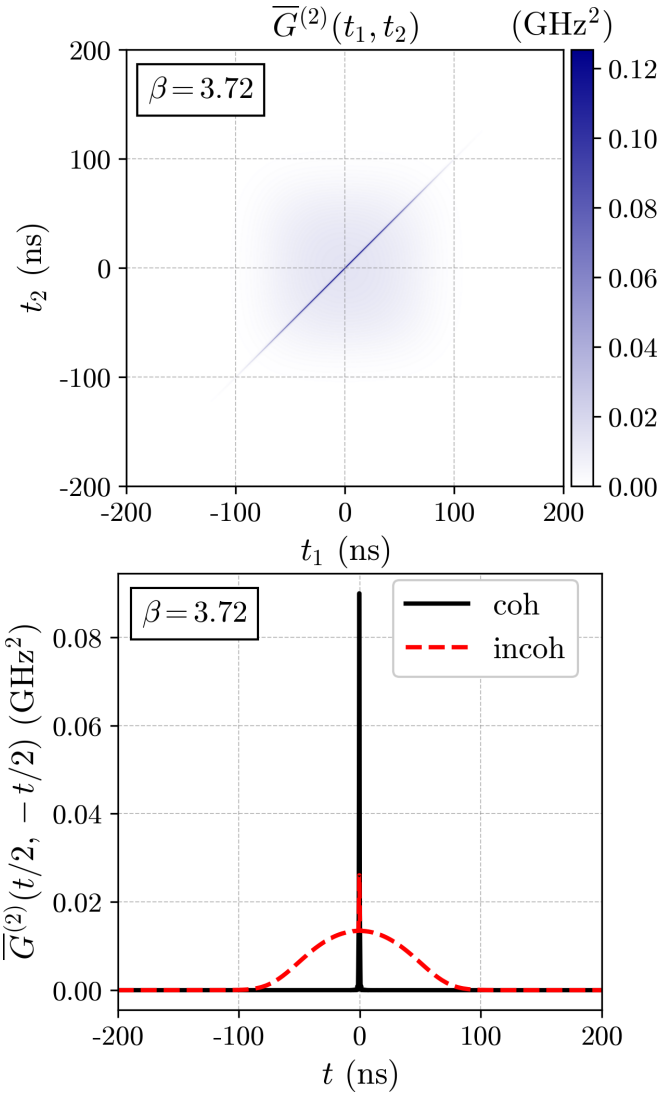

FIG. 25. Plot of $G^{(2)}(t_1, t_2)$ (top) and the coherent and incoherent contribution to $G^{(2)}(t/2, -t/2)$ calculated using the Whittaker-Shannon decomposition.

Schmidt number that identifies the number of pseudo-Schmidt modes required for the decomposition. This is useful because in the long-pulse limit, where $|\beta| \gg 1$ and $N_{\text{pulse}} \gg 1$, the quantity $|\beta|/\sqrt{\mathcal{N}}$ remains finite. Despite there being a large number of photons in the pulse, the number of photons in each pseudo-Schmidt mode can be relatively small.

To consider more general joint amplitudes, where there is a range of Schmidt amplitudes, we generalized the pseudo-Schmidt decomposition to any approximately bandlimited joint amplitude by using the Whittaker-Shannon interpolation formula. While the exponent in the squeezing operator then involves a double sum instead of the usual single sum, we can nevertheless define a packet expansion where each packet typically has a duration short compared with that of the pulse, with the packets thus analogous to the pseudo-Schmidt modes. In general, if the squeezing is weak to moderate, the correlation functions at a particular time are associated with only a few packets, allowing us to deconstruct the squeezed light and the resulting photon statistics. Finally we showed that if one is only interested in some finite-time regions that form part of the pulse duration, an effective ket can be written as a product of kets associated with those time regions. Then in the weakly squeezed limit, which we can take to be set by the limit $|\mathring{\beta}| \ll 1$, there will be on average only a few photons within each time region, although in the long-pulse limit the total number of photons will be very large.

In extensions of this work, we will consider two-mode squeezing, which is fairly straightforward, and we will apply this formalism to quantum optics-based experiments such as coincidence-accidental-detection ratios and SU(1,1) interferometry. And instead of describing squeezed light in

the spectral-temporal domain, one could expand this formalism to describe squeezed light with a large correlation between the photon wave vector and the conjugate position variables in two, or three dimensions. Another interesting focus is the formulation of relationships between the Schmidt number, the effective Schmidt number discussed here, and the Shannon number (or time-bandwidth product) and its generalizations. Here there is the opportunity to apply the vast mathematical formalism that has already been developed to describe the information content of classical signals and images [9–18,26,27,29–32].

With the continuous advancement of custom engineered nonlinear optical systems, the generation of nonclassical "tri-photon" states is slowly becoming a reality [35]. Such states and their "troint amplitudes" are the generalization of squeezed states and the joint amplitudes discussed here. To characterize these states, generalizations of the Schmidt decomposition (singular-value decomposition) need to be employed. One such example is the canonical polyadic decomposition (or CP decomposition) [36]; however, an orthogonal decomposition is not guaranteed to exist. Other generalizations of the Schmidt decomposition exist, such as the Tucker decomposition [36], which gains orthogonality but loses the single-sum behavior of the Schmidt decomposition. An alternative description can be provided using the Whittaker-Shannon interpolation formula. In the same way that we used the Whittaker-Shannon interpolation formula for two-dimensional functions in this work, it can be directly applied to any number of dimensions in a very straightforward way. Thus the formalism applied here can easily be generalized to situations where other decompositions are not possible.

ACKNOWLEDGMENTS

We thank Xanadu Quantum Technologies for allowing access to their proprietary code repository used in Sec. IX and Luke Helt for answering related questions. We also thank Marco Liscidini and Nicolás Quesada for valuable discussions. This work was supported by the Natural Sciences and Engineering Research Council of Canada (NSERC). C.D. acknowledges support by an Ontario Graduate Scholarship.

APPENDIX A: FIELD OPERATOR

For a quasi-1D structure, if z is the direction in which light is propagating, the electric field operator in the Heisenberg picture takes the form [4]

$$\boldsymbol{E}(x,y,z;t)=\sum_n\int_{-\infty}^{\infty}\frac{dk}{\sqrt{2\pi}}\,\boldsymbol{e}_n(k;x,y)b_n(k)e^{ikz}e^{-i\omega t}+\text{H.c.}, \tag{A1}$$

where the dependence of ω on k is identified by the dispersion relation, the $\boldsymbol{e}_n(k;x,y)$ is a properly normalized field profile for a transverse mode n propagating with k at frequency ω, and $b_n(k)$ is the associated lowering operator, $[b_n(k),b_m^\dagger(k')]=\delta_{nm}\delta(k-k')$. We assume that only one transverse mode is of interest and drop the index n, and that only $k>0$ are of interest. Taking $\omega=vk>0$, where v is the group velocity, we identify modes by their frequency ω, putting $c(\omega)=v^{-1/2}b(k)$ so that $[c(\omega),c^\dagger(\omega')]=\delta(\omega-\omega')$ holds, and we can then write

$$\boldsymbol{E}(x,y,z;t)\to\int_0^{\infty}\frac{d\omega}{\sqrt{2\pi}}\frac{\boldsymbol{e}\left(\frac{\omega}{v};x,y\right)}{v^{1/2}}c(\omega)e^{i\omega z/v}e^{-i\omega t}+\text{H.c.} \tag{A2}$$

Assuming that over the frequency range of interest $\boldsymbol{e}(\omega/v;x,y)$ varies little from its value $\boldsymbol{e}(\omega_o/v;x,y)$ at a center frequency ω_o, we can write

$$\begin{aligned}\boldsymbol{E}(x,y,z;t)&\to\frac{\boldsymbol{e}\left(\frac{\omega_o}{v};x,y\right)}{v^{1/2}}\int_0^{\infty}\frac{d\omega}{\sqrt{2\pi}}c(\omega)e^{i\omega z/v}e^{-i\omega t}+\text{H.c.}\\&=\frac{\boldsymbol{e}\left(\frac{\omega_o}{v};x,y\right)}{v^{1/2}}e^{i\omega_o z/v}e^{-i\omega_o t}\\&\quad\times\int_0^{\infty}\frac{d\omega}{\sqrt{2\pi}}c(\omega)e^{i(\omega-\omega_o)z/v}e^{-i(\omega-\omega_o)t}+\text{H.c.}\end{aligned} \tag{A3}$$

Then putting $a(\omega-\omega_o)\equiv c(\omega)$, the commutation relations [Eq. (1.2)] hold and for the range of frequencies much less than ω_o and we have

$$\begin{aligned}\boldsymbol{E}(x,y,z;t)&=\frac{\boldsymbol{e}\left(\frac{\omega_o}{v};x,y\right)}{v^{1/2}}e^{i\omega_o z/v}e^{-i\omega_o t}\\&\quad\times\int_{-\infty}^{\infty}\frac{d\omega}{\sqrt{2\pi}}a(\omega)e^{i\omega z/v}e^{-i\omega t}+\text{H.c.}\end{aligned} \tag{A4}$$

This gives

$$\boldsymbol{E}(x,y,0;t)=\frac{\boldsymbol{e}\left(\frac{\omega_o}{v};x,y\right)}{v^{1/2}}e^{-i\omega_o t}\overline{a}(t)+\text{H.c.}, \tag{A5}$$

where

$$\overline{a}(t)=\int_{-\infty}^{\infty}\frac{d\omega}{\sqrt{2\pi}}a(\omega)e^{-i\omega t}. \tag{A6}$$

Now since the Schrödinger operator for $\boldsymbol{E}(x,y,z)$ is just the Heisenberg operator $\boldsymbol{E}(x,y,z;0)$, for that Schrödinger operator we have

$$\boldsymbol{E}(x,y,z)=\frac{\boldsymbol{e}\left(\frac{\omega_o}{v};x,y\right)}{v^{1/2}}e^{i\omega_o z/v}\overline{a}\left(-\frac{z}{v}\right)+\text{H.c.} \tag{A7}$$

That is, the operator $\overline{a}(t)$ is associated with the electric field at time t and $z=0$, and as well with the electric field at zero time and position $z=-vt$, as would be expected because of the propagation with group velocity v.

APPENDIX B: SCHEMATIC OF SINC-HAT JOINT INTENSITY

Consider the schematic sinc-hat joint intensity shown in Fig. 26, where we drop the sinc "tails" along the antidiagonal (diagonal) direction for the joint temporal (spectral) intensity. Of course, because of the sinc tails the joint intensities extend to infinity in either direction, but for T_p/T_c sufficiently large these contributions are small enough that the behavior in the antidiagonal (diagonal) direction is effectively captured by the width T_c (Ω_p) set at $t_2=0$ ($\Omega_2=0$).

In the schematic one can see that along the lines $t_1=t_2$ ($\omega_1=-\omega_2$) the joint temporal (spectral) intensity ranges over $-T_p/2\to T_p/2$ ($-\Omega_c/2\to\Omega_c/2$), however this is not the *full*

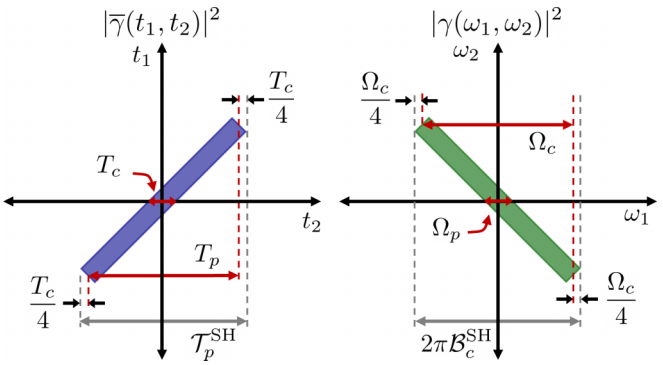

FIG. 26. Schematic of the sinc-hat joint intensities showing the extra contributions to the horizontal widths in the respective corners.

horizontal extent of the joint intensities. For the joint temporal intensity there are two extra contributions in the lower left-hand and upper right-hand corners. Using simple geometry one finds that each corner adds a duration of size $T_p/4$ to the horizontal width for a combined width of $\mathcal{T}_p^{\mathrm{SH}} = T_p + T_c/2$. A similar argument follows for the joint spectral intensity leading to a combined width of $2\pi\mathcal{B}_c^{\mathrm{SH}} = \Omega_c + \Omega_p/2$.

APPENDIX C: JOINT TEMPORAL AMPLITUDE SCALING

Consider the joint temporal amplitude schematically shown in Fig. 1, characterized by $\mathcal{T}_p$ and $\mathcal{T}_c$. To show how the maximum value of the joint temporal amplitude scales with $\mathcal{T}_p$ and $\mathcal{T}_c$ we consider a change of variables

$$\tilde{t}_1 = \frac{1}{\sqrt{2}}\frac{t_1+t_2}{\mathcal{T}_p}, \quad \tilde{t}_2 = \frac{1}{\sqrt{2}}\frac{t_1-t_2}{\mathcal{T}_c},$$
$$t_1 = \frac{1}{\sqrt{2}}(\tilde{t}_1\mathcal{T}_p + \tilde{t}_2\mathcal{T}_c), \quad t_2 = \frac{1}{\sqrt{2}}(\tilde{t}_1\mathcal{T}_p - \tilde{t}_2\mathcal{T}_c), \tag{C1}$$

which are aligned with the long and short axis of the joint temporal amplitude, see Fig. 27. The new variables $\tilde{t}_1, \tilde{t}_2$ are normalized and dimensionless; as they vary over the range $\tilde{t}_1, \tilde{t}_2 \in [-1/\sqrt{2}, 1/\sqrt{2}]$, t_1, t_2 vary over the range of the joint amplitude specified by $\mathcal{T}_p$ and $\mathcal{T}_c$. The Jacobian of this coordinate transformation is $\det(J) = \mathcal{T}_p\mathcal{T}_c$. Then setting

$$\tilde{\gamma}(\tilde{t}_1,\tilde{t}_2) = \sqrt{\mathcal{T}_p\mathcal{T}_c}\overline{\gamma}\left(\frac{1}{\sqrt{2}}(\tilde{t}_1\mathcal{T}_p + \tilde{t}_2\mathcal{T}_c), \frac{1}{\sqrt{2}}(\tilde{t}_1\mathcal{T}_p - \tilde{t}_2\mathcal{T}_c)\right)$$
$$= \sqrt{\mathcal{T}_p\mathcal{T}_c}\overline{\gamma}(t_1,t_2), \tag{C2}$$

$\tilde{\gamma}(\tilde{t}_1,\tilde{t}_2)$ is a normalized and dimensionless joint amplitude that satisfies

$$\int dt_1 dt_2 |\overline{\gamma}(t_1,t_2)|^2 = \int d\tilde{t}_1 d\tilde{t}_2 |\tilde{\gamma}(\tilde{t}_1,\tilde{t}_2)|^2 = 1. \tag{C3}$$

Since the rotated coordinates vary roughly over $\tilde{t}_1, \tilde{t}_2 \in [-1/\sqrt{2}, 1/\sqrt{2}]$ and $|\tilde{\gamma}(\tilde{t}_1,\tilde{t}_2)|$ is always positive, we can infer that the approximate maximum of $|\tilde{\gamma}(\tilde{t}_1,\tilde{t}_2)|$ is on the order of one. Then rewriting Eq. (C2), we have

$$\overline{\gamma}(t_1,t_2) = \frac{\tilde{\gamma}(\tilde{t}_1,\tilde{t}_2)}{\sqrt{\mathcal{T}_p\mathcal{T}_c}}, \tag{C4}$$

and since the location of the maximum of $|\overline{\gamma}(t_1,t_2)|$ must be the same as that of $|\tilde{\gamma}(\tilde{t}_1,\tilde{t}_2)|$, and the latter maximum is of order unity, in general the maximum value of $\overline{\gamma}(t_1,t_2)$ scales with $1/\sqrt{\mathcal{T}_p\mathcal{T}_c}$.

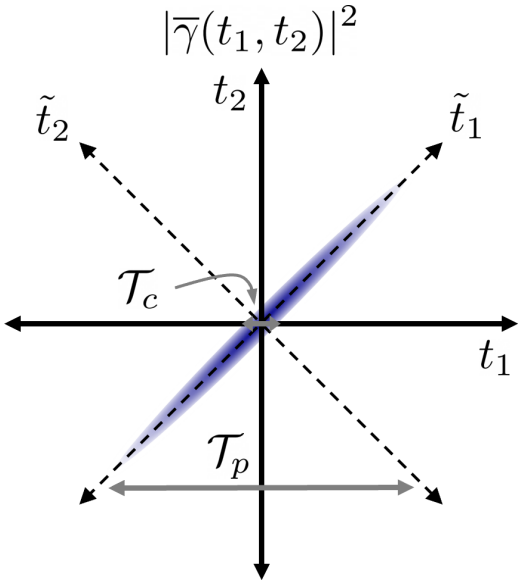

FIG. 27. Schematic of a general joint temporal amplitude with a pulse duration and coherence time denoted by $\mathcal{T}_p$ and $\mathcal{T}_c$, respectively, in the original and rotated coordinate system.

APPENDIX D: RELATION BETWEEN K AND $\mathcal{K}$

We begin with an alternate expression [9,10] for the Schmidt number,

$$\frac{1}{K} = \int dt_1 dt_2 dt_1' dt_2' \overline{\gamma}(t_1,t_2)\overline{\gamma}^*(t_1',t_2)\overline{\gamma}(t_1',t_2')\overline{\gamma}(t_1,t_2'), \tag{D1}$$

which can be confirmed by using the Schmidt decomposition [Eq. (3.1)] in Eq. (D1) and recalling the orthogonality of the Schmidt modes. If a Whittaker-Shannon decomposition [Eq. (5.11)] constructed with an appropriate bandwidth limit is put in Eq. (D1), with the use of the orthogonality relations of $\overline{\chi}_n(t)$ we find

$$\frac{1}{K} = \tau^4 \sum_{a,b,c,d} \overline{\gamma}_{ab}\overline{\gamma}^*_{cb}\overline{\gamma}_{cd}\overline{\gamma}^*_{ad} = \tau^4 \mathrm{Tr}(\bar{\boldsymbol{\gamma}}\bar{\boldsymbol{\gamma}}^\dagger\bar{\boldsymbol{\gamma}}\bar{\boldsymbol{\gamma}}^\dagger), \tag{D2}$$

where we have written $\overline{\gamma}_{ab}$ as shorthand for $\overline{\gamma}(a\tau, b\tau)$, and in the second equality we use $\bar{\boldsymbol{\gamma}}$ to indicate the matrix with components $\overline{\gamma}_{ab}$.

We now make use of the identity

$$|\mathrm{Tr}(\mathbf{A}\mathbf{B}^\dagger)|^2 \leqslant \mathrm{Tr}(\mathbf{A}\mathbf{A}^\dagger)\mathrm{Tr}(\mathbf{B}\mathbf{B}^\dagger), \tag{D3}$$

which is the generalization of the Cauchy–Schwarz inequality to matrices under the trace inner product [37]. For $\mathbf{A}$ an $l \times l$ matrix, we put $\mathbf{B} = \mathbf{1}_{l\times l}$, the identity matrix of size $l \times l$, and find

$$|\mathrm{Tr}(\mathbf{A})|^2 \leqslant \mathrm{Tr}(\mathbf{A}\mathbf{A}^\dagger)l, \tag{D4}$$

or rather

$$\mathrm{Tr}(\mathbf{A}\mathbf{A}^\dagger) \geqslant \frac{|\mathrm{Tr}(\mathbf{A})|^2}{l}. \tag{D5}$$

Next we set $\mathbf{A} = \bar{\boldsymbol{\gamma}}\bar{\boldsymbol{\gamma}}^\dagger$ and since $\mathrm{Tr}(\bar{\boldsymbol{\gamma}}\bar{\boldsymbol{\gamma}}^\dagger) \geqslant 0$ the inequality in Eq. (D5) leads to

$$\mathrm{Tr}(\bar{\boldsymbol{\gamma}}\bar{\boldsymbol{\gamma}}^\dagger\bar{\boldsymbol{\gamma}}\bar{\boldsymbol{\gamma}}^\dagger) \geqslant \frac{\mathrm{Tr}(\bar{\boldsymbol{\gamma}}\bar{\boldsymbol{\gamma}}^\dagger)^2}{l}. \tag{D6}$$

After inputting this result into the equation (D2) for the Schmidt number, we arrive at

$$\frac{1}{K} \geqslant \frac{[\tau^2\mathrm{Tr}(\bar{\boldsymbol{\gamma}}\bar{\boldsymbol{\gamma}}^\dagger)]^2}{l}. \tag{D7}$$

This can be significantly simplified by noting that the joint amplitude is normalized to unity, and inputting the Whittaker-Shannon decomposition [Eq. (5.11)] into

$$\int dt_1 dt_2 |\overline{\gamma}(t_1, t_2)|^2 = 1, \tag{D8}$$

we find $\tau^2\mathrm{Tr}(\bar{\boldsymbol{\gamma}}\bar{\boldsymbol{\gamma}}^\dagger) = 1$, and then from Eq. (D7) we have

$$K \leqslant l. \tag{D9}$$

Now l is the dimension of the matrix $\boldsymbol{\gamma}$, but because $\overline{\chi}_n(t)$ has a width set by τ one needs on the order of $l = \mathcal{T}_p/\tau$ functions to interpolate the joint amplitude; see the discussion around Eq. (5.20). If we choose $\tau = \mathcal{T}_c$, then $l = \mathcal{T}_p/\mathcal{T}_c = \mathcal{K}$ and we find

$$K \leqslant \mathcal{K}, \tag{D10}$$

which completes the argument.

APPENDIX E: CORRELATION FUNCTIONS

We begin by using the inverse relation given by Eq. (5.13) to write the correlation functions (2.4) as

$$\overline{G}^{(1)}(t_1, t_2) = \overline{\chi}^*_x(t_1)\langle\Psi|B^\dagger_x B_y|\Psi\rangle\overline{\chi}_y(t_2), \tag{E1a}$$

$$\overline{G}^{(2)}(t_1, t_2) = \overline{\chi}^*_w(t_1)\overline{\chi}^*_x(t_2)\langle\Psi|B^\dagger_w B^\dagger_x B_y B_z|\Psi\rangle\overline{\chi}_y(t_2)\overline{\chi}_z(t_1), \tag{E1b}$$

we use the same summation convention as in the text. Then using the transformation given by Eq. (6.2) we evaluate

$$\begin{aligned}\langle\Psi|B^\dagger_x B_y|\Psi\rangle &= \langle\mathrm{vac}|\,\nu^*_{xa}B_a\nu_{yb}B^\dagger_b\,|\mathrm{vac}\rangle = \nu^*_{xa}\nu_{ya} = (\boldsymbol{\nu}^*\boldsymbol{\nu}^T)_{xy}\\ &= [\mathbf{U}^*(\sinh\mathbf{P}^*)(\sinh\mathbf{P}^T)\mathbf{U}^T]_{xy} = (\sinh^2\mathbf{P})_{xy},\end{aligned} \tag{E2}$$

and

$$\begin{aligned}\langle\Psi|B^\dagger_w B^\dagger_x B_y B_z|\Psi\rangle &= \langle\mathrm{vac}|\,\nu^*_{wa}B_a(\mu^*_{xb}B^\dagger_b + \nu^*_{xb}B_b)(\mu_{yc}B_c + \nu_{yc}B^\dagger_c)\nu_{zd}B^\dagger_d\,|\mathrm{vac}\rangle\\ &= S^*_{wa}\mu^*_{xb}\mu_{yc}\nu_{zd}\,\langle\mathrm{vac}|\,B_aB^\dagger_bB_cB^\dagger_d\,|\mathrm{vac}\rangle + \nu^*_{wa}\nu^*_{xb}\nu_{yc}\nu_{zd}\,\langle\mathrm{vac}|\,B_aB_bB^\dagger_cB^\dagger_d\,|\mathrm{vac}\rangle\\ &= \nu^*_{wa}\mu^*_{xa}\mu_{yc}\nu_{zc} + \nu^*_{wa}\nu^*_{xb}\nu_{yb}\nu_{za} + \nu^*_{wa}\nu^*_{xb}\nu_{ya}\nu_{zb}\\ &= (\boldsymbol{\nu}\boldsymbol{\mu}^T)^*_{wx}(\boldsymbol{\nu}\boldsymbol{\mu}^T)_{zy} + (\boldsymbol{\nu}^*\boldsymbol{\nu}^T)_{wz}(\boldsymbol{\nu}^*\boldsymbol{\nu}^T)_{xy} + (\boldsymbol{\nu}^*\boldsymbol{\nu}^T)_{wy}(\boldsymbol{\nu}^*\boldsymbol{\nu}^T)_{xz}\\ &= [\mathbf{U}(\sinh\mathbf{P})(\cosh\mathbf{P})]^*_{wx}[\mathbf{U}(\sinh\mathbf{P})(\cosh\mathbf{P})]_{zy} + (\sinh^2\mathbf{P})_{wz}(\sinh^2\mathbf{P})_{xy} + (\sinh^2\mathbf{P})_{wy}(\sinh^2\mathbf{P})_{xz}.\end{aligned} \tag{E3}$$

So $\overline{G}^{(1)}(t_1, t_2)$ is given by

$$\overline{G}^{(1)}(t_1, t_2) = \overline{\chi}^*_x(t_1)(\sinh^2\mathbf{P})_{xy}\overline{\chi}_y(t_2) = \overline{\boldsymbol{\chi}}^\dagger(t_1)(\sinh^2\mathbf{P})\overline{\boldsymbol{\chi}}(t_2), \tag{E4}$$

where $\overline{\boldsymbol{\chi}}(t) = (\ldots, \overline{\chi}_{-1}(t), \overline{\chi}_0(t), \overline{\chi}_1(t), \ldots)^T$ is the column vector formed from the set $\{\overline{\chi}_n(t)\}$ for a given t, and

$$\begin{aligned}\overline{G}^{(2)}(t_1, t_2) &= \overline{\chi}^*_w(t_1)\overline{\chi}^*_x(t_2)[\mathbf{U}(\sinh\mathbf{P})(\cosh\mathbf{P})]^*_{wx}[\mathbf{U}(\sinh\mathbf{P})(\cosh\mathbf{P})]_{zy}\overline{\chi}_y(t_2)\overline{\chi}_z(t_1)\\ &\quad+\overline{\chi}^*_w(t_1)\overline{\chi}^*_x(t_2)(\sinh^2\mathbf{P})_{wz}(\sinh^2\mathbf{P})_{xy}\overline{\chi}_y(t_2)\overline{\chi}_z(t_1)\\ &\quad+\overline{\chi}^*_w(t_1)\overline{\chi}^*_x(t_2)(\sinh^2\mathbf{P})_{wy}(\sinh^2\mathbf{P})_{xz}\overline{\chi}_y(t_2)\overline{\chi}_z(t_1)\\ &= |\overline{\boldsymbol{\chi}}^T(t_1)\mathbf{U}(\sinh\mathbf{P})(\cosh\mathbf{P})\overline{\boldsymbol{\chi}}(t_2)|^2 + [\overline{\boldsymbol{\chi}}^\dagger(t_1)(\sinh^2\mathbf{P})\overline{\boldsymbol{\chi}}(t_1)][\overline{\boldsymbol{\chi}}^\dagger(t_2)(\sinh^2\mathbf{P})\overline{\boldsymbol{\chi}}(t_2)] + |\overline{\boldsymbol{\chi}}^\dagger(t_1)(\sinh^2\mathbf{P})\overline{\boldsymbol{\chi}}(t_2)|^2\\ &= |\overline{\boldsymbol{\chi}}^T(t_1)\mathbf{U}(\sinh\mathbf{P})(\cosh\mathbf{P})\overline{\boldsymbol{\chi}}(t_2)|^2 + \overline{G}^{(1)}(t_1)\overline{G}^{(1)}(t_2) + |\overline{G}^{(1)}(t_1, t_2)|^2.\end{aligned} \tag{E5}$$

APPENDIX F: MODE-BY-MODE CALCULATION

In this Appendix we show that the photon statistics of the sinc-hat joint amplitude can be described on a "mode-by-mode" basis using the pseudo-Schmidt decomposition. We then generalize this to the Whittaker-Shannon decomposition, and show that at least approximately a "mode-by-mode" description can be introduced.

1. Pseudo-Schmidt decomposition

We start by considering the analytical form of $\overline{G}^{(2)}(\Delta t)$ (4.27) in the cw limit,

$$\overline{G}^{(2)}(\Delta t)|_{|\Delta t|\lesssim T_c} \approx \overline{G}^{(2)}(\Delta t = 0) = \frac{1}{T_c^2}\left(3N^2_{\mathrm{mode}} + N_{\mathrm{mode}}\right), \tag{F1}$$

where we have approximated the sinc function as unity and used Eq. (4.20). As expected, we recover the usual standard result for $G^{(2)}(\Delta t = 0)$ [19,38], and for $\Delta t > T_c$ we have $\overline{G}^{(2)}(\Delta t) \leqslant \overline{G}^{(2)}(\Delta t = 0)$, the condition for "bunched light" [39]. Since $\overline{G}^{(2)}(\Delta t)$ varies little over a length of time $|\Delta t| \lesssim T_c$, the quantity $T_c\overline{G}^{(2)}(\Delta t)$ is a "coincidence rate," and

$$T_p(T_e\overline{G}^{(2)}(\Delta t)|_{\Delta t \lesssim T_c}) \approx \mathcal{N}\left(3N_{\text{mode}}^2 + N_{\text{mode}}\right) \tag{F2}$$

is the total coincidence count over the duration of the pulse.

To gain insight into the scaling of $\overline{G}^{(2)}(\Delta t)$ with N_{mode}, we note that, for a single pseudo-Schmidt mode labeled by n, the probability of detecting $2x$ photons is [19]

$$P_n(2x) = \frac{1}{c}\left(\frac{\sqrt{(2x)!}}{2^x x!}\right)^2\left(\frac{s}{c}\right)^{2x}, \tag{F3}$$

where we put $s \equiv \sinh(r)$ and $c \equiv \cosh(r)$, and $r = |\beta|/\sqrt{\mathcal{N}}$ is the squeezing parameter which is independent of n for the values of n for which it is nonzero [see Eq. (4.15)]. Since each pseudo-Schmidt mode is normalized we have

$$1 = \sum_{x=0}^{\infty} P_n(2x) \Rightarrow c = \sum_{x=0}^{\infty}\left(\frac{\sqrt{(2x)!}}{2^x x!}\right)^2\left(\frac{s}{c}\right)^{2x}. \tag{F4}$$

Taking the derivative of both sides with respect to r, and simplifying using hyperbolic trigonometry identities followed by a re-indexing of the sum, we find

$$\sum_{x=0}^{\infty}(2x)P_n(2x) = s^2 = N_{\text{mode}}, \tag{F5}$$

as expected, the average number of photons in each pseudo-Schmidt mode is given by N_{mode}. Notice that we can rewrite the expectation value as

$$\begin{aligned} N_{\text{mode}} &= \sum_{x=0}^{\infty}(2x)P_n(2x) = \sum_{x=0}^{\infty}\frac{(2x)!}{(2x-1)!}P_n(2x) \\ &= \sum_{x=0}^{\infty}\mathcal{P}(2x,1)P_n(2x), \end{aligned} \tag{F6}$$

where $\mathcal{P}(2x,1)$ is the number of permutations of $2x$ objects when we select one object. Again taking the derivative of both sides with respect to r, after further hyperbolic trigonometry manipulations and a re-indexing of the sum, we find

$$\sum_{x=0}^{\infty}(2x)(2x-1)P_n(2x) = 3N_{\text{mode}}^2 + N_{\text{mode}}, \tag{F7}$$

where the right-hand side is the familiar scaling of $\overline{G}^{(2)}(\Delta t)$ with N_{mode}. However, playing the same game, we can rewrite this as

$$\begin{aligned} \sum_{x=0}^{\infty}(2x)(2x-1)P_n(2x) &= \sum_{x=0}^{\infty}\frac{(2x)!}{(2x-2)!}P_n(2x) \\ &= \sum_{x=0}^{\infty}\mathcal{P}(2x,2)P_n(2x) \\ &= 3N_{\text{mode}}^2 + N_{\text{mode}}, \end{aligned} \tag{F8}$$

where $\mathcal{P}(2x,2)$ is the number of permutations of $2x$ objects when we select two of them.

Thus, for short time differences on the order of T_c, the coincidence rate is the expectation value of the total number of ways of picking two photons from any pseudo-Schmidt mode, and to calculate the total coincidence count we multiply by $\mathcal{N}$ (F2), the total number of pseudo-Schmidt modes [cf. (4.20) and (4.21)]. Indeed, for time differences less than T_c we can set $n = m$ for both terms in Eq. (4.17), so that to good approximation we have

$$G^{(2)}(t_1,t_2) \approx \left(3N_{\text{mode}}^2 + N_{\text{mode}}\right)\sum_n |\overline{\eta}_n(t_1)|^2|\overline{\eta}_n(t_2)|^2. \tag{F9}$$

For such time differences the coincidence count at a particular t_1, t_2 is associated with only a few pseudo-Schmidt modes, unlike in the Schmidt decomposition, where the inclusion of the contributions of a large number of Schmidt modes is needed.

2. Whittaker-Shannon decomposition

We now consider the Whittaker-Shannon decomposition, starting with the exact results for the correlation functions (6.6) and (6.7). The photon density is given by

$$\begin{aligned} \overline{G}^{(1)}(t) &= \overline{\boldsymbol{\chi}}^{\dagger}(t)(\sinh^2\mathbf{P})\overline{\boldsymbol{\chi}}(t) = \sum_{n,m}\overline{\chi}_n^*(t)(\sinh^2\mathbf{P})_{nm}\overline{\chi}_m(t) \\ &\approx \sum_n(\sinh^2\mathbf{P})_{nn}|\overline{\chi}_n(t)|^2, \end{aligned} \tag{F10}$$

where in the second line we expanded the matrix multiplication and in the third line approximated the double sum as just the diagonal contributions. In reducing the double sum to a single sum we are losing significant contributions to the photon density because typically $(\sinh^2\mathbf{P})_{nm}$ will be nonzero over a small range of $|n-m|$; further, the product of two neighboring Whittaker-Shannon modes is not negligible. While the final result of Eq. (F10) provides a crude approximate at best, it is similar to the pseudo-Schmidt result given by Eq. (4.16). This suggests that we should identify

$$\Gamma_n^2 = (\sinh^2\mathbf{P})_{nn} \tag{F11}$$

as the number of photons in each mode, and indeed we find this to be the case in Sec. VI A.

We now turn our attention to $\overline{G}^{(2)}(t_1,t_2)$, starting with the coherent contribution

$$\begin{aligned} \overline{G}^{(2)}_{\text{coh}}(t_1,t_2) &= |\overline{\boldsymbol{\chi}}^T(t_1)\mathbf{U}(\sinh\mathbf{P})(\cosh\mathbf{P})\overline{\boldsymbol{\chi}}(t_2)|^2 \\ &= \sum_{n,m,p,q}\overline{\chi}_n^*(t_1)(\mathbf{U}\sinh\mathbf{P}\cosh\mathbf{P})^*_{nm}\overline{\chi}_m^*(t_2)\overline{\chi}_p(t_1) \\ &\quad\times(\mathbf{U}\sinh\mathbf{P}\cosh\mathbf{P})_{pq}\overline{\chi}_q(t_2) \\ &\approx \sum_{n,m}|(\mathbf{U}\sinh\mathbf{P}\cosh\mathbf{P})_{nm}|^2|\overline{\chi}_n(t_1)|^2|\overline{\chi}_m(t_2)|^2, \end{aligned} \tag{F12}$$

where in the last line we used the same approximation that we did for the photon density. Then if we consider times t_1, t_2 such that $|t_1 - t_2| \lesssim \tau$, the significant contribution to the sum

is when $n = m$, and we have

$$\overline{G}^{(2)}_{\rm coh}(t_1, t_2) \approx \sum_n |(\mathbf{U}\text{sinh}\mathbf{P}\text{cosh}\mathbf{P})_{nn}|^2 |\overline{\chi}_n(t_1)|^2 |\overline{\chi}_n(t_2)|^2. \tag{F13}$$

Following the same steps for the incoherent contribution, for times t_1, t_2 such that $|t_1 - t_2| \lesssim \tau$, $\overline{G}^{(2)}(t_1, t_2)$ is given by

$$\overline{G}^{(2)}(t_1, t_2) = \sum_n \left[|(\mathbf{U}\text{sinh}\mathbf{P}\text{cosh}\mathbf{P})_{nn}|^2 + 2\Gamma_n^4\right] \times |\overline{\chi}_n(t_1)|^2 |\overline{\chi}_n(t_2)|^2. \tag{F14}$$

While again a crude approximation at best, we do note the similarity between the final result and the pseudo-Schmidt result in Eq. (F9).

APPENDIX G

We start with equation (6.9) for $\overline{\rho}_n(t)$, and invert it by multiplying by $(\text{sinh}\mathbf{P})^{-1} = \text{csch}\mathbf{P}$

$$\overline{\chi}_n(t) = \sum_m (\text{csch}\mathbf{P})_{nm} \Gamma_m \overline{\rho}_m(t). \tag{G1}$$

Taking the term inside the squared norm for the coherent contribution [Eq. (6.13)] and writing it in its index representation, we insert the form of $\overline{\chi}_n(t)$ in terms of $\overline{\rho}_m(t)$ using (G1), so that

$$\begin{aligned}
&\overline{\boldsymbol{\chi}}^T(t_1)\mathbf{U}(\text{sinh}\mathbf{P})(\text{cosh}\mathbf{P})\overline{\boldsymbol{\chi}}(t_2) \\
&\quad = \overline{\chi}_x(t_1) U_{xa} (\text{sinh}\mathbf{P})_{ab} (\text{cosh}\mathbf{P})_{by} \overline{\chi}_y(t_2) \\
&\quad = (\text{csch}\mathbf{P})_{xm} \Gamma_m \overline{\rho}_m(t_1) U_{xa} (\text{sinh}\mathbf{P})_{ab} (\text{cosh}\mathbf{P})_{by} \\
&\qquad \times (\text{csch}\mathbf{P})_{yn} \Gamma_n \overline{\rho}_n(t_2) \\
&\quad = \Gamma_n \Gamma_m \overline{\rho}_m(t_1) \overline{\rho}_n(t_2) [(\text{csch}\mathbf{Q})\mathbf{U}(\text{sinh}\mathbf{P})(\text{cosh}\mathbf{P})(\text{csch}\mathbf{P})]_{mn} \\
&\quad = \Gamma_n \Gamma_m \overline{\rho}_m(t_1) \overline{\rho}_n(t_2) (\mathbf{U}\text{coth}\mathbf{P})_{mn},
\end{aligned} \tag{G2}$$

where in deriving this result we used the properties of $\mathbf{P}$, $\mathbf{Q}$ and $\mathbf{U}$ discussed in Sec. VI, and we set $\text{coth}\mathbf{P} = (\text{tanh}\mathbf{P})^{-1} = (\text{cosh}\mathbf{P})(\text{csch}\mathbf{P})$. The resulting coherent contribution to the correlation function is then given by

$$\overline{G}^{(2)}_{\rm coh}(t_1, t_2) = \sum_{n,m} |\Gamma_n \Gamma_m (\mathbf{U}\text{coth}\mathbf{P})_{mn} \overline{\rho}_m(t_1) \overline{\rho}_n(t_2)|^2. \tag{G3}$$

[1] S. Pirandola, B. R. Bardhan, T. Gehring, C. Weedbrook, and S. Lloyd, Advances in photonic quantum sensing, Nat. Photonics **12**, 724 (2018).

[2] P.-A. Moreau, E. Toninelli, T. Gregory, and M. J. Padgett, Imaging with quantum states of light, Nat. Rev. Phys. **1**, 367 (2019).

[3] J. E. Bourassa, R. N. Alexander, M. Vasmer, A. Patil, I. Tzitrin, T. Matsuura, D. Su, B. Q. Baragiola, S. Guha, G. Dauphinais *et al.*, Blueprint for a scalable photonic fault-tolerant quantum computer, Quantum **5**, 392 (2021).

[4] N. Quesada, L. Helt, M. Menotti, M. Liscidini, and J. Sipe, Beyond photon pairs—nonlinear quantum photonics in the high-gain regime: a tutorial, Adv. Opt. Photonics **14**, 291 (2022).

[5] N. Quesada and J. E. Sipe, Effects of time ordering in quantum nonlinear optics, Phys. Rev. A **90**, 063840 (2014).

[6] R. J. Glauber, The quantum theory of optical coherence, Phys. Rev. **130**, 2529 (1963).

[7] A. M. Chebotarev and A. E. Teretenkov, Singular value decomposition for the Takagi factorization of symmetric matrices, Appl. Math. Comput. **234**, 380 (2014).

[8] M. Houde, W. McCutcheon, and N. Quesada, Matrix decompositions in quantum optics: Takagi/Autonne, Bloch-Messiah/Euler, Iwasawa, and Williamson, arXiv:2403.04596.

[9] M. Fedorov, M. Efremov, P. Volkov, and J. Eberly, Short-pulse or strong-field breakup processes: a route to study entangled wave packets, J. Phys. B: At., Mol. Opt. Phys. **39**, S467 (2006).

[10] Y. M. Mikhailova, P. A. Volkov, and M. V. Fedorov, Biphoton wave packets in parametric down-conversion: Spectral and temporal structure and degree of entanglement, Phys. Rev. A **78**, 062327 (2008).

[11] M. V. Fedorov, M. A. Efremov, P. A. Volkov, E. V. Moreva, S. S. Straupe, and S. P. Kulik, Spontaneous parametric down-conversion: Anisotropical and anomalously strong narrowing of biphoton momentum correlation distributions, Phys. Rev. A **77**, 032336 (2008).

[12] B. Brecht and C. Silberhorn, Characterizing entanglement in pulsed parametric down-conversion using chronocyclic Wigner functions, Phys. Rev. A **87**, 053810 (2013).

[13] H. J. Landau and H. O. Pollak, Prolate spheroidal wave functions, Fourier analysis and uncertainty—III: the dimension of the space of essentially time-and band-limited signals, Bell Syst. Tech. J. **41**, 1295 (1962).

[14] F. J. Simons, Slepian functions and their use in signal estimation and spectral analysis, in *Handbook of Geomathematics*, edited by W. Freeden, M. Z. Nashed, and T. Sonar (Springer, Berlin, Heidelberg, 2010).

[15] W. Freeden, M. Z. Nashed, and T. Sonar, *Handbook of Geomathematics* (Springer Science & Business Media, 2010).

[16] D. A. Miller, Communicating with waves between volumes: evaluating orthogonal spatial channels and limits on coupling strengths, Appl. Opt. **39**, 1681 (2000).

[17] H. Di Lorenz Pires, C. H. Monken, and M. P. Van Exter, Direct measurement of transverse-mode entanglement in two-photon states, Phys. Rev. A **80**, 022307 (2009).

[18] J. B. Pors, S. S. R. Oemrawsingh, A. Aiello, M. P. Van Exter, E. R. Eliel, G. W. tHooft, and J. P. Woerdman, Shannon dimensionality of quantum channels and its application to photon entanglement, Phys. Rev. Lett. **101**, 120502 (2008).

[19] R. Loudon, *The Quantum Theory of Light* (Oxford University Press, Oxford, 2000).

[20] B. Dayan, Theory of two-photon interactions with broadband down-converted light and entangled photons, Phys. Rev. A **76**, 043813 (2007).

[21] A. Edrelyi *et al.*, *Higher Transcendental Functions* (McGraw-Hill Book Co, Inc., New York,1953), Vol. II, p. 194.

[22] F. W. J. Olver, *NIST Handbook of Mathematical Functions Hardback and CD-ROM* (Cambridge University Press, Cambridge, UK, 2010).

[23] J. J. Sakurai and E. D. Commins, *Modern Quantum Mechanics, Revised Edition* (Addison-Wesely, 1995).
[24] M. G. Raymer and T. Landes, Theory of two-photon absorption with broadband squeezed vacuum, Phys. Rev. A **106**, 013717 (2022).
[25] P. Cutipa and M. V. Chekhova, Bright squeezed vacuum for two-photon spectroscopy: simultaneously high resolution in time and frequency, space and wavevector, Opt. Lett. **47**, 465 (2022).
[26] D. Slepian and H. O. Pollak, Prolate spheroidal wave functions, fourier analysis and uncertainty—I, Bell Syst. Tech. J. **40**, 43 (1961).
[27] L.-L. Wang, A review of prolate spheroidal wave functions from the perspective of spectral methods, J. Math. Study **50**, 101 (2018).
[28] M. L. Cohen and S. G. Louie, *Fundamentals of Condensed Matter Physics* (Cambridge University Press, 2016).
[29] E. T. Whittaker, XVIII.—On the functions which are represented by the expansions of the interpolation-theory, Proc. R. Soc. Edinburgh **35**, 181 (1915).
[30] C. E. Shannon, Communication in the presence of noise, Proc. IRE **37**, 10 (1949).
[31] P. L. Butzer and R. L. Stens, Sampling theory for not necessarily band-limited functions: a historical overview, SIAM Rev. **34**, 40 (1992).
[32] D. Slepian, Some comments on Fourier analysis, uncertainty and modeling, SIAM Rev. **25**, 379 (1983).
[33] C. F. Lo and R. Sollie, Generalized multimode squeezed states, Phys. Rev. A **47**, 733 (1993).
[34] X. Ma and W. Rhodes, Multimode squeeze operators and squeezed states, Phys. Rev. A **41**, 4625 (1990).
[35] M. Banic, M. Liscidini, and J. E. Sipe, Resonant and nonresonant integrated third-order parametric down-conversion, Phys. Rev. A **106**, 013710 (2022).
[36] T. G. Kolda and B. W. Bader, Tensor decompositions and applications, SIAM Rev. **51**, 455 (2009).
[37] S. Friedberg, A. Insel, and L. Spence, *Linear Algebra* (Pearson Education, 2014).
[38] C. Drago and J. E. Sipe, Aspects of two-photon absorption of squeezed light: The continuous-wave limit, Phys. Rev. A **106**, 023115 (2022).
[39] D. F. Walls, Squeezed states of light, Nature (London) **306**, 141 (1983).